Cenozoic Antarctic Glaciation: an integrated climate – ice sheet model approach.

Dissertation
vorgelegt von
Luisa Cristini
aus Verona (Italien)

zur Erlangung des Doktorgrades
Dr. rer. nat.

Fachbereich Physik und Elektrotechnik,
Universität Bremen

1. Gutachter	Prof. Dr. G. Lohmann
2. Gutachter	Prof. Dr. P. Lemke
Eingereicht am:	27.04.2010
Datum des Kolloquiums:	7.06.2010

To the sweetness,
to the patience,
to the constancy,
to the fate,
to the truth,
to the love.

To Torben

Contents

Abstract

One of the most prominent climate changes of the Earth system was the onset of Antarctic glaciation near the Eocene-Oligocene transition (~34 million years ago). The causes of this change are not yet well understood. The most common hypothesises are that glaciation resulted from a cooling of Antarctica due to plate tectonic repositioning and associated changes in ocean circulation or by a response to declining atmospheric pCO_2 supported by the Earth's orbital configuration relative to the Sun. In this thesis these hypotheses are tested through sensitivity experiments with a new climate-ice sheet modelling approach, which takes into account the global oceanic and atmospheric circulation and the Antarctic cryosphere. The first chapter describes the Antarctic Ice Sheet (AIS) and its climatic evolution. It also explains the forcing mechanisms for the Antarctic glaciation and the scientific questions addressed in this study.

The detailed representation of the AIS and its response to oceans and atmosphere is the way by which the processes capable to drive the Antarctic climate evolution can be examined. To achieve this goal with a modelling approach, the models adopted must be able to describe reliably the present AIS and the global circulation of oceans and atmosphere. The numerical models chosen for this study are Huybrechts (1993) ice sheet model (ISM) for the Antarctic cryosphere, and the Earth System Model COSMOS, composed of the atmospheric general circulation model ECHAM5 and the ocean general circulation model MPI-OM, coupled by the ocean-atmosphere-sea ice-soil coupler (OASIS3). MPI-OM is initialised by runs of the Large Scale Geostrophic ocean model (LSG). The second chapter illustrates numerical modelling concepts and previous studies of ice-sheet dynamics. It also describes briefly the four models as well as the methodology employed in the experiments.

The new modelling procedure is validated for modern climate in Chapter 3 and the results compared to observational data. Furthermore the robustness of the method is assessed by analysing the climate and AIS response to a doubling of the global atmospheric carbon dioxide partial pressure (pCO_2). The AIS modelled with this methodology is comparable with observations. This method is also usable to investigate changes in the atmospheric pCO_2 as component of the global climate boundary conditions. The incorporation of the AIS in the climate model via the iterative procedure constitutes an important advancement in the representation of the Antarctic surface topography in general circulation models.

The response of the Antarctic continent to the opening of the Drake Passage (DP) and to the establishment of the Antarctic Circumpolar Current (ACC) is examined in Chapter 4. Two different climate states have been reproduced with global tectonic configurations similar to the Late Eocene and to the Late Oligocene (i.e. before and after the opening of the DP). A reduced southward heat flux and a decrease of both water and air temperature is found around and over Antarctica when the gateway is open. A more massive ice sheet develops on the continent in this case compared to the configuration with the DP closed.

The influence of a specific concentration of carbon dioxide in the atmosphere for

the onset of a major AIS is investigated in the fifth chapter. The dynamics of the climate with a tectonic configuration similar to the Late Eocene and under different pCO_2 are analysed and the response of the Antarctic cryosphere is examined. Lower atmospheric pCO_2 levels result in lower surface atmospheric temperature over the Antarctic continent and, consequently, in larger ice volumes.

The effect of a favourable set of orbital parameters on the early formation of the AIS is analysed in the sixth chapter. Four different experiments are conducted with the land-sea distributions similar to the Late Eocene and to the Late Oligocene by applying two distinct orbital setups, the modern and a favourable one for yielding the coldest Antarctic summer. The effect of a favourable orbital position is to help the initial growth of the AIS under both tectonic configurations, but it seems to have minor impact with respect to the other two main forcings, namely the atmospheric pCO_2 level and the establishment of the ACC.

In conclusion, this study provides results from experiments with a new climate-ice sheet model simulating present and past AIS as well as the global climate. The results support the idea that the establishment of the ACC and low atmospheric pCO_2 levels could have comparable significance in creating the conditions for a wide continental glaciation. On the other hand, orbital forcings, although they certainly support the initial AIS formation, do not seem to have a major impact.

Chapter 1
Introduction

Polar Regions play a key role in global climate change with an impact on sea level and atmospheric as well as oceanic circulation. The Antarctic Ice Sheet (AIS) exists since approximately 35 million years, but has fluctuated considerably throughout the Late Cenozoic era. The assessment of the response of its huge ice mass to climatic forcing is of critical importance for both the understanding of its evolution as well as the prediction of its future behaviour.

In this chapter the description of the present AIS is presented. The evolution of the Antarctic continent throughout the Cenozoic is briefly illustrated, including the potential causes of the Antarctic glaciation: the opening of the Southern Ocean gateways and the consequent establishment of the Antarctic Circumpolar Current (ACC), the decrease in atmospheric carbon dioxide and the favourable orbital configuration. Finally the scientific questions as well as the structure of the thesis are delineated.

1.1 The Antarctic Ice Sheet (AIS)

Antarctica is known as being the highest, driest, windiest and coldest continent on Earth (Turner et al., 2009). The continent covers an area of $14 \cdot 10^6$ km^2, which is about 10% of the Earth's land surface. The land surface rises rapidly from the coast, and the continent has the highest mean elevation of any continent on Earth, of around 2200 m. The surrounding seabed comprises a number of features, which constrain ocean circulation. A map of Antarctica is shown in the Figure 1.1.

The Antarctic continent is dominated by the Antarctic Ice Sheet (AIS), a vast mass of glacial ice containing around $25 \cdot 10^6$ km^3 of ice or 70% of the Earth's freshwater and covering around 99.6 % of the continental area (Fox and Cooper, 1994). The ice sheet consists of East Antarctica, covering an area of $10.35 \cdot 10^6$ km^2, West Antarctica, $1.97 \cdot 10^6$ km^2, and the Antarctic Peninsula, $0.52 \cdot 10^6$ km^2 (Turner et al., 2009). East and West Antarctica are separated by the Transantarctic Mountains, which extend from Victoria Land to the Ronne Ice Shelf (Figure 1.1).

The East Antarctic Ice Sheet (EAIS) comprises the largest part of the ice sheet. In many places the ice at the bedrock is at the pressure melting point as a consequence of the thick ice sheet and heat flux from the Earth beneath, giving rise to a number of subglacial lakes (Siegert et al., 2005). The West Antarctic Ice Sheet (WAIS) rests on a bed that is substantially below sea level. For this reason it is described as a "marine ice sheet" and is considered unstable, being vulnerable to collapse if it loses its fringing ice shelves (e.g., Bamber et al., 2009). The WAIS is generally warmer than the near EAIS, with basal ice close to the melting point in most areas. The Antarctic Peninsula is the only part of the continent that extends significantly northwards, reaching the latitude 63ºS. It is a narrow mountainous region with an average width of 70 km and a mean elevation of 1500 m. The ice that covers the Antarctic Peninsula consists of ice caps that cover the central mountainous spine and some of the larger surrounding islands. These ice caps drain into the sea through narrow, steep and fast, alpine-type glaciers. In contrast to the WAIS and the EAIS, which lose mass primarily through iceberg calving and melt of the base of the ice shelves, the Antarctic Peninsula experiences much higher summer temperatures, making runoff from surface melt a significant component in the budget of its ice cover (Turner et al., 2009).

Ice shelves constitute 11% of the total area of Antarctica, with the two largest being the Filchner-Ronne Ice Shelf in the Weddell Sea and the Ross Ice Shelf in the Ross Sea, which have areas of $0.53 \cdot 10^6$ km^2 and $0.54 \cdot 10^6$ km^2, respectively (Turner et al., 2009). The ice shelves are several hundreds up to more than 1500 metres thick and the ocean currents underneath carry seawater into the cavities beneath the ice shelves. The seawater interacts with the undersides of the ice shelves either melting the ice or adding to it by refreezing (e.g., Grosfeld and Gerdes, 1998). The cooled ocean water becomes fresher with the addition of melt water and emerges from beneath the ice shelves in this modified condition known as Ice Shelf Water (Nicholls et al, 2008).

The continent is surrounded for most of the year by a zone of sea ice of 1 or 2 m thickness. By late austral winter, this sea ice covers an area up to $20 \cdot 10^6$ km^2, more than the area of the continent itself (Summerhayes et al., 2009). Most of the Antarctic sea ice melts during the austral summer, so that by autumn it only covers an area of about $3 \cdot 10^6$

km^2. Most Antarctic sea ice is therefore thin first year ice, with the largest area of multi-year ice covering the western Weddell Sea (Summerhayes et al., 2009).

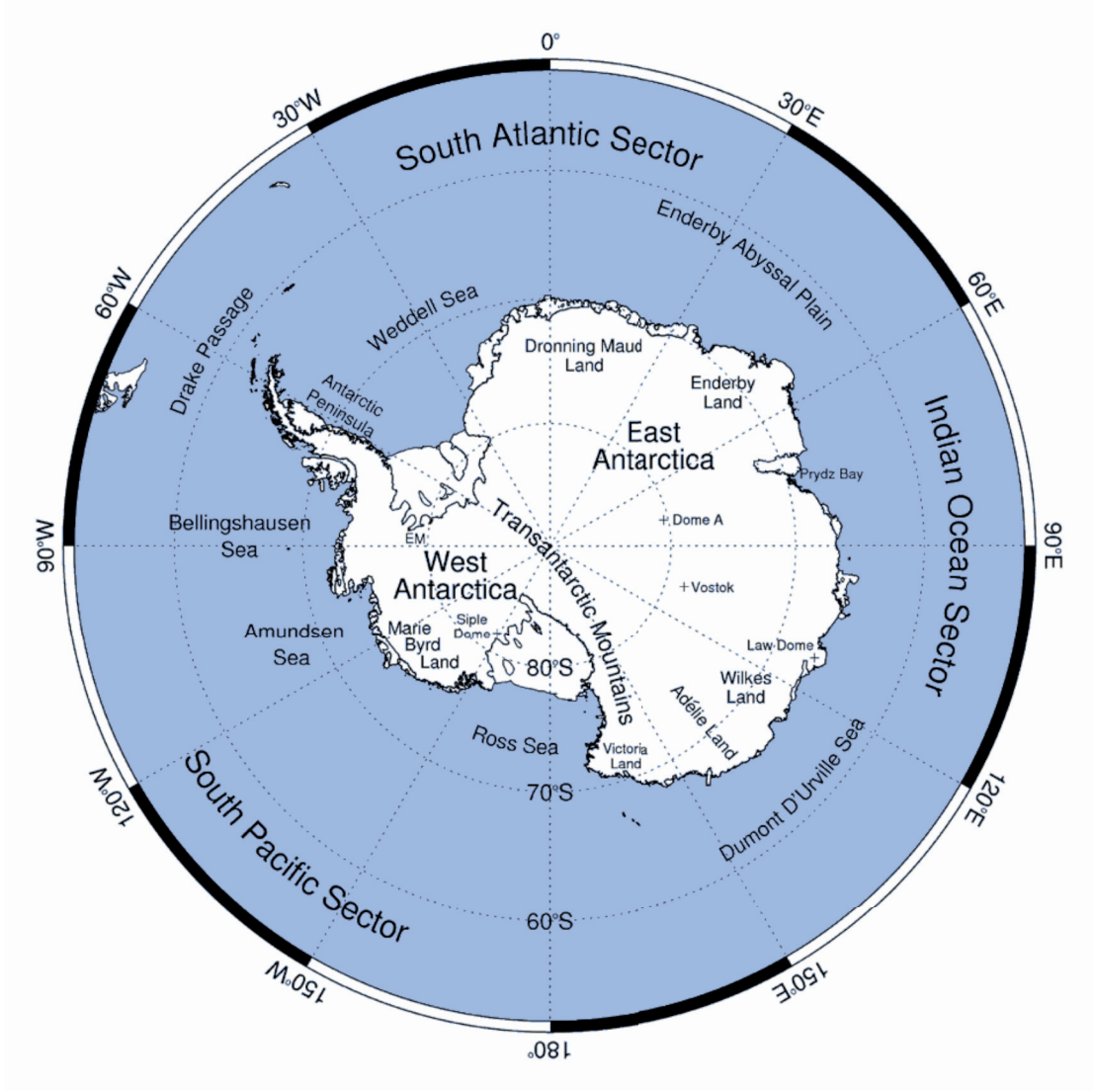

Figure 1.1: Map of Antarctica and associated main features (Turner et al., 2009).

The coldest, driest, and least windy regions are located at the highest plateaus of East Antarctica, while warmer, wetter, and windier regions are generally located along the coastal margins (Monaghan and Bromwich, 2008). The Polar Plateau of East Antarctica experiences very low temperatures because of its high elevation, the lack of clouds and water vapour in the atmosphere and the isolation of the region from the relatively warm maritime air masses found over the Southern Ocean. Temperatures are much less extreme in the Antarctic coastal region than on the plateau. The surface air temperature (SAT) controls surface melting (e.g., Picard et al. 2007) and is the most important factor determining precipitation because the moisture-carrying capacity of air diminishes strongly as its temperature decreases. Snowfall is the largest contributor to the growth of the ice sheet (Bromwich, 1988; Van de Berg et al., 2005). Over the vast interior of the continent, precipitation rates are on the order of a few centimetres ice

equivalent per year. In the more marginal parts of the ice sheet the accumulation regime is more linked to the synoptic situation and the intensity of cyclonic activity and therefore snowfall rates are higher (Simmonds et al., 2003). The AIS acts also as a sink of energy of the Earth-atmosphere system. This is due to the high snow albedo (0.8 – 0.9), and the high emissivity. The surface loses almost continually more energy than it receives. This loss is compensated by the advection of warmer air from over the ocean, followed by the transport of heat by vertical eddy motions and by particles of falling snow to the surface (Schwerdtfeger, 1984). Because of the lack of incoming solar radiation, the Antarctic stratosphere in winter is extremely cold. A strong temperature gradient develops between the continent and mid-latitude, isolating a pool of very cold air above Antarctica and very strong winds evolve along this thermal gradient (Turner et al., 2009).

The AIS interacts actively with the global climate system by amplifying, pacing and potentially driving global climate change over different time scales. Its direct and indirect influence causes changes in ocean surface temperatures and circulation, sea-level changes, land-surface albedo and radiation balance, which in turn cause additional feedbacks in the climate system and help to synchronize global climate change. The Antarctic climate system varies on time scales from the sub-annual to the millennial and is closely coupled to other parts of the global climate system. Given its importance in the Earth system, establishing what controls its evolution and behaviour is necessary to understand its influence on the different components of the climate. The modern climate over Antarctica and the Southern Ocean results from the interactions within the ice sheet – ocean – sea ice – atmosphere system. Knowledge of its response to past and present climate forcing is essential for understanding Earth's past and future global climate.

1.2 The Antarctic climate evolution

The East Antarctic plate formed a significant component of the super continent Gondwana during the Jurassic (Talarico and Kleinschmidt, 2008). Starting at 180 Ma (before present, BP), this continent broke up into what are recognised today as distinct continental landmasses with the repositioning of Antarctica at southern polar latitudes in the Early Cretaceous (ca. 120 Ma BP). In spite of its polar position, Antarctica is thought to have remained mostly ice-free, vegetated and with mean annual temperatures above freezing until the latter half of the Cenozoic (around 34-35 Ma). Immediately afterwards the continent became subject to repeated phases of glaciation at a variety of temporal and spatial scales (Siegert and Florindo, 2008).

The deep-ocean sedimentary record (Fig. 1.2) documents clearly the long-term cooling of climate over the past 50 million years and large-scale variability in the last 3–5 million years. Proxy measurements, in particular oxygen isotopes, provide general details, but initiation, growth and extent of the ice sheets are still debated (e.g., DeConto and Pollard, 2003; Merico, 2008; Zachos, 2001 and 2008). During the Cenozoic, the Antarctic region experienced tectonic, climatic and oceanographic events that led to a geographical isolation and the establishment of colder conditions. The deepening of the separations from other continental masses and the removal of the last

barriers (e.g. between Antarctica and South America) enhanced a circumpolar flow of water masses and allowed the establishment of the Antarctic Circumpolar Current (ACC) and of the Antarctic Polar Front (APF), a roughly circular oceanic and atmospheric system located between 50°S and 60°S (Barker, 2001).

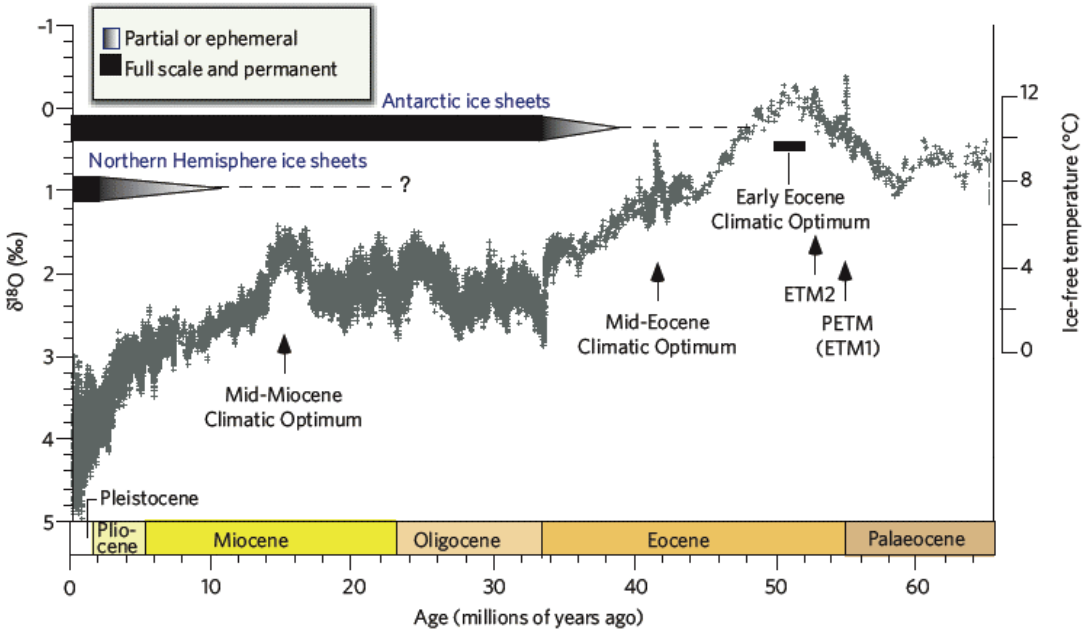

Figure 1.2: Deep-sea benthic foraminiferal oxygen-isotope curve based on sedimentary records from Deep Sea Drilling Project and Ocean Drilling Program sites (Zachos et al., 2008). The $\delta^{18}O$ temperature scale, on the right axis, was computed with the assumption of an ice-free ocean; it therefore applies only to the time preceding the onset of large-scale glaciation on Antarctica (about 35 million years ago).

The change from a warm, ice-free greenhouse world to the glacial icehouse occurred during the Late Eocene–Early Oligocene (Liu et al., 2009). Stable oxygen isotope data of benthic foraminifera are the most significant proxy for documenting the Eocene-Oligocene (E-O) climatic change (e.g., Lear et al. 2008; Coxall et al. 2005). The principal controls on benthic $\delta^{18}O$ are seawater temperature and $\delta^{18}O$ of seawater (δ_w), which depends on global ice volume, the $\delta^{18}O$ of the ice and local variations. Therefore the $\delta^{18}O$ proxy helps constraining deep-water temperatures and global ice volumes. As the Southern Ocean was probably the dominant deep-water source since at least the Late Eocene (e.g. Wright and Miller 1993), benthic $\delta^{18}O$ also provides an estimate of high latitude surface water temperatures.

A stepwise cooling trend is recognizable during the Eocene. By the Late Eocene, the Antarctic climate appears to have deteriorated enough to allow for the formation of small, ephemeral ice sheets, a state that persisted until 34 Ma, when a stable cold dry climate was established in Antarctica and most of East Antarctica became glaciated by a large ice sheet. A temperate glacier regime is suggested for the Early Oligocene (Barrett, 2007). For the remainder of the Oligocene, this ice sheet was a permanent feature of Antarctica and waxed and waned in response to orbital forcing (Naish et al., 2001). High-resolution records of marine sediment cores show that ice

volume and ocean temperatures varied periodicly concentrated in the long eccentricity and obliquity bands (Coxall et al., 2005).

1.3 Potential forcing mechanisms for the Antarctic Glaciation

A huge volume of geochemical data from drilling projects allows us to gain insight into the broader environmental and climatic evolution through E-O transition (Barrett, 2007). However the real pattern of climate cooling and the causes of glaciation are far from being well understood. The long-term cooling trend during the Cenozoic that facilitated the formation and stabilization of continental ice sheets on Antarctica has been attributed to changes in the paleo-geography and in the atmospheric concentration of greenhouse gases.

1.3.1 Opening of the Southern Ocean Gateways

The classical hypothesis of the Southern Ocean Cenozoic climate evolution is that climatic cooling and Antarctic cryosphere development were related to the opening of tectonic seaways: the Drake Passage (DP), between Antarctica and South America and the Tasman Gateway between Antarctica and Australia. This could have permitted the unrestricted development of the Antarctic Circumpolar Current (ACC) and consequently of the Polar Frontal Zone (PFZ), which is believed to have progressively thermally isolated the Antarctic continent (e.g., Kennett, 1977; 1978; Exon et al., 2001). In the modern ocean, the ACC is a powerful surface-to-bottom current that provides an effective barrier to warm waters flowing southward. Different tectonic configurations result in different flow patterns, therefore understanding how the boundaries influenced past ocean circulation patterns might offer insight into the dynamics of other important atmospheric and cryospheric processes.

Precise timing of the opening of these tectonic gateways is necessary for assessing their importance as possible mechanisms of E-O climate change and initiation of major Antarctic glaciation. However, there are great uncertainties in the age estimates, especially for the opening of the DP. Tectonic constraints on the separation of the DP range between about 45 and 22 Ma (Barker and Burrell, 1977; Lawver and Gahagan, 1998; Scher and Martin, 2006), obscuring the direct cause and effect relationship between this gateway, cooling of the climate and Antarctic Glaciation. The uncertainty lies in the tectonic complexity of the region and the question of what constitutes an effective opening for water to flow through.

The idea of a connection between gateways opening and Antarctic Glaciation is supported by the results of ocean general circulation model (OGCM) simulations that demonstrated that the ocean's overturning circulation, heat transport and resulting surface temperature distribution are sensitive to changes in ocean gateways. The opening of Drake Passage and the organization of an ACC would have reduced southward oceanic heat transport and facilitated cooling of Southern Ocean sea surface

temperatures (Mikolajewicz et al., 1993; Toggweiler and Samuels, 1995; Nong et al., 2000; Toggweiler and Bjornsson, 2000;). However, these ocean model approaches lack the link to the atmosphere and hence to Antarctic Glaciation. Modelling efforts for the glacial history of Antarctica have been performed with general circulation models (GCMs) including different climate components and their interactions (DeConto and Pollard, 2003), but a definite answer about the importance of this gateway for the Southern Ocean climate could not been given yet. The main reason is the absence of a model approach including a full oceanic GCM. The three-dimensional oceanic flow regime is the main precondition for the patterns of heat fluxes that force the atmosphere. Vice versa, the distribution of energy (heat), moisture (net precipitation) and momentum (wind stress) are the prevalent driving mechanisms for the ocean as well as for the waxing and waning of continental ice on Antarctica. The examination of different flow regimes can give the significant clues for the understanding of climate variability under different tectonic boundary conditions.

1.3.2 Decline in atmospheric CO_2

The second possible mechanism for the glaciation of Antarctica is the decline in atmospheric temperature related to a decrease in the partial pressure of atmospheric carbon dioxide (pCO_2). Climate sensitive proxies record processes related to the global carbon cycle, either as cause or effect, and have the potential to influence and be influenced by atmospheric CO_2 concentration. A significant part of the discussion on the causative mechanisms for E-O climate change concentrates on the role of declining greenhouse gases in permitting substantial ice build-up on Antarctica. According to Tripati et al. (2005), the transition from a “greenhouse” to an “icehouse” climate is due to the decreasing atmospheric carbon dioxide concentration.

Changes in pCO_2 are thought to be amplifiers of climate change (Raymo 1991; Berner 1992; Crowley, 2000) especially during transitions into and out of glaciations (e.g., Barnola et al., 1987; Petit et al., 1999; Royer et al., 2004). Reconstructing E-O pCO_2, therefore, is a primary goal for constraining the links between climate and radiative forcing of the Earth's surface temperatures through the E-O transition. A variety of proxies are used to estimate pCO_2 during the Early Cenozoic (Boucot and Gray, 2001; Royer et al., 2001). In Figure 1.3 a compilation of various proxy data, published by Zachos et al. (2008) is shown. Estimates of pCO_2 using boron-isotope ratios of planktonic foraminifera (e.g. Pearson and Palmer, 2000; Hönisch and Hemming, 2004; Pagani et al., 2005) and carbon stable isotope composition of marine alkenones (Pagani et al., 2005) indicate a decline. Although there are issues with the timing of the decline in pCO_2, it is very likely that the decrease was a critical factor that allowed expansion of ice sheets on Antarctica. The most recent reconstructions of Cenozoic pCO_2 (Pearson et al., 2009) also depict a decreasing carbon level for the Eocene and Oligocene.

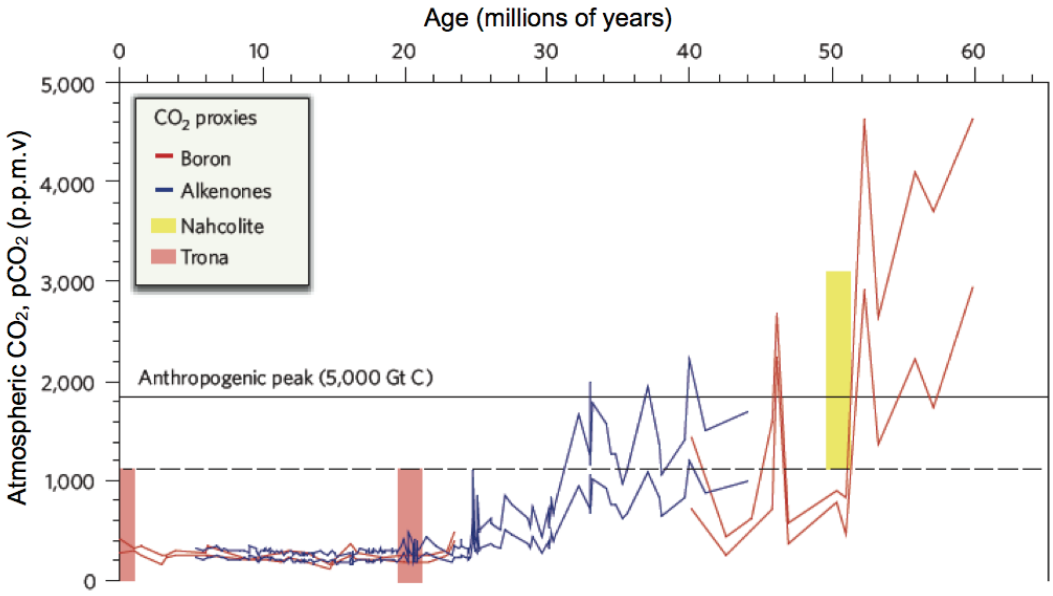

Figure 1.3: Evolution of atmospheric CO_2 levels over the past 65 million years. Data are a compilation of proxy records. The dashed horizontal line represents the maximum pCO_2 for the Neogene (Miocene to present) and the minimum pCO_2 for the Early Eocene (1,125 p.p.m.v.). The vertical distance between the upper and lower coloured lines shows the range of uncertainty for the alkenone and boron proxies. Adapted from Zachos et al., 2008.

Model simulations based on changes in carbon burial on land, due to the evolution of land plants, and weathering changes, caused by organic acids in soils, suggest a general decline in the Early Cenozoic (e.g. Berner, 1990). Despite the fact that there is a good first order agreement between model results and proxy CO_2 estimates on long time scales (Berner, 1990; Berner, 1997; Crowley, 2000; Berner and Kothavala, 2001), the records mostly lack the detail and accuracy to fully resolve the magnitude and timing of decline during the E-O transition and other key climatic events. In addition, general circulation models have been used to show that continuous decrease of pCO_2, amplified by Milankovitch forcing and ice-albedo feedbacks, could cause significant temperature reduction resulting in permanent continental ice sheets in high latitudes (DeConto and Pollard, 2003; Zachos and Kump, 2005). These studies suggest that the ice-sheet formation might have been triggered when atmospheric pCO_2 fell below a critical threshold of 750 ppm. Nevertheless these studies do not include a realistic ocean component, necessary for a proper representation of the global climate.

1.3.3 Favourable orbital configuration

Orbital dynamics that affect the amount and distribution of incoming solar radiation received by the Earth are thought to have been the principal pacemaker of Quaternary climate cycles, forcing the repeated growth and decay of continental glaciers (Imbrie et al., 1984). In the mid-19th century Croll (1867a, 1867b) proposed an astronomical theory linking the Pleistocene (2 million to 10 thousand years ago) ice

ages with periodic changes in the Earth's orbit around the Sun. Croll's ideas were later refined and elaborated by Milankovitch (1941). The original Milankovitch theory identifies three types of orbital variations, which could act as climate forcing mechanisms: obliquity of the Earth's axis, eccentricity of the Earth orbit around the Sun, and precession of the equinoxes.

However, the effects of orbital fluctuations in the Early Cenozoic, when climate boundary conditions differed and global ice volumes were significantly less than in the Quaternary, have been difficult to resolve. Astronomical models have been extended back to the Early Oligocene and beyond (Laskar et al., 2004; Pälike et al., 2004), allowing orbital tuning of Eocene-Oligocene records (Coxall et al., 2005; Gale et al., 2006; Jovane et al., 2006). Spectral analysis of $\delta^{18}O$ from deep-sea sediment cores at the E-O transition underlines the influence of orbital parameters for temperature and ice volume (Coxall et al., 2005). The shift coincides with an orbital configuration comprising a phase of low eccentricity and low-amplitude change in obliquity, favouring cool austral summers and permitting to hinder the melting of summer snow. This probably tipped the balance towards glaciation (Coxall et al., 2005). Therefore the galciation of the Antarctic continent could have occurred at a time when Earth's orbital parameters favoured ice-sheet growth and was probably accelerated by positive feedbacks as a massive high-albedo ice cap was assembled. At this point an "icehouse" climate mode characterized by pronounced orbitally-paced climate cycles was initiated.

Obliquity

Today the Earth is tilted with its rotational axis at an angle of 23.45° relative to a perpendicular to the orbital plane of the Earth. This angle of inclination fluctuates between 22° and 24.5° over a 41000-year time period (Fig. 1.4). Obliquity does not influence the total amount of solar radiation received by the Earth, but it affects its distribution in space and time. As obliquity increases, so does the amount of solar radiation received at high latitudes in summer, while insolation decreases in winter. Changes in obliquity have little effect at low latitudes, since the strength of the effect decreases towards the equator. Consequently, variations in the Earth's axial tilt affect the strength of the latitudinal temperature gradient. Increased tilt has the effect of raising the annual receipt of solar energy at high latitudes, with a consequent reduction in the latitudinal temperature gradient.

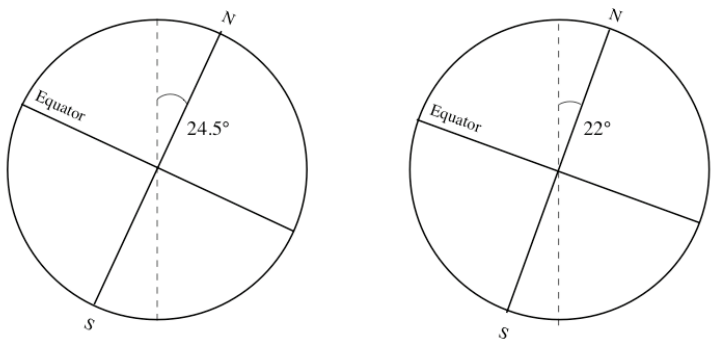

Figure 1.4: Schematic representation of the obliquity of the Earth's axis. Adapted from Roeckner et al. (2003).

Eccentricity

The Earth's orbit around the Sun is not perfectly circular but follows an elliptical path (Fig. 1.5). The second orbital variation therefore involves the strength of the ellipse, or eccentricity. This parameter, e, is determined by:

$$e = \frac{a^2 - b^2}{2a} \tag{1.1}$$

When the orbit is circular, the semi major axis a and semi minor axis b are equal and e=0. The Earth's orbit has been found to vary from being near circular (e=0.005) to elliptical (e=0.05) with two primary periodicities of approximately 96 ky and 413 ky (Berger, 1976). The current value of e is 0.0167 (Meeus, 1998). Variations in eccentricity influence the total amount of solar radiation incident at the top of the Earth's atmosphere. With maximum eccentricity, differences in solar radiation income of about 30% occur between perihelion (closest approach) and aphelion (farthest approach) (Goodess et al., 1992).

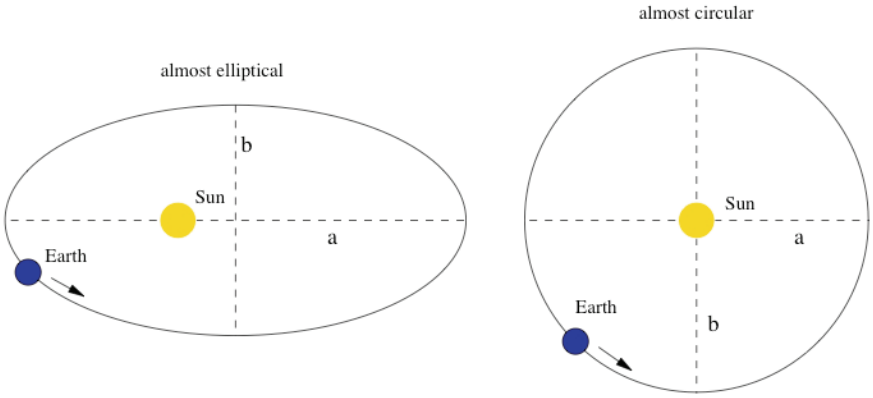

Figure 1.5: Schematic representation of the eccentricity of the Earth's orbit. Adapted from Roeckner et al. (2003).

Precession

The third orbital variation is that of precession (Fig. 1.6). The Sun lies at one of the focal points of the Earth's orbital ellipse. Due to the gravitational interaction of other planetary bodies in the solar system, primarily the Moon and the planet Jupiter, the perihelion, the point at which the Earth passes closest to the Sun, moves in space with a consequent shifting of the elliptical orbit. This phenomenon is known as the precession of the equinoxes, and affects the intensity of the seasons.

Precession has two components: an axial precession, in which the torque of the other planets exerted on the Earth's equatorial bulge causes the rotational axis to rotate like a spinning top, and an elliptical precession, in which the elliptical orbit of the Earth itself rotates about one focus. The net effect describes the precession of the equinoxes

with a period of 22 ky. This term is modulated by eccentricity, which splits the precession into periods, of 19 ky and 23 ky (Crowell and North, 1991).

Like obliquity, precession does not affect the total amount of solar energy received by the Earth, but only its hemispheric distribution over time. If the perihelion occurs in mid-June i.e. when the Northern Hemisphere is tilted toward the Sun, then the receipt of summer solar radiation in the Northern Hemisphere will increase. Conversely, if the perihelion occurs in December, the Northern Hemisphere will receive more solar radiation in winter. The direction of changes in solar radiation receipt at the Earth's surface is opposite in each hemisphere.

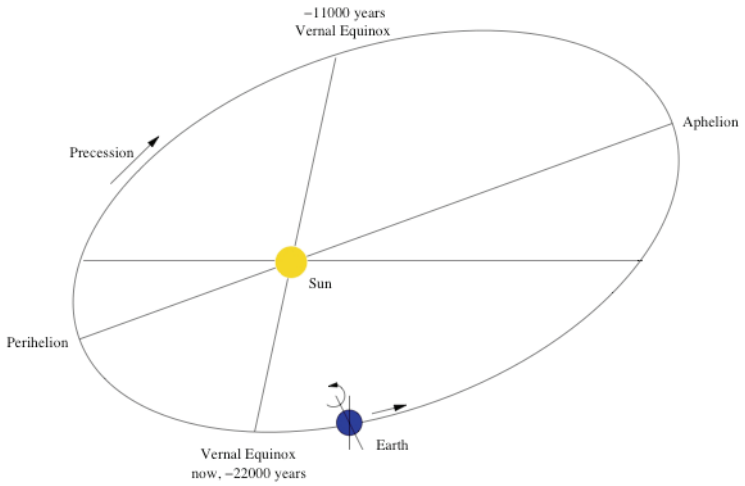

Figure 1.6: Schematic representation of the precession of the Earth's equinoxes. Adapted from Roeckner et al. (2003).

1.4 Scientific questions

One of the most fascinating challenges in the study of Earth history is to understand the fundamental climate change from the past greenhouse world, with no major polar ice caps, to our present icehouse, dominated by the huge ice sheets on Antarctica and on Greenland. This change across a major climate threshold holds evidence that will help us to understand the potential changes our world may undergo in the future. Ice-sheet models are used to predict how the cryosphere responds to climate change. As ice sheets, oceans and the atmosphere interact with each other, it is important that ice-sheet models are coupled with models of atmospheric and ocean circulation in order to predict how the ice–ocean–atmosphere system has behaved in the past and behaves in the future.

The onset of glaciation in Antarctica is not yet well constrained, largely because no sediment core has yet been obtained that unequivocally provide a continuous transition from no-ice to ice-sheet scale glaciation. Factors such as different levels of atmospheric CO_2, tectonic changes and orbital forcing could all have played a part in cooling the polar climate. Previous oceanic, atmospheric and ice-sheet modelling

studies have shown the importance of each of these factors. Nevertheless, as these studies suffered a lack of a complete representation of the climate system, an explicit answer on the sensitivity of the AIS to changes in the various climate sub-systems is still missing.

In particular, finding answers to the following methodological and scientific questions is crucial:

1. *Is it possible to achieve a complete model representation of the Antarctic climate system, including the ocean, the atmosphere and the Antarctic cryosphere?*

   Obviously there are limitations for reaching this goal, the first being the difference in the time scales at which those subsystems evolve. As the climate subsystems interact with each other in a complex manner and on very broad range of timescales, climate modelling reduces to the process of identifying and isolating subsystems and processes that are relevant to the problem at hand. It is, at the moment, impossible to build an exact model of the climate system. As an alternative, the system can be split into discrete macroscopic elements (oceans, atmosphere, cryosphere). The state of and interaction between these discrete elements follow physical laws and can therefore be determined with numerical models asynchronously coupled.

2. *To what amount does the opening of the Drake Passage and the subsequent establishment of the Antarctic Circumpolar Current change the oceanic circulation? How does this affect the glacial evolution of the Antarctic Ice Sheet?*

   The classical theory of the opening of this Southern Ocean gateway as primary reason for the establishment of the Antarctic Circumpolar Current (ACC) and for the Antarctic climatic isolation and resulting formation of the Antarctic Ice Sheet (AIS) is the goal of answering this question. The point is to simulate how the global oceanic and atmospheric systems evolve under different tectonic configurations and how the Antarctic continent evolves under the outcoming climates.

3. *How sensitive was the Late Eocene Antarctica to the atmospheric carbon dioxide concentration?*

   This question tests the hypothesis that a decline in the atmospheric CO_2, together with a favourable orbital configuration, was the primary driver of the decrease in surface atmospheric temperature and, therefore, favour of the expansion of the AIS. It can only be addressed by representing the possible Late Eocene global climatic conditions under different atmospheric pCO_2 and investigating the genesis of the AIS under these different scenarios.

4. *How much can a favourable orbital configuration promote the initial AIS growth?*

   Independently of the global tectonic configuration or of the atmospheric greenhouse gases concentration, the origin of the AIS could have been facilitated

by a specific orbital configuration yielding the coldest austral summer. Addressing the sensitivity of the Antarctic continent to different orbital geometries under distinct continental distribution means to help in clarifying the role of the insolation forcing in the early stage of AIS development.

1.5 Thesis outline

This thesis is organized in seven chapters, additional to this introduction, which are shortly described in the following.

Chapter 2: Numerical models and methodology.

One aim of this study is to achieve the most complete description of the Antarctic and the global climate system and of the interactions of the Antarctic cryosphere with the global oceanic and atmospheric circulations. In order to achieve such goal with a modelling approach, the models adopted must be able to describe reliably the modern AIS and the global circulation of oceans and atmosphere. The numerical model chosen for this study are Huybrechts (1993) ice sheet model (ISM) for the Antarctic cryosphere, and the Earth system model COSMOS, a fully coupled Atmosphere and Ocean General Circulation Model (AOGCM). The latter is in turn composed of the atmospheric general circulation model (AGCM) ECHAM5 and the ocean general circulation model (OGCM) MPI-OM, coupled through the ocean-atmosphere-sea ice-soil coupler (OASIS3). The ocean model MPI-OM is initialized by runs of the Large Scale Geostrophic model (LSG). This chapter shortly describes numerical modelling concepts. It then explains briefly the four models used in this study and it delineates the methodology employed in the experiments as well as the coupling procedure used to combine the three mathematical models.

Chapter 3: Model validation and response to climate forcings

This chapter addresses the first, methodological, question. It illustrates an explicit representation of the present-day AIS using a global description of climate. It also compares the modelled results with the available observational data. Furthermore it assesses the robustness of the method by analysing the climate and AIS response to a doubling of the global atmospheric pCO_2 level. The conditions of the Antarctic climate system are reproduced coupling iteratively the ISM and the climate model COSMOS, simulating the global ocean and atmosphere. At the steady state the atmospheric carbon dioxide concentration is doubled and the climate and AIS response analysed. The AIS modelled with this methodology is comparable with observations, although there are still some differences in the representation of the West Antarctic Ice Sheet (WAIS) and of the Antarctic Peninsula (AP). Moreover this method allows the ice sheet to be able to respond to changes in the atmospheric CO_2 and therefore in global climate boundary conditions. The incorporation of the AIS in the climate model via the iterative procedure constitutes an important advancement in the representation of the

Antarctic surface topography in general circulation models (GCMs) such as COSMOS. This empowers the study of the feedback of the AIS to changes in the climate state. Hence the new ice sheet-climate modelling approach is an efficient tool for reconstructing the modern Antarctic climate and can be also used for investigating past time slices.

Chapter 4: Sensitivity of Antarctica to the opening of the Drake Passage.

This chapter addresses the second research question. The goal is to examine the importance of the opening of an oceanic gateway such as the Drake Passage for the development of the Antarctic Circumpolar Current (ACC) and for the consequent development of the AIS. We evaluate if this possibility could have served as major cause to generate extensive ice sheets on the Antarctic continent. Two different climate states are reproduced with tectonic configurations similar to the Late Eocene and to the Late Oligocene (i.e. with closed and open Drake Passage) in order to test the sensitivity of Antarctica to different land-sea distributions and oceanic regimes.

Chapter 5: Sensitivity of the Late Eocene Antarctica to atmospheric pCO_2

This chapter addresses the third research question. The aim is to investigate the influence of different concentrations of carbon dioxide in the atmosphere for the onset of the AIS. The dynamics of the climate system under different carbon dioxide levels are analysed and the response of the Antarctic cryosphere is investigated. Four different climate states are reproduced with Late Eocene tectonic configuration in order to perform a set of sensitivity experiments with the different pCO_2 with respect to pre-indstrial levels $8\times CO_2$ (2240 ppm), $4\times CO_2$ (1120 ppm), $2\times CO_2$ (560 ppm) and $1\times CO_2$ (280 ppm). It is found that the surface atmospheric temperatures over the Antarctic continent are lower for lower carbon dioxide level. Consequently more ice is connected with lower pCO_2.

Chapter 6: Sensitivity of the AIS to orbital configuration

This chapter addresses the fourth research question and considers the significance that a particular astronomical configuration could have had on the origin of an early AIS. It is assessed if a favourable set of orbital parameters (obliquity, eccentricity and precession), permitting a cold austral summer, serves as pre-condition for the establishment of the AIS. Four different experiments are conducted with the land-sea distributions used in the previous chapters, similar to the Late Eocene and Late Oligocene, and applying two distinct orbital setups, the modern and an advantageous one yielding the coldest Antarctic summer. The effect of a favourable orbital position is to help the growth of the AIS in the first phase of the glaciation under both topographic conditions. The effectiveness of the "cold" orbit is more marked in case of Late Eocene continental distribution.

Chapter 7: Discussion

This chapter discusses all the experiments performed and the results achieved in this study. It reconsiders and answers the scientific questions posed at the

beginning of the thesis in view of the findings. Moreover, it compares the results achieved with previous similar studies. As any modelling study, this has limitations, mostly concerning the paucity of information needed to model paleo-climates and the technical restrictions. Nevertheless it has been possible to design specific experiments and to analyse the single-acting mechanisms investigating their relative importance.

Chapter 8: Conclusions and outlook

This chapter draws the general conclusions of the work. It also illustrates the improvements, which could be done to the method and the next research questions, which could be addressed. A complete modelling approach allowing for a detailed representation of the AIS and its sensitivity to (paleo)climate forcings has been reached. The experimental results support the idea that the decrease in atmospheric pCO_2 and the opening of the Drake Passage could have had comparable significance in creating the conditions for a wide continental glaciation, whereas an advantageous orbital configuration, although it has certainly promoted the AIS growth, seems to have not been essential.
This study shows that this modelling procedure can simulate present and past AIS in the global climate. Still some features in the modelling strategy could be improved and other scientific issues could be investigated, involving the Antarctic and global climate evolution throughout the Cenozoic.

Chapter 2
Numerical models and methodology

One of the objectives of this study is to simulate the Antarctic and global climate system as realistic as possible. A comprehensive representation of the Antarctic Ice Sheet (AIS) and its response to climate forcings allows examining the processes, which drive the Antarctic climate evolution. The models chosen for this study are Huybrechts (1993) ice sheet model (ISM) and the Earth system model COSMOS, a fully coupled Atmosphere and Ocean General Circulation Model (AOGCM) composed by the atmospheric general circulation model (AGCM) ECHAM5 and the ocean general circulation model (OGCM) MPI-OM. ECHAM5 and MPI-OM are coupled through the ocean-atmosphere-sea ice-soil coupler (OASIS3). MPI-OM is initialized by spin-up runs of the Large Scale Geostrophic ocean model (LSG). The first paragraph of this chapter illustrates briefly the ice-sheet modelling concepts. Then the general features of the models used in this study are described as well as the coupling procedure between them.

2.1 Numerical modelling of the Antarctic Ice Sheet

Studies on Antarctic climate evolution have benefited increasingly over the last years from numerical ice-sheet modelling. Such activities have led to the testing of geological hypotheses concerning past ice-sheet changes and a better understanding of macro-scale glaciological processes through space and time. Ice-sheet modelling allows quantitative predictions of how large ice masses behave and respond to environmental change. Hence, the use of ice-sheet modelling to test geologically based hypotheses has increased in recent years. However, ice-sheet models have limitations concerning the necessary simplification of ice flow processes, and incomplete model input data, such as bedrock topography and climate forcing (Siegert, 2009).

Studies of ice rheology (the flow and deformation of ice) have distinguished three main mechanisms by which ice masses move. These processes are internal deformation of the ice, basal sliding and the deformation of underlying water-saturated weak sediments. (Fig. 2.1). The flow by internal ice deformation takes place in all ice masses whereas basal motion occurs only at the interface between ice and bedrock where compression leads to partial melting of the ice. At the centre of an ice sheet, the flow speed is relatively low (of the order of metres per year) and is controlled by internal deformation. A particle of ice on the ice-sheet surface will be buried by subsequent snowfall and thus will have a relatively significant vertical velocity component downwards into the ice. The flow of ice radiates outward from the ice divide, where there is no lateral flow. Ice-sheet interiors are characterized by divides that define the margins of ice drainage basins. Ice sheets are drained by ice streams, transporting ice from the interior to the ice margin (Bennett, 2003). Ice streams flow quickly because water at their bases causes a reduction of friction allowing them to effectively slide over the subglacial bedrock.

When a large amount of ice accumulates on the Earth's crust, the weight acts to displace the crust towards the viscous asthenosphere, beneath the solid lithosphere, which adjusts to isostatic equilibrium on time scales of a few thousand years, depending on the mantle viscosity. The process involves flow in the asthenosphere and elastic deflection of the lithosphere. When the ice load is removed, as in the case of deglaciation, the asthenosphere and lithosphere relax back to their original state. This process is called isostatic uplift or recovery.

The concept behind numerical ice-sheet modelling is that an ice sheet can be divided into ice columns, each of which representing a cell in the model's two-dimensional horizontal grid. Ice-sheet models are normally organized in a loop beginning by applying algorithms, determining the flow of ice, the mass balance and interaction with the subglacial surface in each cell. The loop is completed by a continuity equation on the full grid to calculate the interaction and flow of ice between cells. Each iteration of the loop moves forward the model through one time step. The accuracy of the model depends on the width of the grid cells and on the time step length. In some models, the depth-averaged ice velocity is calculated by the sum of depth-averaged internal ice deformation and basal motion. These models use the so-called "shallow-ice approximation" and assume that a single horizontal vector can describe the ice flow (Siegert, 2009 and references therein).

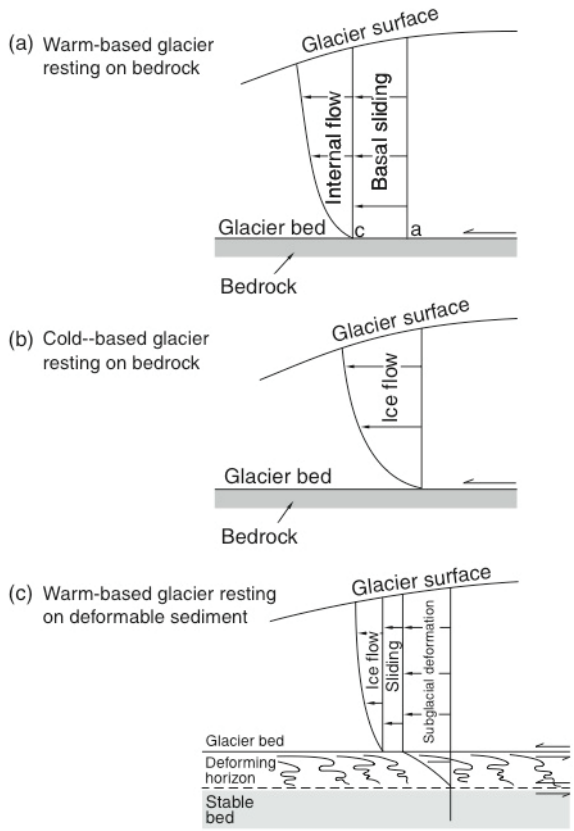

Figure 2.1: Processes controlling the flow of large ice sheets. Ice flows through internal deformation in all situations. If the ice rests on bedrock and is warm based (a) then basal sliding can occur. If the base is frozen (b) then only ice deformation will take place. If the base is warm and loose unconsolidated sediments are present (c) then their own deformation can add to ice deformation and basal sliding as a contribution to ice flow. Each of these processes can be accounted for in ice-sheet models. Adapted from Siegert (2001).

Ice-sheet models can be used to test geological hypotheses regarding past changes in Antarctica. Whereas the boundary conditions of the present ice sheet can be established reasonably well, past conditions are difficult to quantify. Huybrechts (1993) provided the first detailed modelling investigation into Pliocene AIS. He addressed the problem of whether the EAIS was stable at this time, or susceptible to significant changes. By running an ice-sheet model with shallow-ice approximation under a selection of climate forcing parameters, Huybrechts showed that the EAIS could resist to a mean annual temperature rise of around 10 K and that several degrees in excess of this amount of warming was required to significantly alter the ice-sheet configuration (Fig. 2.2). Air temperatures needed to rise by around 15 K with respect of modern values in order to reduce the ice sheet to a series of small isolated ice caps. As such warming is unlikely for the Pliocene, Huybrechts concluded that the idea of widespread retreat of ice at this time is not supported by ice-sheet modelling.

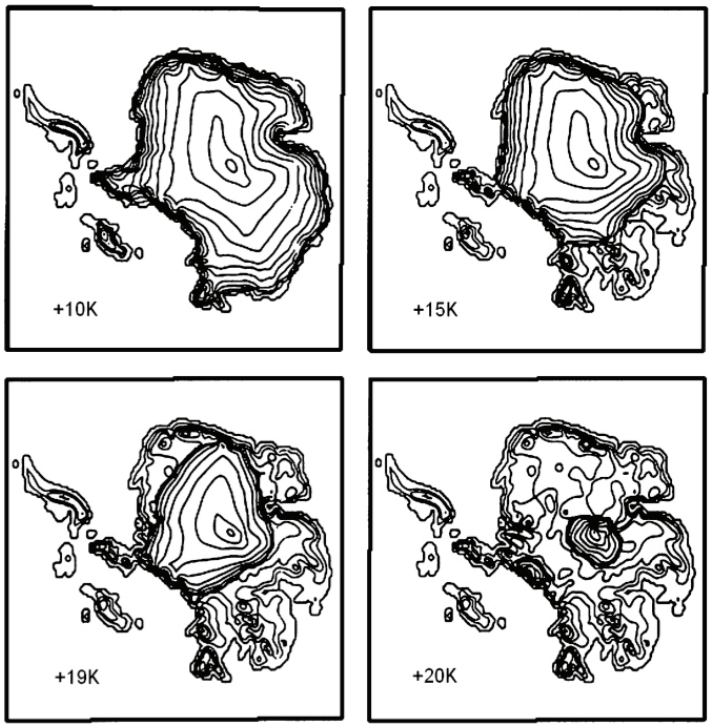

Figure 2.2: Numerical modelling results of the AIS under a variety of climate warming scenarios (Huybrechts, 1993).

There have been several models of recent (last glacial cycle) ice-sheet behaviour (e.g. Ritz et al., 2001; Huybrechts, 2002), which demonstrated the differences between East and West Antarctica and showed that these differences are controlled to a large amount by the topography. The Western AIS is a marine-based ice sheet, with a bed resting below sea level in most places. This is in contrast to the terrestrial Eastern AIS, where the bed elevation is generally above sea level. Marine ice sheets are known to be more vulnerable to environmental changes than terrestrial ice sheets. This is due to many factors such as grounding line retreats caused by the disintegration of ice shelves, nature and stability of ice streams and deepening of the bedrock inland of ice-sheet margins leading to a positive feedback of ice retreat. This retreat may be further amplified when sea level rises.

2.2 The ice sheet model

The ice sheet model employed in this study is the one developed by Huybrechts (1993). The AIS is represented as an interactive component within the global climate system. In polar ice sheets ice flow and its thermodynamics are strongly linked because temperature determines the viscosity of ice. Changes in ice thickness arise from the combined effect of fluctuations in the mass balance, due to surface accumulation or basal melting, and variations in the divergence of the ice-mass flux.

The model is able to respond realistically to fluctuations in environmental conditions. It is time-dependent and computes the full set of coupled thermo-mechanical equations for ice flow in three dimensions as well as the geographical distribution of ice mass. The model also includes basal sliding, which is restricted to regions that are at the pressure melting point. It considers the response of the underlying bedrock to changing ice load, taking into account both the rigidity of the lithosphere and the viscosity of the asthenosphere, and including a temperature calculation. The finite difference scheme used to solve the equations is based upon the Alternating-Direction-Implicit method and the vertical coordinate is scaled to local ice thickness. The horizontal grid point distance is 40 km and there are 11 layers in the vertical, which have closer spacing towards the bedrock surface, where the shear concentrates.

The basic equations solved by the model are the conservation equations for ice mass and heat, supplemented with stress-equilibrium equations and constitutive relation for the ice, relating the strain rate components to some form of the stress components. The conservation equations are expressed by:

$$\frac{\partial H}{\partial t} = -\nabla \cdot (\vec{\bar{v}} H) + M \tag{2.1}$$

$$\frac{\partial T}{\partial t} = \frac{k}{\rho c_p} \nabla^2 T - \vec{V} \cdot \nabla T + \frac{\Phi}{\rho c_p} \tag{2.2}$$

where H is the ice thickness (in m) and T the temperature (in °C), t the time (in years), $\vec{\bar{v}}$ is the depth-averaged horizontal velocity vector (in m/s), M the mass balance, ρ is the ice density (910 kg/m^3), $\vec{V}$ is the three-dimensional ice velocity, Φ is the layer heating and k and c_p are the temperature-dependent thermal conductivity and heat capacity, respectively. The thermodynamic equation accounts for vertical heat conduction, three-dimensional advection and heat generation by internal deformation. Boundary conditions are the mean annual air temperature at the upper surface and a temperature gradient at the lower surface incorporating the effects of geothermal heating and heat dissipation by sliding. A geothermal heat flux of 54.6 mWm^{-2} is taken, an average value for the entire Antarctic continent (Huybrechts, 1993; Van der Wateren and Cloetingh, 1999). Only grounded ice flow is taken into account.

Ice deformation is assumed to result from shearing in horizontal planes and longitudinal deviatoric stresses are disregarded. Expressions for the horizontal velocity components are derived by substituting equations for the shear stress distribution τ(z) in the flow law, which is assumed to be of Glen's type with exponent n=3. The equations for the shear stress distribution and for the horizontal velocity components are:

$$\vec{\tau}(z) = -\rho g (H + h - z) \nabla (H + h) \tag{2.3}$$

$$\vec{v}(z) - \vec{v}(h) = -2(\rho g)^3 \left[\nabla (H + h) \cdot \nabla (H + h)\right] \nabla (H + h) \int_h^z A(T^*)(H + h - z)^3 \, dz \tag{2.4}$$

where $\vec{v}(h)$ is the basal boundary condition on velocity, h its bed elevation, z is the vertical, g is the gravity and $A(T^*)$ expresses the temperature dependence of the flow-law parameter, which is given by an Arrhenius equation of the following type.

$$A(T^*) = m \cdot ae^{-\frac{Q}{RT^*}} \tag{2.5}$$

where R is the gas constant (8.314 Jmol-1K-1), Q the activation energy for creep and T* is the absolute temperature corrected for the dependence of the melting point on pressure: $T^* = T + 8.7 \cdot 10^{-4} (H + h - z)$, with T measured in K. m is an enhancement factor and the following values for a and Q are used: $a=1.14 \cdot 10^{-5}$ $Pa^{-3}y^{-1}$ and Q=60 $kJmol^{-1}$ if T*<263.15 K and $a=5.47 \cdot 10^{10}$ $Pa^{-3}y^{-1}$ and Q=139 $kJmol^{-1}$ if T* ≥263.15 K.

Basal sliding takes place when the basal temperature is within 1 K of the pressure melting point:

$$\vec{v}(h) = -A_S(\rho g)^3 H^2 \left[\nabla(H+h) \cdot \nabla(H+h)\right] \nabla(H+h) \tag{2.6}$$

where $A_S = 1.8 \cdot 10^{-11}$ $N^{-3}y^{-1}m^7$. The mean horizontal ice mass flux is calculated as:

$$\vec{v}(h) = \int_h^{H+h} \vec{v}(z)dz \tag{2.7}$$

while the vertical motion, as a result of accumulation and vertical strain, is computed from the incompressibility condition:

$$w(z) - w(h) = -\int_h^z \nabla \cdot \vec{v}(z)dz \tag{2.8}$$

In order to calculate bedrock adjustments, the steady state deflection is given by local isostatic equilibrium, whereas the time-dependent response is modelled as a damped return with a characteristic time scale Θ of 3000 years.

$$\frac{\partial h}{\partial t} = -\frac{1}{\Theta}\left(h - h_0 + d\right) \tag{2.9}$$

with:

$$d = \frac{\rho}{\rho_m} H \tag{2.10}$$

where ρ_m is the mantle density (3300 kg/m^3), d is the lithospheric deflection and h_0 is the undisturbed bed elevation when the ice sheet is removed and the isostatic rebound is complete.

The present grounding line position is taken as constrain, beyond which all ice is lost in the ocean. The expansion of grounded ice over terrain below sea level is still possible, but is entirely controlled by the surface mass balance and the ability of the ice sheet to extend down to the sea level. All ice is treated as grounded ice irrespective of the bedrock elevation, with the limitation that it cannot expand beyond its present limits.

This approach is not considered a problem here, because the ice sheet is restricted to the East Antarctic continent in a warmer climate and does no longer interact with the ocean directly.

The primary inputs to the model are bedrock elevation and surface mass balance at any time and place in the model domain. These determine entirely the ice sheet geometry. The dataset for the ice-free bedrock topography is given by the BEDMAP project (Lythe et al., 2001). The mass balance components of accumulation rate and runoff are calculated separately and parameterised in terms of temperature, which is the ultimate forcing variable. The parameterizations used in the stand-alone model are based on the assumption that temperature remains the main controlling factor for precipitation over the Antarctic continent and follow analyses by Giovinetto et al. (1990) and Fortuin and Oerlemans (1990):

$$TMA = 34.46 - 0.00914\ H_{sur} - 0.68775\ Lat \quad (2.11)$$
$$TMS = 16.81 - 0.00692\ H_{sur} - 0.27937\ Lat \quad (2.12)$$
$$ACC = 0.78 + 2.525 \cdot 10^{-2}\ TMA + 2.225 \cdot 10^{-4}\ TMA^2 \quad (2.13)$$

where TMA (°C) is the mean annual surface air temperature and ACC is the parametrized accumulation rate, H_{sur} is the surface elevation (m) above sea level, Lat is the latitude (°S) and T_{for} is the applied temperature change with respect to present conditions. TMS is the summer temperature needed to construct the yearly temperature march in the ablation model, which is based on the degree-day method. The model estimates the number of positive degree-days (PDDs, Ambach, 1988) accounting for the daily cycle and for random temperature variations from the regular long-term annual cycle by using a statistic, normally distributed and centred on the curve of the mean daily temperature TD:

$$PDD = \frac{1}{\sigma\sqrt{2\pi}} \int_0^A \left(\int_0^{TD+2.5\sigma} Te^{\left(\frac{-(T-TD)^2}{2\sigma}\right)} dT \right) dt \quad (2.14)$$

where σ is 5 K, TD is defined as a cosine with mean of TMA and amplitude of (TMA-TMS) and A is one year. The calculated annual number of PDDs represents a melt potential, which is used to melt snow and ice with degree-day factors of 0.003 my^{-1}/PDD and 0.008 my^{-1}/PDD respectively.

In this study, the forcing fields (temperature and accumulation) are not parameterized, but rather provided by runs of the climate model COSMOS, described below.

2.3 The Earth System Model COSMOS

The climate model employed in this study is the first version of the one developed within the COSMOS (COmmunity Earth System MOdelS) network. COSMOSv1 is an

Earth System Model (ESM) constituted by various model components, which can be coupled in order to give different configurations. The configuration used in this study includes the atmospheric general circulation model (AGCM) ECHAM5.4 and the ocean general circulation model (OGCM) MPI-OM.

Atmosphere and ocean are coupled by means of the Ocean–Atmosphere–Sea Ice–Soil (OASIS) coupler (Valcke et al. 2003). The ocean passes the SST, sea ice concentration, sea ice thickness, snow depth, and the ocean surface velocities to the atmosphere. River run off and glacier calving are treated interactively in the atmosphere model and the respective fresh water fluxes are passed to the ocean as part of the atmospheric freshwater flux field. The land hydrology model includes a river routing scheme (Hagemann and Dümenil, 1998; Hagemann and Dümenil-Gates, 2001).

2.3.1 The atmospheric general circulation model ECHAM5

ECHAM5.4 is the fourth version of the fifth-generation AGCM developed at the Max Planck Institute for Meteorology in Hamburg, Germany (MPI-M). It is the most recent version in a series of ECHAM models evolving originally from the spectral weather prediction model of the European Centre for Medium Range Weather Forecasts in Reading, UK (ECMWF). A detailed description of the model dynamics and of the physical parameterization can be found in the technical report by Roeckner et al. (2003). A summary of its main components can be found in Appendix A1.

ECHAM5.4 employs a spectral dynamical core: vorticity, divergence, temperature and the logarithm of surface pressure are represented in the horizontal by a truncated series of spherical harmonics. The general form of the corresponding equations follows that of the early multi-level spectral models (e.g., Hoskins and Simmons, 1975). In this study the triangular truncation is applied at wave number T31, which corresponds to a Gaussian grid with a grid point spacing of approximately 3.75°. The model utilizes a semi-implicit leapfrog time differencing scheme. The vertical direction uses a hybrid coordinate system from sigma (surface, lowest model level) to pressure (uppermost level) with 10 hPa at uppermost level. A second-order energy and angular momentum conserving scheme is used for finite differencing in the vertical (Simmons and Burridge, 1981).

Transport of water vapour, cloud liquid water, and cloud ice is computed on a Gaussian grid, using a flux-form semi-Lagrangian scheme (Lin and Rood, 1996). All physical parameterization schemes are computed in grid point space. The physical parameterizations are radiation (shortwave/longwave), cloud schemes (stratiform/cumulus convection), surface fluxes, land surface processes and vertical diffusion.

To allow proper representation of orbital variations for climate simulations in ECHAM, two orbital schemes are given. The first one is based on precise orbit determination principles to reflect short term variations for today's climate. It uses the VSOP (Variations Seculaires des Orbites Planetaires) analytical solution by Bretagnon and Francou (1988). The second orbit given is using the basic Kepler laws only,

allowing for simple adjustment for paleoclimate studies using the long term series expansions for obliquity, eccentricity, and precession by Laskar and Boudin (1993).

2.3.2 The ocean general circulation model MPI-OM

The Hamburg Ocean Model (MPI-OM) is an ocean general circulation model (OGCM) based on the primitive equations for a hydrostatic Boussinesq fluid with a free surface and it includes the representation of thermodynamic processes. It is capable of simulating the oceanic circulation from small scales (oceanic eddies) to gyre scales, in response to atmospheric forcing fields. A detailed explanation of the numerical background can be found in Marsland et al. (2003). A summary is given in Appendix A2.

The vertical discretization is on a so-called "z-coordinate" system. Variables defined on vector points are horizontal velocities, wind stress and coefficients of vertical viscosity. Variables defined on scalar points are potential temperature, salinity, density, pressure, vertical velocity, coefficients of vertical diffusivity, sea surface elevation and heat and freshwater fluxes across the air-sea interface. The vertical discretization includes partial vertical grid cells, i.e. at each point in the horizontal grid the deepest wet cell has a uniform thickness that is adjusted to resolve the discretised bathymetry. The surface layer thickness is also adjusted to account for the sea surface elevation and the sea ice/snow draft. MPI-OM has 40 vertical levels with level thickness increasing with depth.

The horizontal discretization of the MPI-OM model is on a staggered Arakawa C-grid (Arakawa and Lamb, 1977). The model uses a curvilinear coordinate system with variable resolution. In this setup, the North Pole has been placed over Greenland by conformal mapping. While the formal resolution is 3°×1.8° in the global average, the regional resolution varies between about 170 km in the Tropics and 30 km in high latitudes. This arrangement gives high resolution in the main regions associated with deep-water formation. The vertical resolution is 40 levels on z-coordinates. Level thicknesses increase with depth, but bathymetry is captured by partial grid cells.

MPI-OM includes a dynamic-thermodynamic sea ice model based on work by Hibler (1979) and Semtner (1976), consisting of dynamics of sea ice advection, zero-dimensional thermodynamics of sea ice growth and the thermohaline coupling to the ocean model (brine rejection).

2.4 The Large Scale Geostrophic model (LSG)

In all the experiments the ocean model MPI-OM is initialized with three-dimensional thermohaline fields given by integrations of an improved version of the Large Scale Geostrophic (LSG) OGCM (originally developed by Maier-Reimer et al., 1993). The major changes to the original version are explained in Prange et al. (2003) and Butzin et al. (2005).

The model has an effective horizontal resolution of 3.5° on a semi-staggered Arakawa E-grid. Vertical resolution is 22 levels on z-coordinates involving partial grid cells. The original LSG upstream advection scheme for temperature and salinity has been replaced by a less diffusive third-order QUICK scheme (Schäfer-Neth and Paul, 2001). A surface heat flux parametrization with diffusive lateral heat transports based on atmospheric energy balance model considerations permits that sea surface temperature can freely evolve (Prange et al., 2003). The hydrologic cycle is closed by a runoff scheme, which enables that sea surface salinities can freely adjust to changes in the continental configuration.

In addition to a control run with modern bathymetry (PD), two paleo-runs with ocean gateway changes mimicking the Late Eocene (called EOC and including closed Drake Passage, narrowed South African and Tasman Passages, open Central American Seaway and Eastern Tethys) and Late Oligocene (called LOL and including modern Southern Ocean seaways, open Central American Seaway and Eastern Tethys) have been considered (Butzin, pers. comm.; see land-sea distributions in Fig. 4.1). All the experiments use present-day atmospheric forcings to create a background climate (Lohmann and Lorenz, 2000) and adjustment through an energy balance model. This is a reasonable procedure to produce an adequate initialization of the global ocean for the different time slices of interest. It furthermore allows for shorter integration time of the fully coupled COSMOS model and therefore increases the number of possible experiments.

2.5 The coupling procedure

The climates of the different time periods studied are simulated by the fully coupled AOGCM COSMOS. The two components, the AGCM ECHAM5 and the OGCM MPI-OM, interact with each other exchanging the heat and momentum fluxes through the coupler OASIS3 every day of integration. The different model set-ups, corresponding to the different time periods analysed, are consistent for the ocean and the atmosphere. The set-ups of the paleo-experiments are generated from the modern ones adapting them to the distinct land-sea masks.

The horizontal grid resolution of the atmospheric model is T31, corresponding to approximately 3.75° and having 96 by 48 horizontal grids cells, while it has 19 vertical levels reaching the highest of 10 hPa. The ocean is resolved on a 3°×1.8° horizontal grid and on 40 vertical levels.

Figure 2.3 shows the scheme of the modelling procedure employed in the experiments.

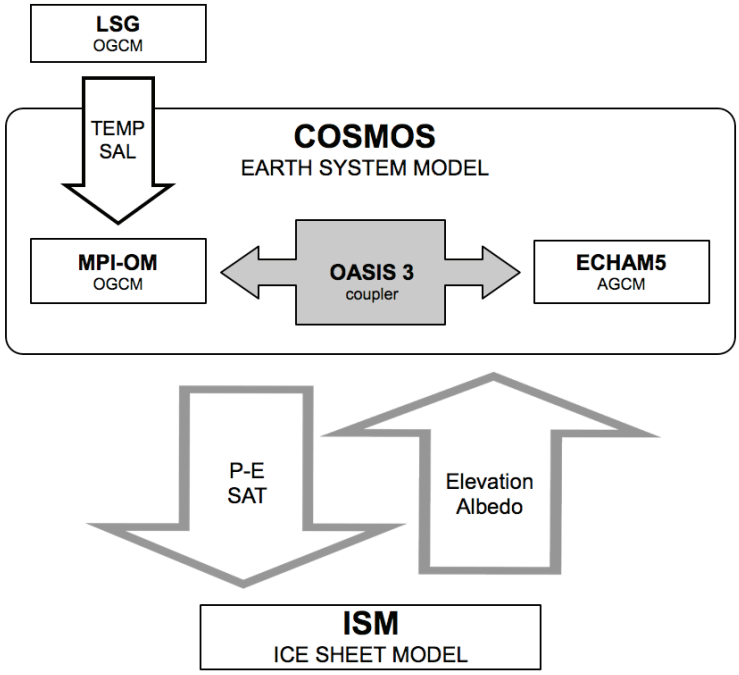

Figure 2.3: Scheme of the modelling procedure employed in the experiments. COSMOS is composed by an OGCM (MPI-OM) and an AGCM (ECHAM5) coupled by OASIS3. It exchanges the net precipitation (P-E), the surface atmospheric temperature (SAT), the Antarctic surface elevation and albedo with the ISM in an iteratively procedure. MPI-OM is initialized by fields (three-dimensional temperature and salinity) from the OGCM LSG.

The initial conditions required by the atmospheric model are the specific humidity and the whole set of surface boundary conditions, such as the land-sea, glacier and lake masks, the surface background albedo, the surface roughness length, the soil data, the vegetation type, the snow depth, the soil wetness, the field capacity of soil, the surface geopotential, the mean orography, the orographic anisotropy, slope and angle, the orographic elevation of peaks and valleys and the orographic standard deviation. Additionally the model needs the monthly climatology of ozone, leaf area index, land surface temperature and of the three dimensional vegetation. Finally the inputs for the radiation scheme and the hydrological model discharge are also required.

The initial and boundary conditions setting up the ocean component are the ocean grid and bathymetry, the geographical positions of the centres and of the edges of the grid cells, the mask of the ocean basins and the initial and surface salinity and temperature.

As mentioned in the previous section, in order to accelerate the computing time needed in the paleo-experiments, the ocean model MPI-OM in COSMOS is initialized with annual mean thermohaline fields obtained by integration of an improved version of the LSG model. LSG is driven by ten-year averaged monthly fields of wind stress, surface air temperature and freshwater flux taken from simulations with the atmosphere general circulation model ECHAM3/T42, which by itself is forced with prescribed values of insolation, CO_2, ice-sheet cover and sea surface temperatures for the present day (Lohmann and Lorenz, 2000). The resulting background climate is considered as

zeroth-order approximation of the EOC and LOL paleoclimates. LSG is integrated over 10 ky to quasi steady-state conditions. The resulting thermohaline fields are used to initialize MPI-OM. During the coupled runs subsurface and deepwater (L4-L40) temperatures and salinities in MPI-OM are restored to their initial values with a relaxation time constant of $f=8\cdot10^{-4}$, corresponding to damping time scale of 120 days. As a consequence, the surface layer can freely adjust to atmospheric changes while the deep ocean stays close to the equilibrium.

In Figures 2.4 and 2.5 the sea surface temperature (SST) and sea surface salinity (SSS) adjustment of the MPI-OM output to the LSG input for the tectonic set-ups used in the experiments (PD, EOC and LOL) are displayed. The anomalies indicate that the surface of the ocean modelled with MPI-OM during 20 years of COSMOS run can adapt to the atmospheric circulation. Sensitivity experiments to different relaxation constants ($8\cdot10^{-4}$ and $5\cdot10^{-1}$) and for different model levels (L4-40, L15-40) have been performed for the three set-ups. It has been found that the combination with three-dimensional restoring between the levels 4 and 40 and using the restoring constant $f=8\cdot10^{-4}$ gives the best results, i.e. smaller SST and SSS anomalies (see also Fig. A1 and Fig. A2 in Appendix A3).

The SST adjustment over 20 years for the PD configuration (Fig. 2.4a) shows a wave-like anomaly pattern in the Northern Hemisphere connected to the atmospheric circulation. In the Southern Hemisphere the adjustment process is visible in the Southern Ocean. The anomalies are in the range of ±1 K and are related to the eddy activity, which is not represented in the ocean model. In the case of EOC configuration (Fig. 2.4b) the ocean adapts to the atmosphere towards a state with colder Arctic and Pacific oceans. In the Arctic region this is related to the sea-ice production, modelled in the MPI-OM but not in the LSG model. Coastal warmer areas are associated with atmospheric advection from the continents and changes in the winds, not included in the LSG. Finally, weaker SST anomalies are visible for the LOL configuration, where the anomaly pattern is more similar to the PD one.

The SSS adjustments over 20 years for all the configurations, shown in Fig. 2.5 are related to the temperature anomalies. In the PD case (Fig. 2.4a) enhanced upwelling near the coasts of Africa and South America are detected, where cold and salty water from the deep ocean is brought to the surface. In both the EOC and LOL configurations (Fig. 2.5b and 2.5c, respectively) salinity anomalies in the Arctic Ocean are related to the sea-ice formation, simulated in the MPI-OM but not in LSG model.

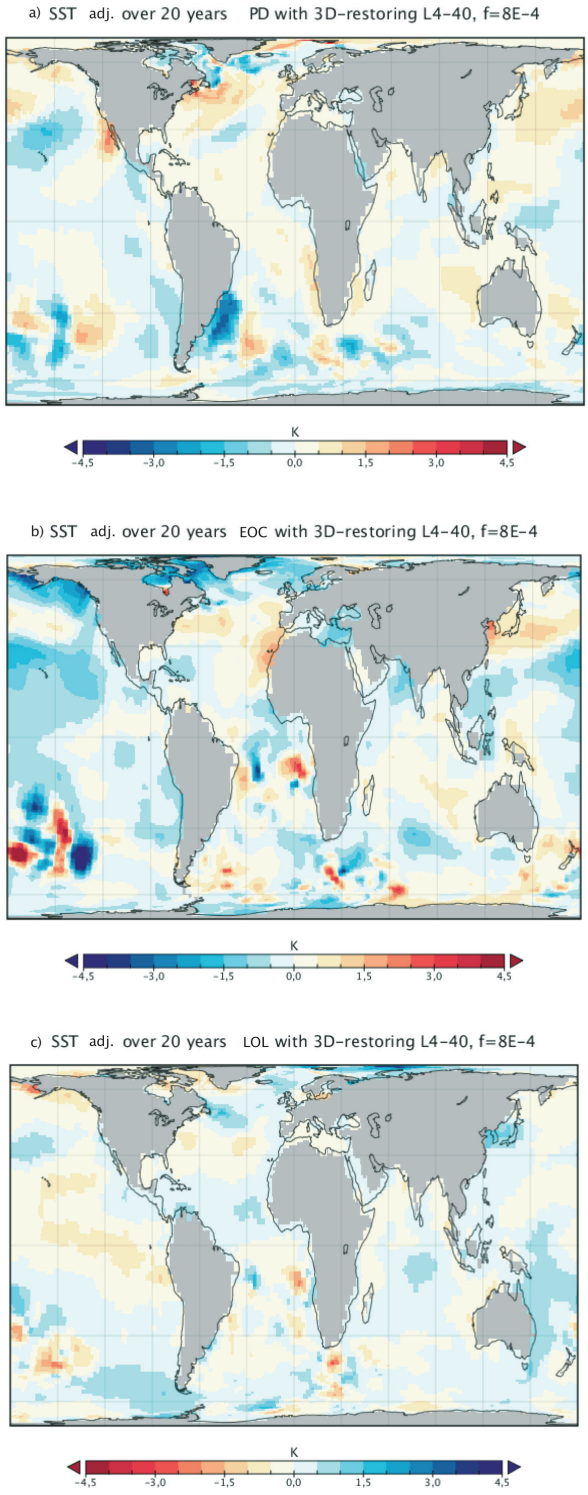

Figure 2.4: Annual mean sea surface temperature (SST) adjustments of the MPI-OM ocean model to the LSG input for the different tectonic configurations present-day (PD, a), Late Eocene (EOC, b) and Late Oligocene (LOL, c, inverted colour scale) using a 3-dimensional restoring between the model levels (L) 4 and 40 and a relaxation constant (f) of $8 \cdot 10^{-4}$. Modified after Butzin (pers. comm.).

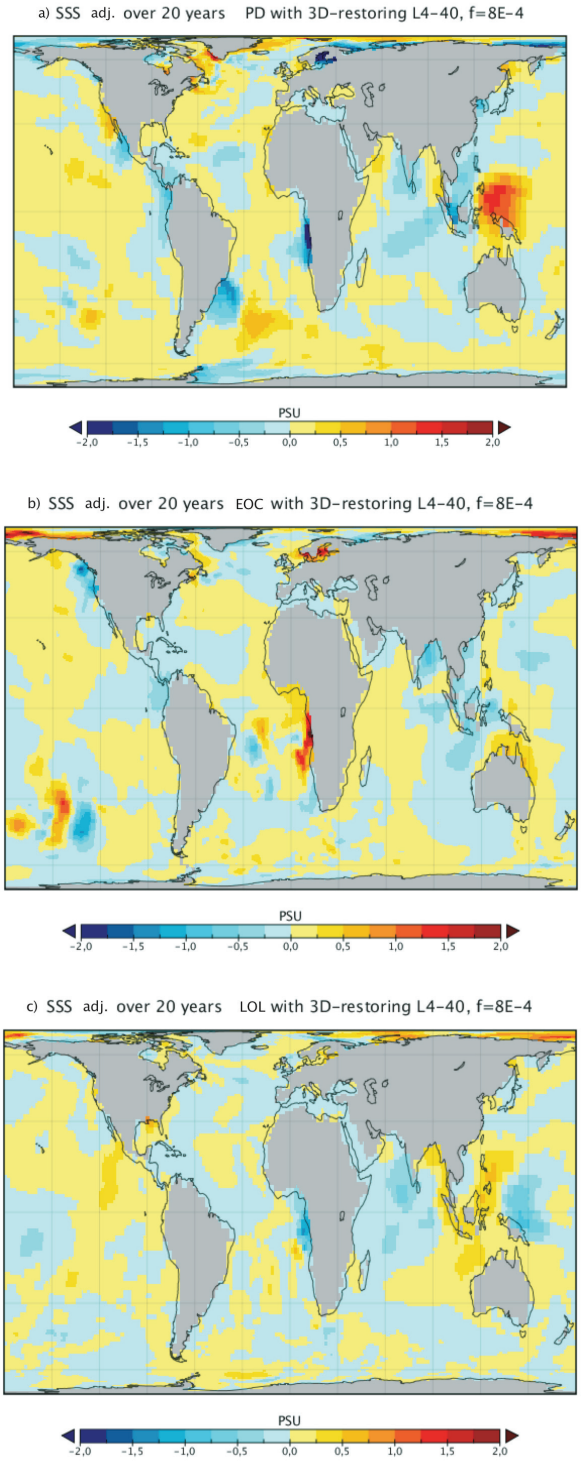

Figure 2.5: Annual mean sea surface salinity (SSS) adjustments of the MPI-OM ocean model to the LSG input for the different tectonic configurations present-day (PD, a), Late Eocene (EOC, b) and Late Oligocene (LOL, c) using a 3-dimensional restoring between the model levels (L) 4 and 40 and a relaxation constant (f) of $8 \cdot 10^{-4}$. Modified after Butzin (pers. comm.).

Along the COSMOS integration the modelled data is post-processed and the monthly means of the meteorological and oceanic fields are saved. After the whole run is completed (i.e., after 50 years of integration of COSMOS), the atmospheric monthly and yearly fields are calculated averaging them over the last 30 years of simulation. The net precipitation (P-E) is computed subtracting the total evaporation from the total precipitation (large scale and convective precipitation). P-E and surface atmospheric temperature (SAT) are transformed from the geographical to Cartesian grid and interpolated to the finer mesh of the ISM.

The initial condition of the ISM is an ice-free Antarctic continent with an isostatically adjusted bedrock. Forced by the accumulation and temperature produced with COSMOS, the ISM is run for 10 ky or for 100 ky, depending on the experiment, in order to simulate the first phase of the Antarctic ice sheet growth or to reach a steady state of the ice sheet, respectively. Outputs of the ISM are the final surface and bedrock elevation, the ice thickness, the basal temperature at the pressure melting point, the flux velocity of the ice and the time series of the ice volume and of the basal temperature during the run.

If successive iterations are required, depending on the experiment and explained in detail for each experimental set-up, the outcoming Antarctic surface elevation is converted and merged into the COSMOS global geopotential height. Starting from the modelled ice cover a new albedo dataset for Antarctica is constructed, converted and included in the global surface background albedo of COSMOS. This iterative procedure between COSMOS and the ISM is repeated until a steady state of the AIS is reached and the climatic equilibrium between the global climate and the Antarctic cryosphere is established.

Chapter 3

Model validation and response to climate forcings

This chapter illustrates the present-day control run and validates the modelling procedure by comparing the model results with observational data. Furthermore it assesses the robustness of the method by analysing the climate and AIS response to a doubling of the global atmospheric pCO_2 level. The state of the Antarctic climate system is reproduced by iteratively coupling of COSMOS and the ISM. When steady state is reached the atmospheric pCO_2 is doubled and the climate and AIS response examined. The inclusion of the AIS in the climate model by means of the iterative procedure constitutes a significant progress in the representation of the Antarctic topographic configuration in general circulation models (GCMs). This allows a more detailed study of the feedbacks of the AIS to changes in the climate system. Therefore the new ice sheet-climate modelling approach is an efficient tool for simulating the modern Antarctic climate and can be used for investigating past time slices, too.

3.1 Experimental set-up

The aim of this experiment is to achieve a complete description of the Antarctic and global climate system and of the interactions of the Antarctic cryosphere, including the global oceanic and atmospheric circulation. Additionally the experiment aims for validating the model results and for testing the robustness of the modelling procedure to changes in the boundary conditions (e.g. doubling in the atmospheric CO_2).

Figure 3.1 shows schematically the iterative modelling procedure applied to this present-day (PD) control experiment. The Earth System Model COSMOS is run with modern tectonics and boundary conditions (including the pre-industrial pCO_2 level of 280 ppm) for 50 years. The ocean is initialized with annual mean present-day thermohaline fields obtained by a 10 ky integration of the LSG model (Butzin et al., 2005). The three-dimensional ocean temperature and salinity are then averaged over the last 50 years and used to initialize the ocean component MPI-OM in COSMOS. Successively the fully coupled COSMOS is run for 50 years. During the MPI-OM run the ocean temperature and salinity at depth of 42 m (level 4) to the ocean bottom, at about 6000 m (level 40), are restored to their initial values (modelled by LSG) with a relaxation time constant of 1/(120 days). After the run is completed, the meteorological fields are calculated and averaged over the last 30 years of integration. The net precipitation (P-E) and the surface atmospheric temperature (SAT) are interpolated and transformed from the larger spherical grid of COSMOS to the finer Cartesian grid of the ISM. The ISM is run for 100000 years (100 ky) in order to reach the equilibrium of the AIS. Outputs of the ISM are the ice thickness and the final surface elevation, accounting of the bedrock elevation and the ice thickness. Subsequently the Antarctic surface elevation is converted and merged into the COSMOS global surface geopotential height. Starting from the modelled ice cover a new albedo dataset for Antarctica is constructed, converted and included in the global surface background albedo of COSMOS.

This iterative procedure between COSMOS and the ISM is repeated until the equilibrium between the models is established. This method guarantees that the global climate model adapts to the new Antarctic orography and radiation balance at each step and hence it returns consistent meteorological forcing fields.

To test the robustness of the modelling approach, a sensitivity experiment to a change in the atmospheric carbon dioxide level has also been performed. After the equilibrium between the two models COSMOS and ISM has been established, the pCO_2 level in the atmosphere has been doubled (560 ppm) and the asynchronous coupling procedure applied again until a new stability has been reached. The subsequent effects on the global climate and on the AIS have been analyzed.

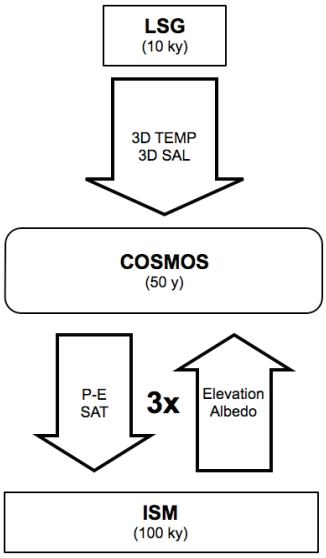

Figure 3.1: Flow-chart of the modelling procedure between LSG, COSMOS and ISM applied to the present-day (PD) control experiment.

Figure 3.2 shows the Antarctic bedrock elevation after the isostatic rebound, which is used as initial Antarctic orography. Because of the high mass of the present ice sheet, vast parts of the bedrock are beneath sea level. After the removal of the ice sheet and the subsequent relaxation of the lithosphere, East Antarctica results to have an average elevation of about 1000 m with peaks reaching 2500 m in the very inner sector of the continent (the Gamburtsev Mountain Range). On the other hand, West Antarctica and the Antarctic Peninsula are composed of isolated islands.

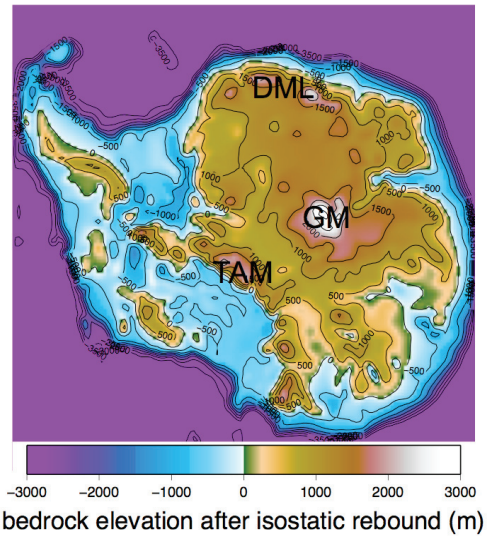

Figure 3.2: The initial Antarctic topography used in the experiment is the rock surface resulting after the removal of the ice load and the consequent isostatic rebound. The three most elevated areas are recognizable: the Transantarctic Mountains (TAM), the Gamburtsev Mountain Range (GM) and the Dronning Maud Land (DML).

3.2 Results

3.2.1 Modern climate and AIS

In Figure 3.3 the annual mean horizontal flow at the ocean model level L3 (corresponding to a depth of 27 m) modelled by the MPI-OM in COSMOS (a) for the PD experiment is compared with a control run performed with the stand-alone MPI-OM (Butzin, pers. comm., b) forced by prescribed present-day climatology. The main features of the modern global circulation are represented in both model simulations, even though some differences are recognizable. In the North Atlantic, the North Atlantic Current and the Gulf Stream are simulated in both models, but the latter has slightly less magnitude in the COSMOS run compared to the MPI-OM alone. The Equatorial Current is modelled in the Atlantic, Pacific and Indian Oceans although with different amplitudes as well. The Subtropical Gyres around the coasts of South America and in the Pacific Ocean are overestimated in the COSMOS run, rather than in the MPI-OM stand-alone run. In COSMOS, the Kuroshio Current, flowing northward in the coastal region off Japan, is underrated. Finally the Antarctic Circumpolar Current (ACC) is modelled in both models, but its magnitude in the COSMOS run is largely underestimated with respect to the stand-alone MPI-OM control run and the turbulent circulation between the coasts of South Africa and East Antarctica is emphasized. A possible explanation for these differences could be that the spinning-up time of the COSMOS set-up is too short (150 years in total) for adapting to the deep ocean restoring by LSG hydrography, and the global ocean in general does not reach quasi-equilibrium, especially in the regions of high transports (e.g., ACC). A feasible solution in this direction could be the execution of the spin-up run directly with the fully-coupled AOGCM COSMOS, before going over to the sensitivity studies. A more detailed analysis of the restoring process is also recommended; nevertheless the experiments of this research are performed with the confidence that these differences have minor impact on the sensitivity experiments.

In order to test the consistency of the results between the two ocean models LSG and MPI-OM (in COSMOS) used in this study, the annual mean zonally-averaged temperature and salinity fields modelled by the LSG and the MPI-OM for the PD control experiment have been compared and are shown in Figure 3.4. The temperature fields for the PD experiment modelled by the LSG model (Fig. 3.4a) and by the MPI-OM (Fig. 3.4b) exhibit the same pattern. In both cases the highest values are found in the tropical region, between 30°N and 30°S. Here the surface water reaches a temperature of 28°C. Values decrease northward and southward and in the deep ocean. The lowest values are found in the Arctic region and in the Southern Ocean, especially near the coasts of Antarctica. The small differences between the two patterns are due to the higher resolution in the MPI-OM, in horizontal and vertical scale, with respect to the LSG. This yields a more detailed structure of the temperature gradient. The annual mean zonally-averaged salinity modelled by the LSG ocean model (Fig. 3.4c) displays a pattern where the highest values (up to 36 psu) are located at the surface in the northern tropical region (around 30°N). Deep ocean waters in general have higher salinities than surface waters, whereas the lowest salinities are observed in the Polar Regions. The salinity field modelled by the MPI-OM ocean model (Fig. 3.4d) displays a pattern

which has more detailed structure, but similar to the one in Figure 3.4c. The highest values are located at the surface in the tropical region. A zone of lower salinity is visible in the Southern Hemisphere deep ocean. In this case the differences between the two models are due to the fact that the MPI-OM includes an interactive sea-ice model, which is absent in the LSG model. This is very important for the representation of the salinity field.

The global Meridional Overturning Circulation (MOC) modelled by LSG is plotted in Figure 3.5. The MOC is a stream function, which indicates the integrated water mass (or volume) transport. Positive numbers indicate clockwise circulation, while negative ones indicate counter clockwise flow. The region with deep water formation in the Northern Hemisphere is visible between 60°N and 80°N, with a maximum volume transport of about 20 Sv (1 Sv = 10^6 m^3s^{-1}). This is due to deep water formation in the North Atlantic (North Atlantic Deep Water, NADW). NADW enters the deep ocean up to a depth of about 2 km. In the Southern Ocean between 40°S and 60°S, Antarctic Intermediate Water (AAIW) formation is recognizable. Negative values along the coasts of Antarctica indicate the formation of Antarctic Bottom Water (AABW) by downwelling along the Antarctic continent.

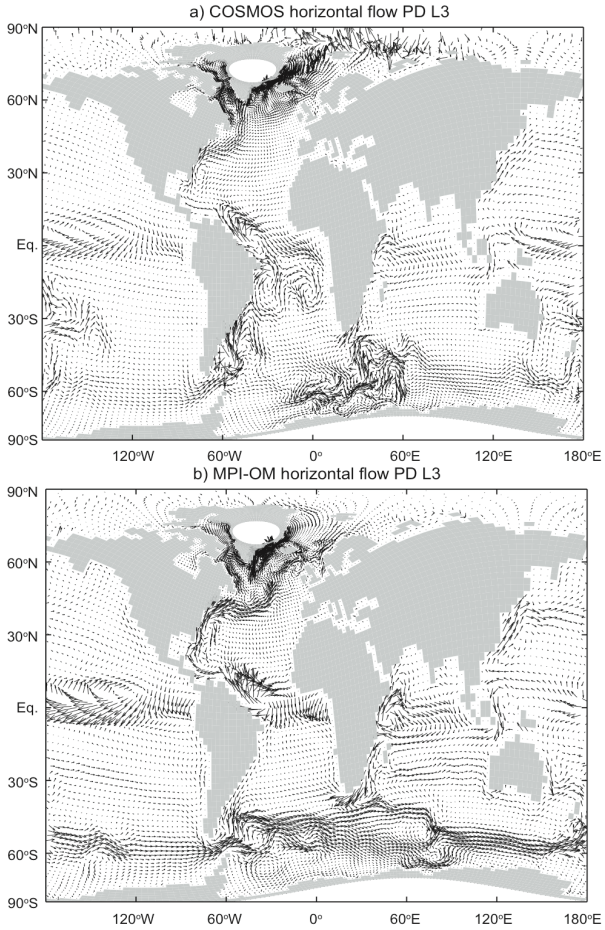

Figure 3.3: The annual mean horizontal flow at the model level L3 (corresponding to a depth of 27 m) modelled by the MPI-OM in COSMOS for the PD experiment (a) is compared with a control run performed with the stand-alone MPI-OM (Butzin, pers. comm., b) forced by prescribed present-day climatology.

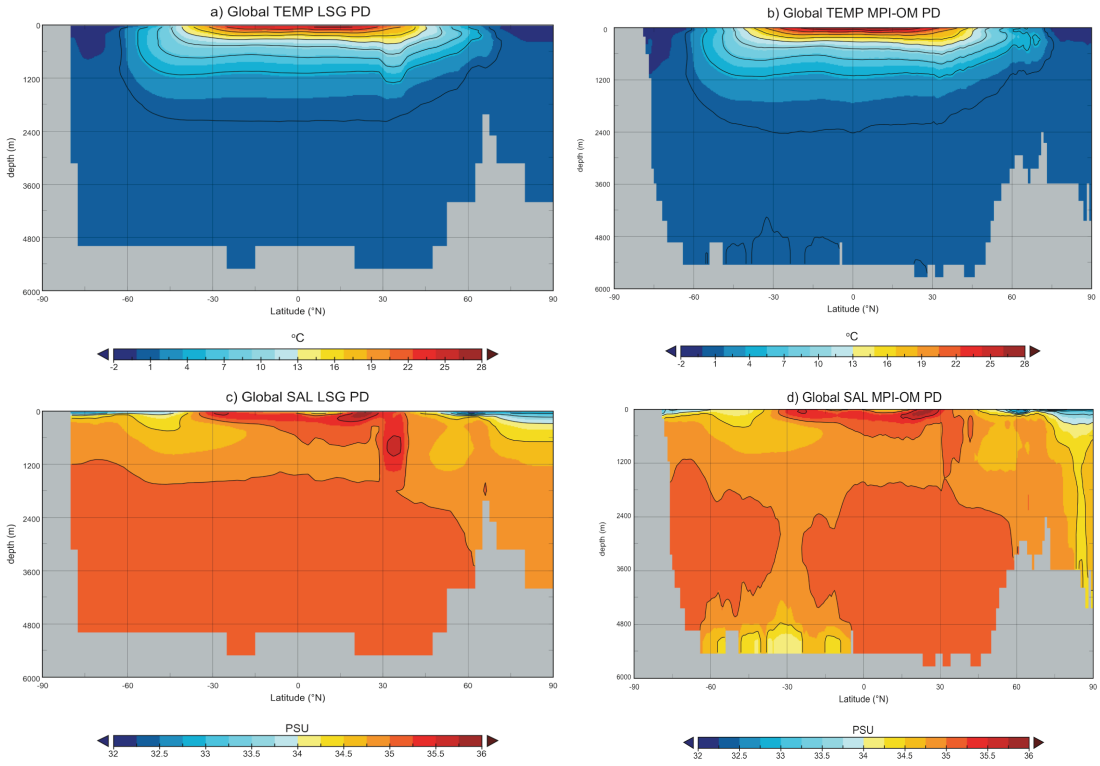

Figure 3.4: The zonally averaged annual mean present-day temperature (TEMP) and salinity (SAL) modelled by the LSG ocean model (panels a and c, respectively; Butzin, pers. comm.) and the same quantities modelled by the MPI-OM ocean model (panels b and d, respectively) for the present-day (PD) control run.

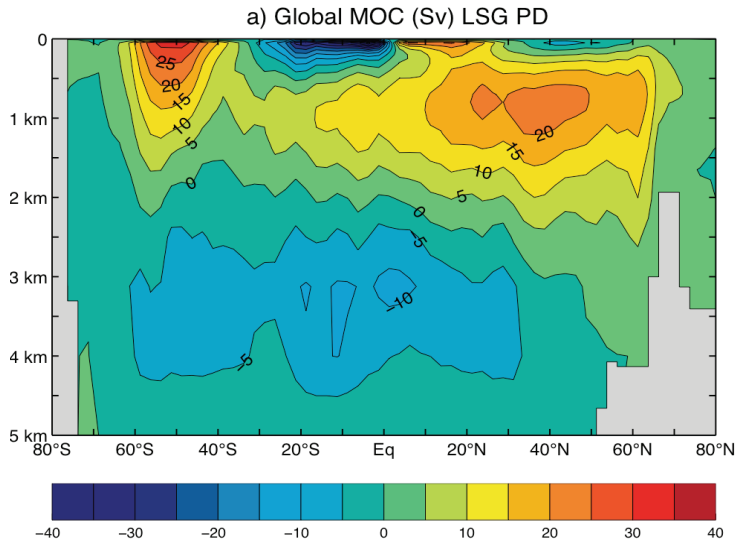

Figure 3.5: The present-day (PD) meridional overturning circulation (MOC, a) modelled by the LSG ocean model for the PD control run. Butzin, pers. comm.

In Figure 3.6 the mean annual sea surface temperature (SST, a), the sea ice thickness in February (b) and in September (c) and the sea surface salinity (d) over the Southern Ocean modelled by the MPI-OM in COSMOS for the present-day (PD) control run are shown. The ocean surface temperature exhibits a latitudinal dependency, with values close to zero near the Antarctic coasts and gradually increasing towards lower latitudes. The modelled pattern and values are similar to the ones provided for the ocean temperature in the World Ocean Atlas 2005 (Locarnini et al., 2006). The highest sea ice thickness in both summer and winter is found in the Weddell Sea (locations in Fig. 1.1) reaching 4 m. The minimum and the maximum sea-ice extents in the Antarctic region have been calculated as $6.73 \cdot 10^6$ km^2 and $19.5 \cdot 10^6$ km^2, respectively. The ones provided by Comiso (2010) for the means from the year 1979 to 2007 are $3 \cdot 10^6$ km^2 and $18.3 \cdot 10^6$ km^2, respectively. While the maximum value modelled by COSMOS is similar, the minimum value is higher by a factor of two. Indeed, sea ice persists in the Weddell Sea fastening to the eastern Antarctic Peninsula (AP) in summer, where also the surface salinity displays a minimum. The modelled results for the surface salinity are comparable to the values given in the World Ocean Atlas 2005 (Antonov et al., 2006).

Figure 3.7 shows the annual mean SAT (a), P-E (b) and 10 m wind speed (c) over the Antarctic continent after the models have reached a common equilibrium. The temperature field exhibits a strong dependency on the latitude and on the elevation, decreasing poleward and with the height. Over the ocean the SAT display a pattern similar to the SST (Fig. 3.6a). The innermost region of the continent, corresponding to the high altitudes of the Gamburtsev Mountains and the overlying Dome Argus, experiences the lowest temperatures (around 230 K). The net precipitation is very low (0.01 m/y to 0.02 m/y, water equivalent WE) over the interior of the continent, due to the low temperatures and the dryness of the air. Values increase along the steep coastal margins and over the surrounding ocean (up to 1 m/y WE) due to orographic lifting of warmer and moister air associated with the transient cyclones that encircle the continent. The wind pattern shows clearly the polar vortex due to the Antarctic Circumpolar Current (ACC). Winds are stronger over the Southern Ocean surrounding the continent, especially over the Indian sector, where values are higher than 10 m/s. The katabatic winds along the Antarctic coastal areas are also distinctly visible, due to the steep slope of the plateau. They carry high-density cold air form the top of the ice sheet down the escarpment under the force of gravity. The modelled meteorological fields over the Antarctic continent and the Southern Ocean are in agreement with the modern observed fields (e.g., the ERA-40 atlas by Kållberg et al., 2005 and Monaghan and Bromwich, 2008).

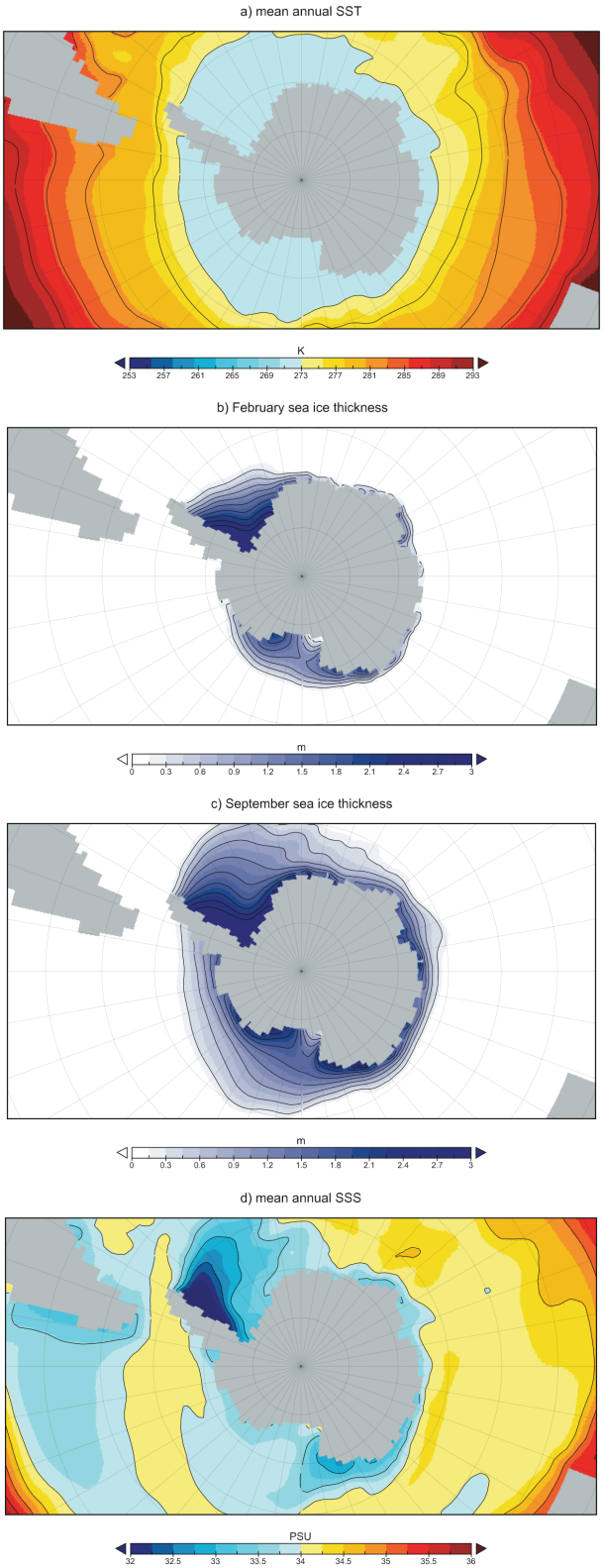

Figure 3.6: The present-day (PD) annual mean sea surface temperature (SST, a), sea ice thickness in February (b) and September (c) and mean annual sea surface salinity (SSS, d) modelled by the MPI-OM ocean model in the Earth System Model COSMOS for the present-day (PD) control run.

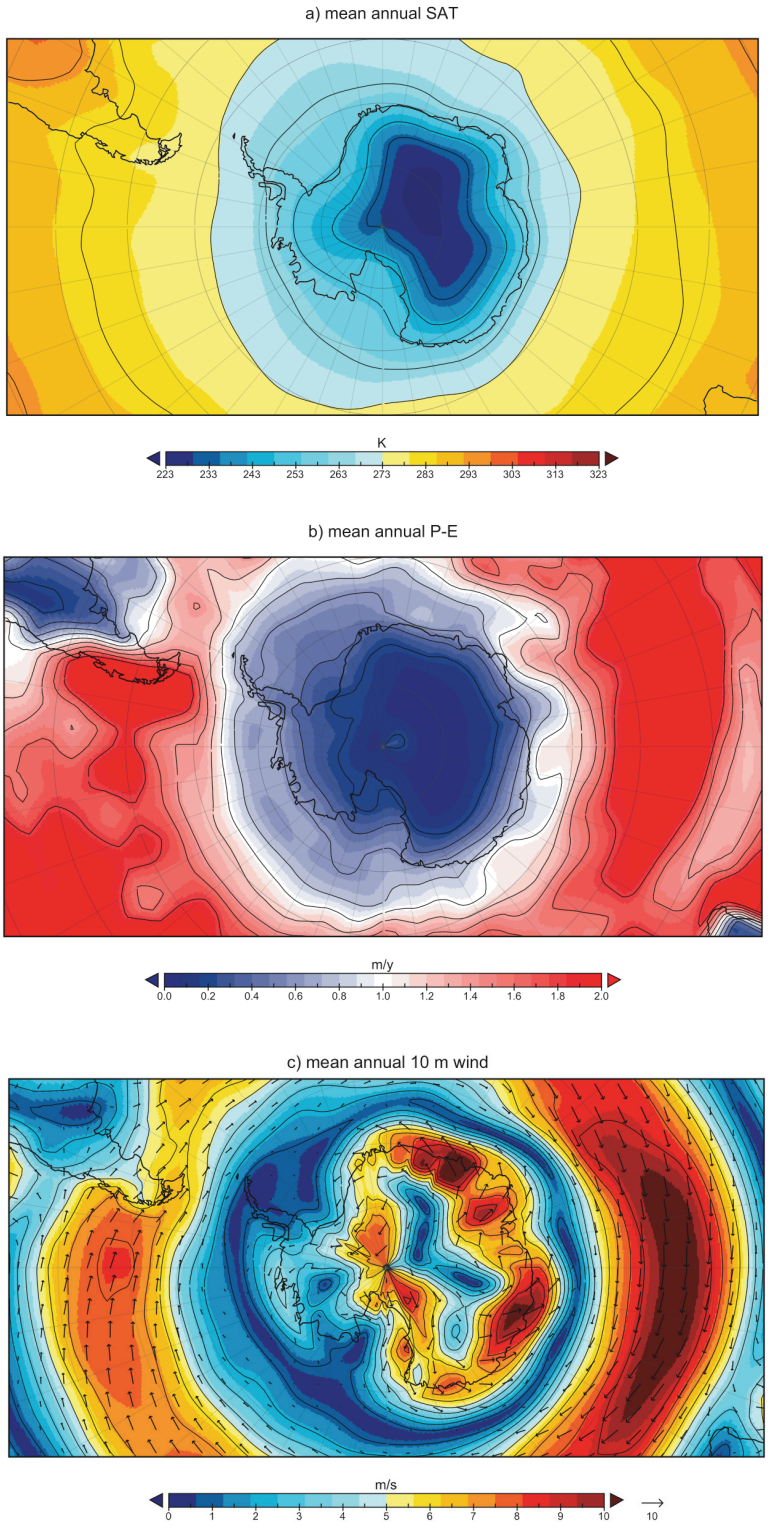

Figure 3.7: The annual mean surface atmospheric temperature (SAT, a), net precipitation (P-E, b) and 10-m wind (c) modelled by the climate model ECHAM5 in the Earth System Model COSMOS for the present-day (PD) control run.

The course of the AIS volume calculated by the ISM along the PD control experiment is shown in Figure 3.8. The behaviour of the AIS volume is visible in each of the three iteration steps (the first from 0 to 100 ky, the second from 100 ky to 200 ky and the third from 200 ky to 300 ky). In each iteration the AIS reaches the equilibrium after about 50 ky. At the beginning of the second and third iterations (i.e. after 100 ky and after 200 ky), the adaptation of the AIS to the new climate forcing fields is visible, with a first, small and rapid decrease in the ice volume and a subsequent, slow increase to the equilibrium value. The trend of the ice volume is very similar for the second and third iterations and the values reached at the end of each of these steps is the same ($2.23 \cdot 10^{16}$ m^3 or $2.23 \cdot 10^7$ km^3) and slightly higher that the volume achieved at the end of the first iteration step ($2.22 \cdot 10^{16}$ m^3 or $2.22 \cdot 10^7$ km^3). The final ice volume achieved is therefore $2.23 \cdot 10^7$ km^3.

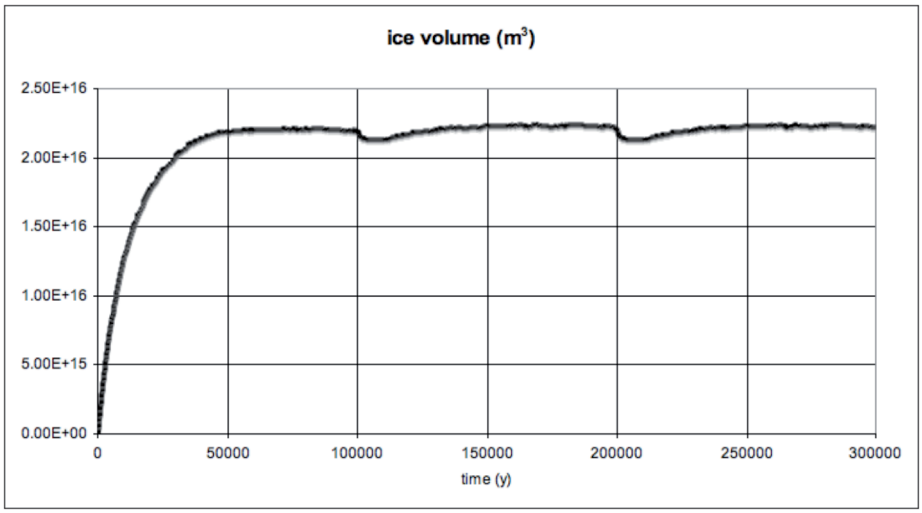

Figure 3.8: The AIS volume modelled by the ISM along the present-day (PD) control run.

Figure 3.9 shows the final surface elevation (a) and ice thickness (b) reached at the end of the experiment (i.e. after in total 300 ky of ISM integration). The biggest ice thickness develops in East Antarctica. There is a clear separation between East Antarctica and the marine based West Antarctica, which in general has a lower ice thickness. The Transantarctic Mountains (TAM, Fig. 3.2), dividing the continent into an eastern and a western part, act like a barrier to the growth of the ice sheet. The final elevation of the EAIS has a dome-shape, which reaches the altitude of about 4000 m, the peak corresponding to Dome Argus over the Gamburtsev Mountains (GM, Fig. 3.2). The Antarctic Peninsula and parts of west Antarctica remain ice-free.

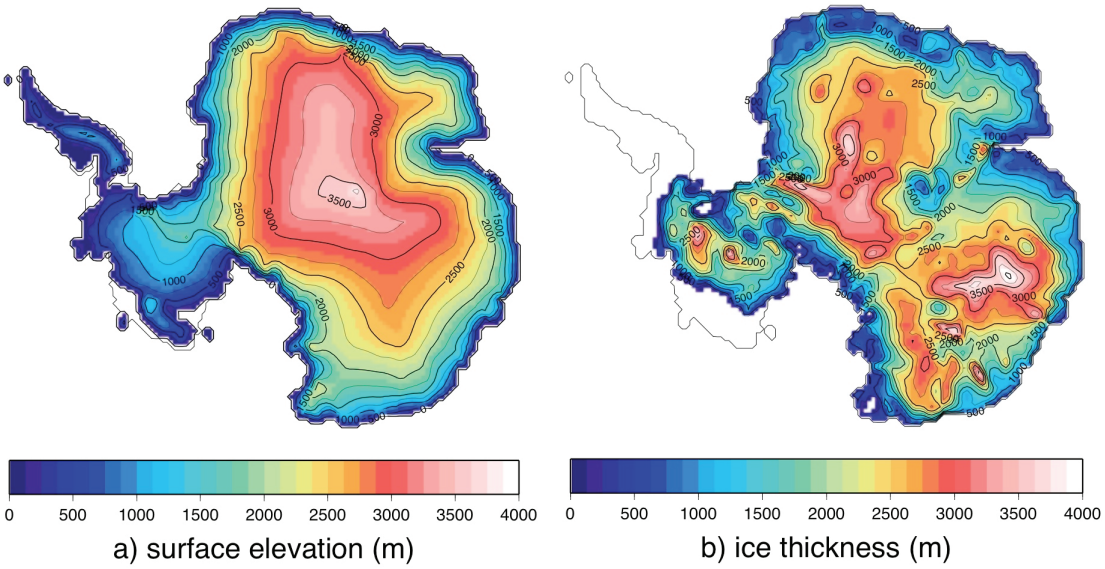

Figure 3.9: The Antarctic surface elevation (a) and ice thickness (b) modelled by the ISM for the present-day (PD) control run.

3.2.2 Comparison with observations

The final AIS volume achieved with this methodology is about 12% lower ($0.31 \cdot 10^7$ km^3) than its observed present-day value of $2.54 \cdot 10^7$ km^3 (BEDMAP dataset, Lythe et al., 2001). Measurements of the AIS ice thickness collected during surveys undertaken over 50 years have been brought together by the BEDMAP project into a single database. From these data, a suite of digital topographic models has been compiled for Antarctica.

The surface elevation and ice thickness deviations between the modelled results and the observations are shown in Figure 3.10. Generally the model underestimates the amount of ice present on the continent. The mean anomalies are 84 m for the surface elevation and 121 m for the ice thickness. More evident differences are found in the WAIS (negative) and along the coasts of the EAIS (positive). The WAIS is still not well resolved by the model, indicating differences up to 1200 m between model results and observation. There are still differences concerning the ice thickness, which are due to the variance in the representation of the meteorological fields on a larger scale, since the horizontal resolution of the climate model is about 10 times coarser than the one of the ice sheet model. The growth of an ice sheet depends mostly on the temperature and precipitation over the continent, which is well represented by the climate model over East Antarctica. On the other hand, over west Antarctica and the Antarctic Peninsula the coarse horizontal resolution of the climate model (about 400 km) does not permit a detailed representation of the meteorological fields over small distances (the Antarctic Peninsula is on average 70 km wide), therefore the ice sheet model, forced by them, underestimates the ice coverage.

On the other hand, even if the BEDMAP database quantifies elevation and ice thickness well in many places, there are several large data gaps where little is known about ice topography. Furthermore, even in regions where coverage is good, radar transects are often separated by several kilometres across which interpolation of data remains necessary. This causes uncertainties in the estimation of the ice thickness, which are assessed between 150 and 300 m (Lythe et al. 2001).

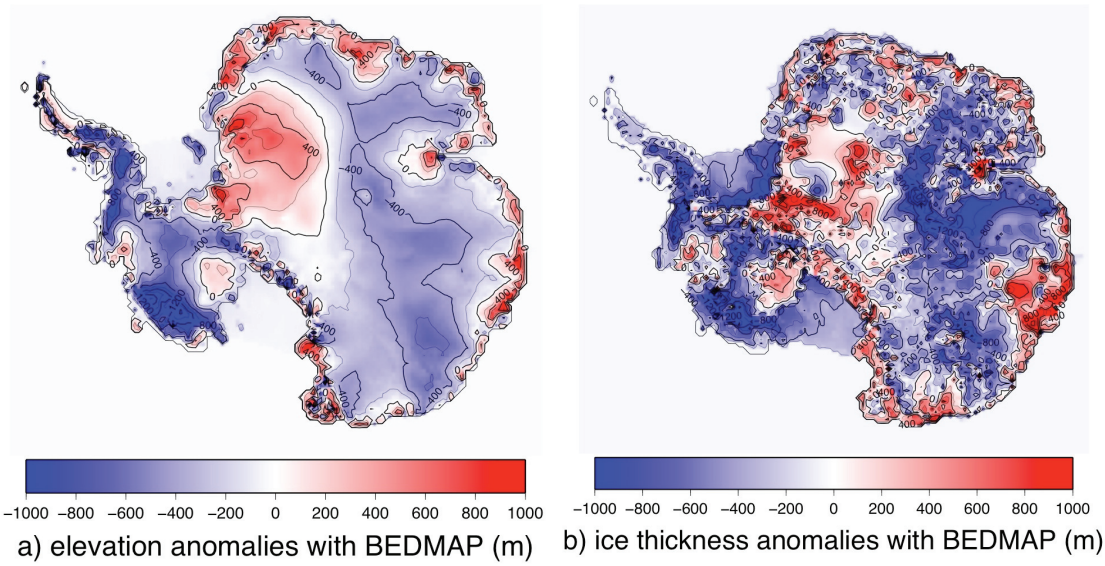

Figure 3.10: Surface elevation (a) and ice thickness (b) differences between the results modelled by the ISM for the present-day (PD) control run and modern observations (BEDMAP Consortium, Lythe et al., 2001).

3.2.3 Comparison with stand-alone models

In order to evaluate if the iteratively coupled modelling procedure between the ISM and COSMOS represents an improvement with respect to earlier modelling studies, the modelled Antarctic surface elevation was compared to the standard dataset included in COSMOS and to the modelled stand-alone one of the ISM. Figure 3.11 shows the surface elevation anomalies between the modelled AIS with stand-alone COSMOS and ISM and with the two models iteratively coupled, in the panels a and b, respectively.

In the first case Figure 3.11a shows a significant improvement in the representation of the AIS. The mean anomaly in the elevation is 81 m. Differences, positive and negative, are present for the entire continent and regard primarily the more detailed representation of the AIS structure incorporated in the AOGCM with the iteratively coupled technique. In the second case (Fig. 3.11b), the mean difference in the AIS elevation between the two methods is 71 m. With respect to the stand-alone version of the ISM, the new approach produces notable differences in the WAIS only, whereas it is in good agreement with the EAIS. The stand-alone version of the ISM is forced by temperature and accumulation calculated with empirical parameterizations following

Giovinetto et al. (1990) and Fortuin and Oerlemans (1990). These parameterizations are based on present-day meteorological observations taken over Antarctica. Although in this way the modern AIS is more precisely simulated, the iterative modelling approach is much more consistent for simulating the AIS during different (paleo)climate states, when no empirical parameterization can be applied. This is very important if one wants to describe consistently the AIS in the global (paleo)climate.

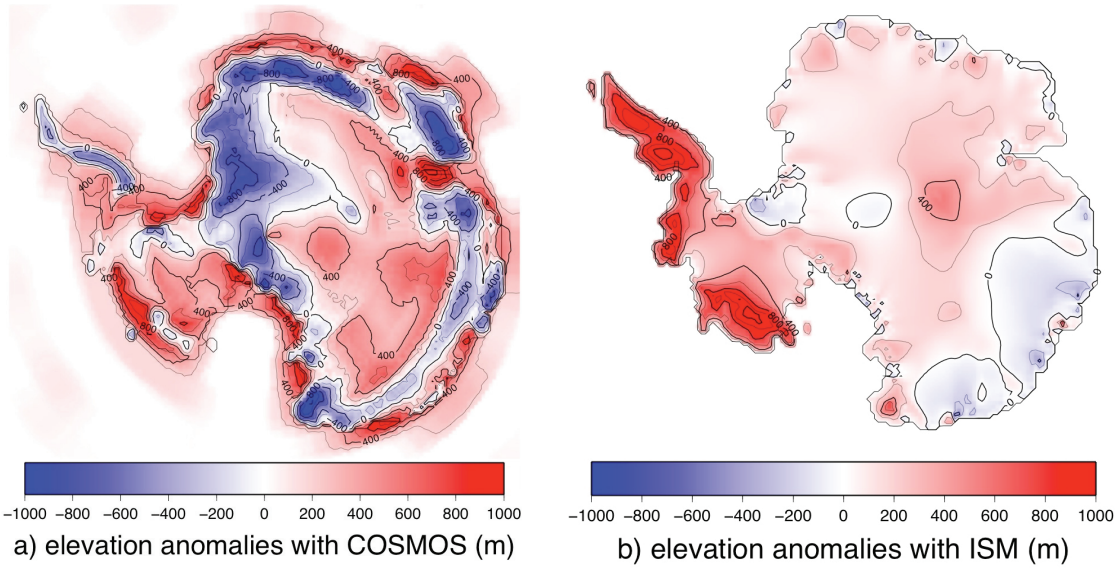

Figure 3.11: Surface elevation differences between the AIS dataset included in the atmospheric component (ECHAM5) of the Earth System Model COSMOS and modelled by the stand-alone ISM and with the two models iteratively coupled for the present-day (PD) control run (panels a and b, respectively).

3.2.4 Response to doubling pCO_2

In order to test the sensitivity of the modelling method, an experiment has been performed, increasing the level of carbon dioxide in the atmosphere. The aim is to examine whether the constructed model is able to react to an alteration of the boundary conditions and to give a corresponding climate response.

Starting from the final condition of the previous present-day control experiment (PD), i.e. from the equilibrium state between the climate model COSMOS and the ISM, the atmospheric CO_2 concentration has been raised to a level of 560 ppm, which is twice the pre-industrial level of 280 ppm used in the PD control experiment. The iterative procedure has been repeated until a new equilibrium has been established (experiment denoted by "PD $2CO_2$").

The zonal annual mean SAT anomaly between the two cases is shown in Figure 3.12 (delta T). There is a globally-averaged increase of the surface temperature of 1.2 K. The SAT anomaly trend over Antarctica is due to the non-linear response of the sea-ice over the surrounding ocean: the change in the sea-ice coverage is small, and

therefore no strong amplification takes place. The difference in the temperature is accentuated at high latitudes in both of the hemispheres, but more in the Arctic region, where the anomalies reach 2.7 K. On the other hand, the Antarctic region experiences a maximum rise in the SAT of about 1.3 K. The polar amplification of the climate change due to increasing in pCO_2 is an expected result, also due to the ice-albedo feedbacks of those regions. This result is indeed confirmed by earlier studies (e.g., Masson-Delmotte et al., 2006).

However, the last report of the Intergovernmental Panel for Climate Change (IPCC), released in 2007, assesses that climate sensitivity, defined as the equilibrium global average surface warming following a doubling of CO_2 concentration, is likely to be in the range of 2 to 4.5 K with a best estimate of about 3 K, and is very unlikely to be less than 1.5 K. With respect to this assessment, the result of this experiment is at the lower bound of the estimate of the climate sensitivity. The climate sensitivity given by the iteratively coupled model has been compared with the one given by the ECHAM5/MPIOM model simulation for 1% per year pCO_2 increase experiment (to doubling) derived from the World Climate Research Programme's Coupled Model Intercomparison Project multi-model data set (CMIP3) (available at http://www-pcmdi.llnl.gov). The anomaly between the last and the first 5 years of the run has been analysed and plotted in Figure 3.12 as well (deltaT_freeModel; Laepple, pers. comm.). Also in this case, the trend of the SAT anomaly over Antarctica is due to the sea ice-albedo feedback: particularly in the coastal areas, the SAT with doubled pCO_2 is high enough that the sea ice is strongly reduced, and therefore the warming is amplified. In general, the iteratively coupled climate-ice sheet model underestimates the global climate sensitivity by a factor of about 3 and of about 4 in Antarctica, if compared to the CMIP3 model run. This occurs because the doubling in the CO_2 concerns mostly the atmosphere, while the ocean is not considerably affected owing to the restoring of the subsurface and deep-ocean temperature to the initial values, as explained in Chapter 2. Therefore, the lower climate sensitivity resulting from this modelling approach has implications that must be considered in the interpretation of the (paleo) modelling results in later discussion.

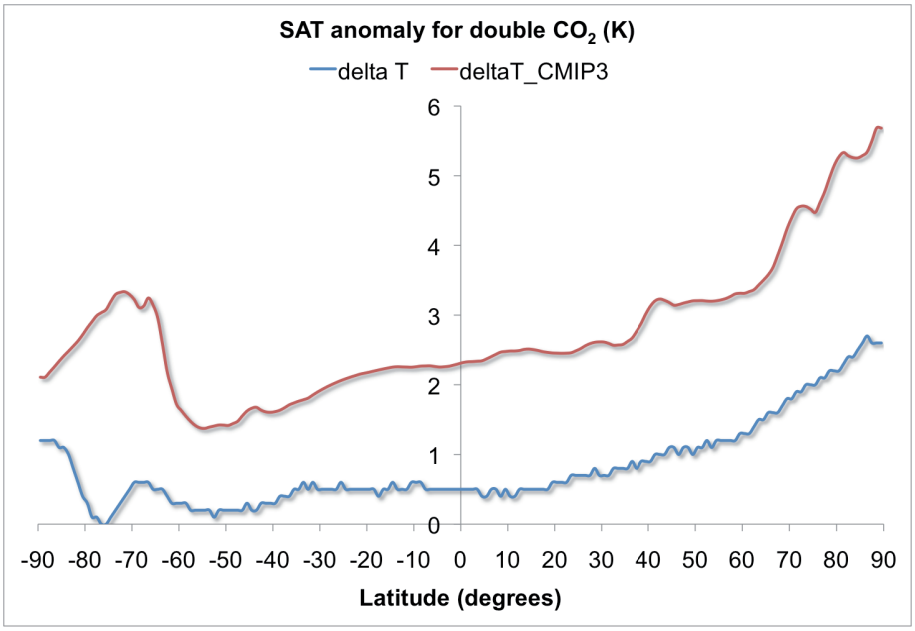

Figure 3.12: In blue (deltaT): the zonal mean SAT anomalies between the PD climate obtained with a CO_2 level of 560 ppm and the one with 280 ppm modelled by the iteratively coupled COSMOS-ISM. In red (deltaT_CMIP3): the anomaly between the last and the first 5 years of the CMIP3 model run for pCO_2 increase experiment (Laepple, pers. comm.).

Figure 3.13 shows the SAT (a) and P-E (b) anomalies between the experiments PD $2CO_2$ and PD over the Antarctic continent. In general the increased pCO_2 causes a rise of the surface temperature, with an average of 0.55 K over the entire continent. An area of negative anomaly is visible over East Antarctica, which corresponds also to an area of decreased net precipitation and is most likely associated with the low atmospheric humidity content. The areas where the SAT anomalies are positive correspond to the areas where also the P-E is positive. This means that an increase in the surface temperature is associated with an increase in the amount of total precipitation with respect of the amount of evaporation.

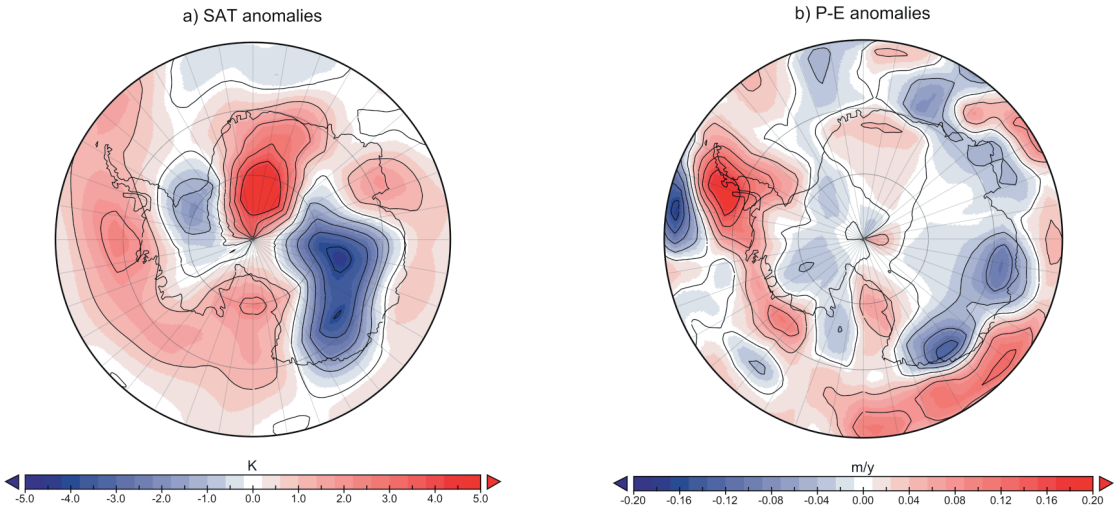

Figure 3.13: SAT (a) and P-E (b) anomalies of the COSMOS-ISM experiment PD $2CO_2$ related to the PD control run.

Figure 3.14 shows the trend of the AIS simulated by the ISM for the experiment PD $2CO_2$ in each of the two iteration steps (the first from 0 to 100 ky and the second from 100 ky to 200 ky). As for the PD control experiment, in each iteration the AIS reaches steady state after 50 ky. At the beginning the adaptation of the AIS to the new climate with the pCO_2 level of 560 ppm is visible, with an initial decrease in the ice volume and the subsequent increase to the equilibrium value. The plot is similar for the first and second iterations and the values reached at the end of each step are the same ($2.15 \cdot 10^7$ km^3). Therefore the final ice volume once the new equilibrium has been established shows a loss of $0.08 \cdot 10^7$ km^3 with respect to the volume achieved in the control run ($2.23 \cdot 10^7$ km^3). This corresponds to about 3.6%.

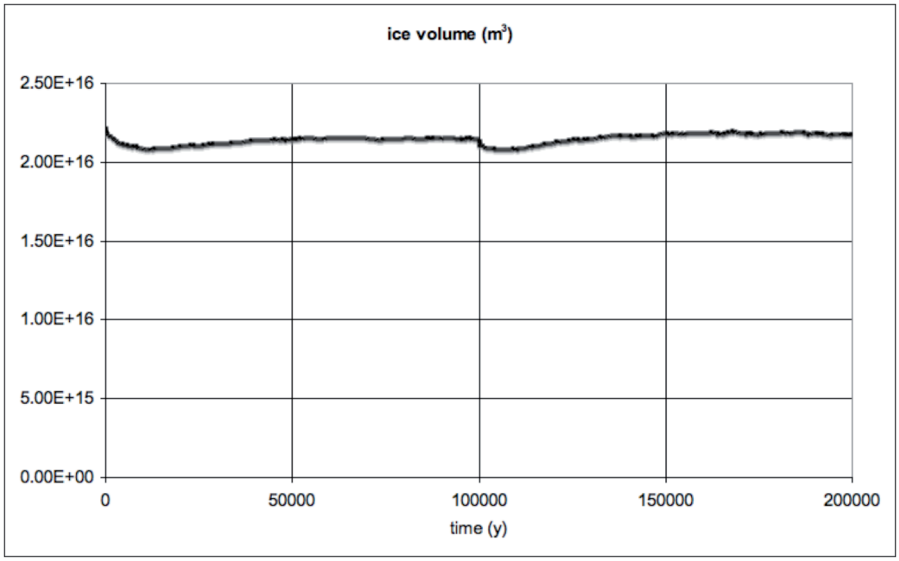

Figure 3.14: The AIS volume modelled by the ISM along the experiment PD $2 \times CO_2$.

Figure 3.15 shows the response of the AIS once the equilibrium is reached. Both, the surface elevation (a) and the ice thickness (b) show generally negative anomalies, meaning that the AIS experiences a decrease in both volume and extent. In both of the cases the drop occurs predominantly in the coastal areas and the west Antarctic region. These regions are in fact more sensitive to changes in temperature due to the thinner ice layer, as mentioned before. The ice sheet flowing towards the Weddell Sea between East Antarctica and the Antarctic Peninsula, and towards the Wilkins and Aurora basins, facing the Pacific sector, presents the higher negative anomalies, up to 200 m and up to 500 m, respectively (locations in Fig. 1.1). Some areas of positive anomalies are visible in correspondence to the locations with increased precipitation (Fig. 3.13b).

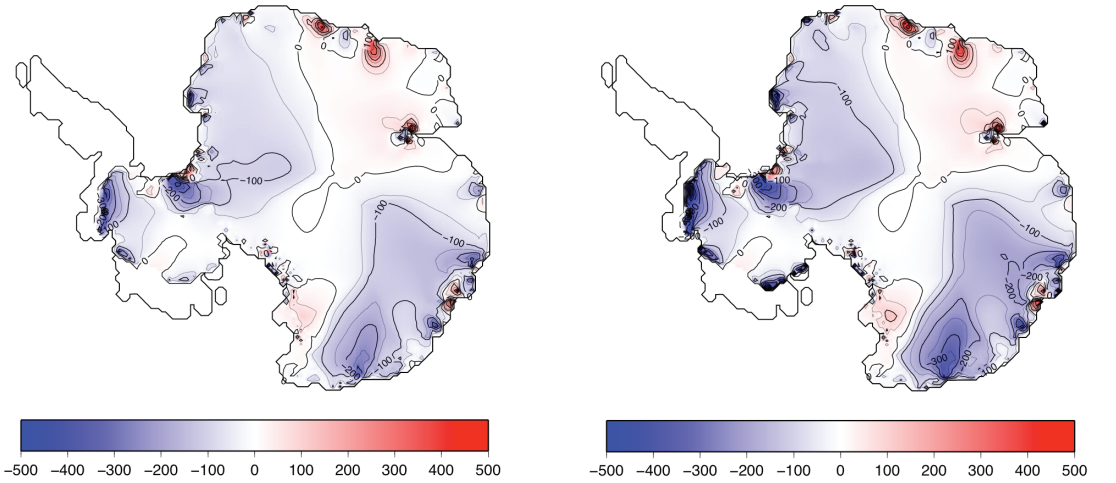

Figure 3.15: Surface elevation (a) and ice thickness (b) anomalies of the COSMOS-ISM experiment PD $2CO_2$ related to the PD control run.

3.3 Summary

The aim of this modelling approach is producing a comprehensive representation of the AIS including the global climate. The presentation of a new modelling procedure must be accompanied by a demonstration of its robustness to changes in the boundary conditions. In order to explore the response of the climate and the modelled AIS to an alteration in the climate constraints, a doubling of the atmospheric carbon dioxide has been applied.

The methodology here developed used a coupled ocean-atmosphere climate model (COSMOS) asynchronously coupled with an ice sheet model (ISM). The ice sheet grows in response to the modelled climate forcings in an iterative procedure, which ensures the adaptation of the model components to the changing forcing fields up to a stable equilibrium. Therefore, the iterative procedure assures that the steady state obtained is representative for the climate at a specific time slice (in this case the modern climate).

The new ice sheet-climate modelling approach proposed is able to respond to changes in the climate boundary conditions, as demonstrated by quantifying the reaction to an increase in the global CO_2. This test was designed to evaluate if such a methodology is capable to capture alterations in the global climate state and to transmit them properly to the AIS in a way in which this can react. At equilibrium of the PD control experiment (i.e., after three successive iterations of the climate and ice sheet model), an increase in the global surface atmospheric temperature has been detected as a consequence of the increased pCO_2. The climate sensitivity is 40% (1.2 K) lower than the best estimate of the IPCC (2007) assessment (3 K), owing to the restoring of the ocean temperature, which dampens the climate response. The modelling strategy is also effective in diagnosing the higher sensitivity of the high latitudes to a rise of the global temperature with respect to the middle and lower latitudes. The resulting ice sheet at the

equilibrium is reduced in size and volume with reference to the initial one, the lowering regarding especially the coastal regions of East Antarctica and the WAIS.

To summarize, the modelling procedure adopted for this study demonstrated to be a valuable tool for representing the present-day Antarctic climate and ice sheet and to be able to respond to changes in the global climate boundary conditions. The inclusion of the AIS in a climate model via the iterative technique establishes a significant progress in the representation of the Antarctic surface geography in general circulation models (GCMs) and allows the test and examination of the feedback of the AIS to variations in the global climate. This method can therefore be an effective instrument for simulating the AIS for certain time slices in the context of paleo-climate. With the performance of time slice experiments with the two models, it will be possible to study the sensitivity of the AIS to the processes, which could have contributed to its glaciation. The glaciation of Antarctica is thought to have started in the eastern side of the continent, for which this model configuration seems to represent satisfactorily the response of climate and ice sheets. A better understanding of past changes in this region is crucial to make improved predictions on future global environmental change and to estimate the role of the AIS in the future.

Chapter 4

Sensitivity of Antarctica to the opening of the Drake Passage

The classical hypothesis that the Antarctic glaciation was generated as a result of the thermal isolation of Antarctica through the opening of a major gateway such as the Drake Pasage (DP) and the subsequent establishment of the Antarctic Circumpolar Current (ACC) is tested in this chapter. The climate - ice sheet model is employed to explore the glacial evolution of Antarctica to different land-sea distributions and associated global oceanic circulations. Two sensitivity experiments with different tectonic settings (Late Eocene and Late Oligocene) provide understanding of the role of the ACC for the development of the AIS.

4.1 Experimental set-up

This set of sensitivity experiments is designed to study two different climate states under different land-sea distributions: with closed and with open Drake Passage (DP). Two separated experiments, different from each other in the tectonic configuration, have been performed (Fig. 4.1): they are called "EOC" and "LOL", respectively because of their tectonic settings, which differ in the open or closed DP. The EOC ocean bathymetry includes closed DP, narrowed South African and Tasman Passages, open Panama Gateway and Eastern Tethys Sea. The LOL ocean bathymetry includes modern Southern Ocean seaways, open Panama Gateway and Eastern Tethys Sea.

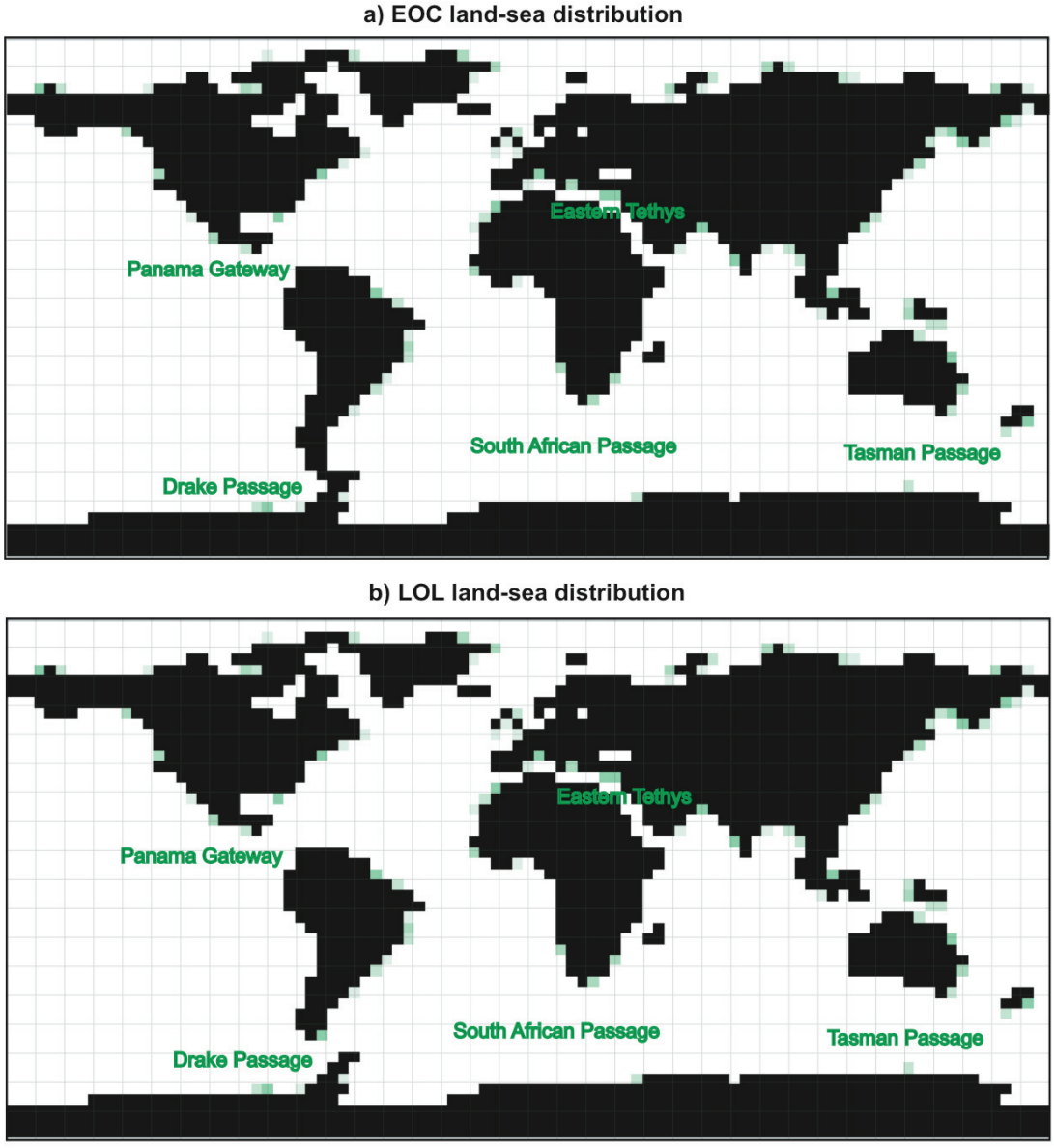

Figure 4.1: The two land-sea distributions used in the EOC (a) and LOL (b) experiments.

In both cases the topography used to force the climate model COSMOS includes an ice-free Antarctica, isostatically relaxed after the removal of the ice sheet (Fig. 3.2). The use of modern, isostatically equilibrated Antarctic bedrock is not ideal for Eocene-Oligocene (E-O) ice sheet simulations, but the detailed paleo-topography of Antarctica is not well known. Since little is known on the Antarctic paleo-vegetation as well, the surface background albedo of the ice-free Antarctica is set at the global mean value 0.3. The atmospheric pCO_2 level is fixed to 280 ppm, i.e. the pre-industrial level. Finally a modern astronomical orbit is applied in both cases. All other boundary conditions are constructed from the modern ones using the different land-sea masks.

The iterative modelling procedure used for the PD control experiment of Chapter 3 and shown schematically in Figure 3.1 is applied in both these experiments as well. The Earth System Model COSMOS is run with EOC and LOL tectonics for 50 years. In both cases the ocean model MPI-OM is initialized with annual mean fields obtained by a 10 ky integration of the LSG model. The LSG runs use the same EOC and LOL configurations and are forced by present-day background climate, as explained in Chapter 2. Successively the fully coupled COSMOS is run for 50 years. During the run the deep ocean temperature and salinity below 40 m are relaxed to their initial values (modelled by LSG), as explained in Chapters 2 and 3. After the COSMOS run is completed the net precipitation (P-E) and the surface atmospheric temperature (SAT) are averaged over the last 30 years of integration, interpolated and used to force the ISM. The ISM is run for 100 ky to the equilibrium of the AIS. Subsequently the Antarctic surface elevation is converted and merged into the COSMOS global surface geopotential height. Starting from the modelled ice cover a new albedo dataset for Antarctica is constructed, converted and included in the global surface background albedo of COSMOS.

In Table 4.1 a summary of the two experiments, with their denomination and schematic description, is given.

Table 4.1: Summary of the COSMOS-ISM experiments performed in this chapter.

Name of the experiment	Description
EOC	Experiment with: • land-sea distribution similar to the Late Eocene (Fig. 4.1a); • ocean temperature and salinity L4-40 restored to LSG run with EOC land-sea distribution; • pCO_2 of 280 ppm (pre-industrial level); • modern orbital configuration.
LOL	Experiment with: • land-sea distribution similar to the Late Oligocene (Fig. 4.1b); • ocean temperature and salinity L4-40 restored to LSG run with LOL land-sea distribution; • pCO_2 of 280 ppm (pre-industrial level); • modern orbital configuration.

4.2 Results

The zonally-averaged temperature field modelled by the LSG and by the MPI-OM ocean models for the EOC experiment (Fig. 4.2a and Fig. 4.2b, respectively) presents values generally higher than the ones modelled for the PD control experiment (Fig. 3.4a and Fig. 3.4b). In both cases the deep ocean is 4 to 5 degrees warmer than today and shows the highest values at the surface of the equatorial region. The structure of the modelled temperature is very similar for the two models. Figure 4.2c and Figure 4.2d show the zonally-averaged salinity modelled by the LSG and the MPI-OM, respectively, for the EOC set-up. In both cases the values are lower than the ones modelled for the PD control run (Fig. 3.4c and Fig. 3.4d), differing of about 1 psu in the deep ocean. Equatorial surface waters are saltier than polar ones, with a maximum salinity of 36 psu. The pattern of the salinity modelled by the MPI-OM is more detailed then the one modelled by the LSG model, due to the higher resolution.

As for the EOC experiment, the zonally-averaged temperature modelled by both the LSG and the MPI-OM ocean models for the LOL set-up (Fig. 4.3a and Fig. 4.3b) is higher than the modern one (Fig. 3.4a and Fig. 3.4b). The pattern of the modelled temperature is very similar in the two cases, but the MPI-OM gives a more detailed structure, as a result of its higher resolution compared to the LSG model. The lowest temperatures are found in the polar surface waters, especially in the Arctic Ocean, where waters have temperature lower than -2°C. In both models (LSG and MPI-OM) the salinity (Fig. 4.3c and Fig. 4.3d) exhibits higher values in the LOL experiment compared to the EOC. Values higher than 36 psu are found in both cases in the surface tropical region. The lowest values are found in the Arctic Ocean, where the salinity is inferior to 32 psu. As in the case of the temperature, the higher resolution of the MPI-OM with respect of the LSG model permits a more accurate description of the pattern, especially in the deep ocean.

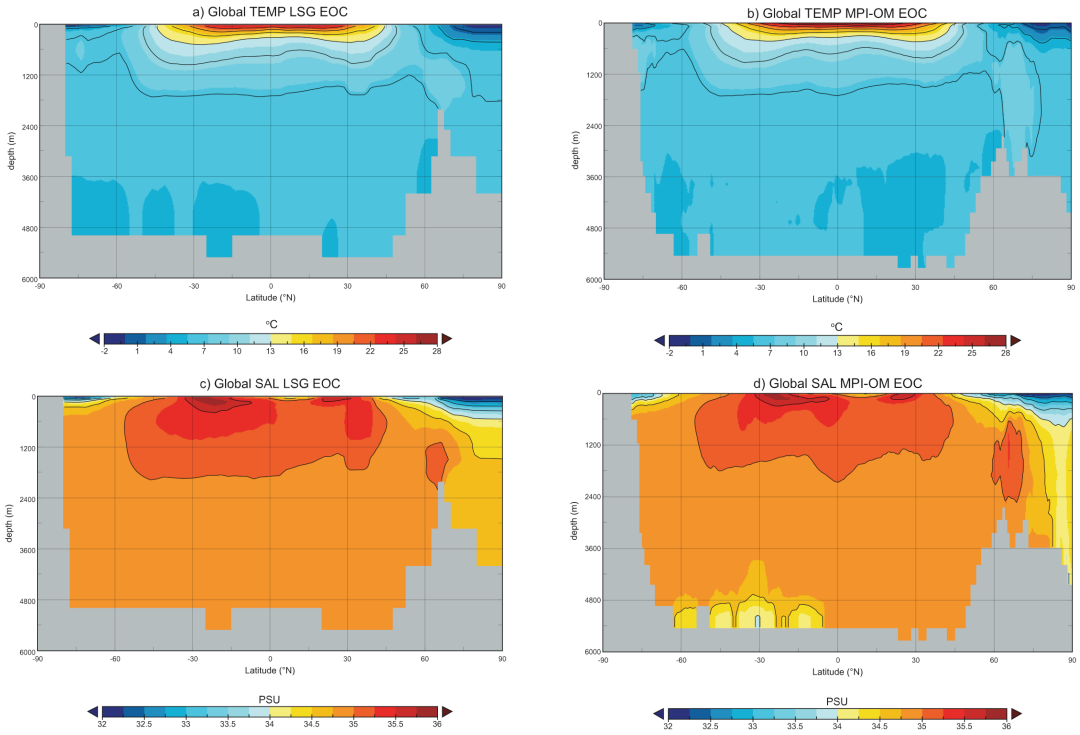

Figure 4.2: The zonally-averaged annual mean temperature (TEMP) and salinity (SAL) modelled by LSG (a and c, respectively) and the same quantities modelled by MPI-OM (b and d, respectively) for the Late Eocene (EOC) experiment.

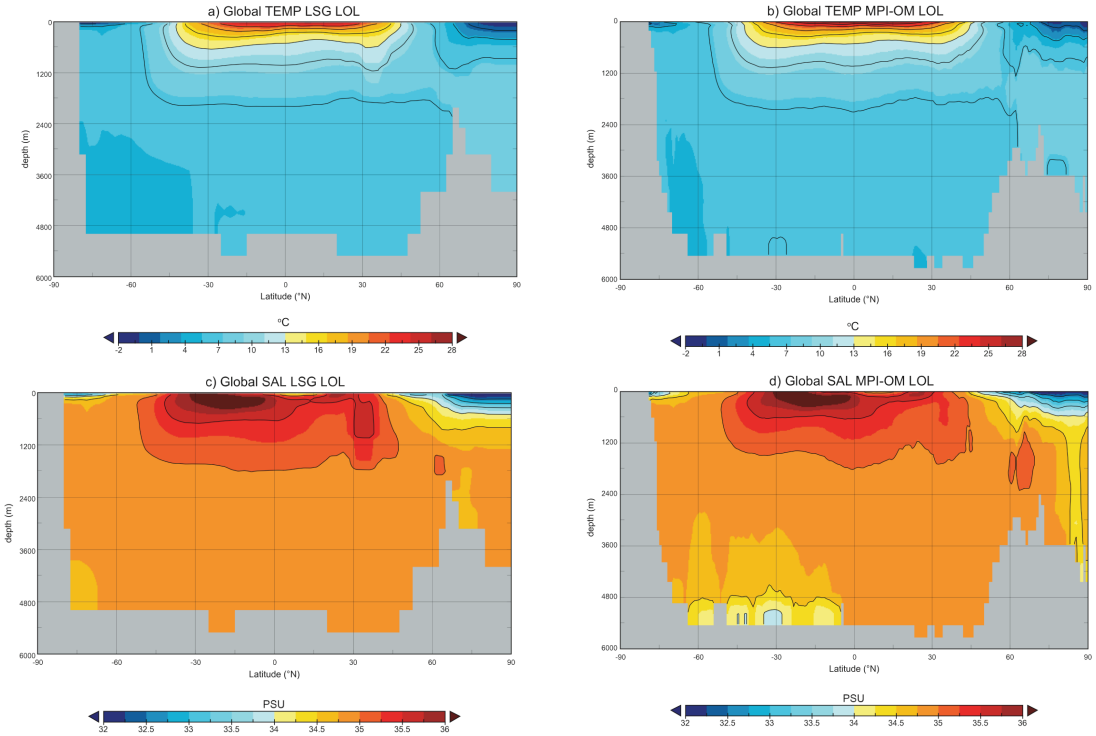

Figure 4.3: The zonally-averaged annual mean temperature (TEMP) and salinity (SAL) modelled by LSG (a and c, respectively) and the same quantities modelled by MPI-OM (b and d, respectively) for the Late Oligocene (LOL) experiment.

Figure 4.4 displays the zonal mean ocean temperature difference between the LOL and the EOC experiments modelled by the MPI-OM. Negative values are recognizable in the SO, denoting lower ocean temperatures in that region when the DP is open (LOL) with respect to the case with DP closed (EOC). Near the coasts of Antarctica temperatures decrease up to 2°C as a result of the change in the ocean circulation caused by the opening of the Drake Passage. In the rest of the global ocean the anomalies are mostly positive, especially in the equatorial region. This is due to the different global ocean circulation with reduced southward heat transport in the LOL experiment.

Figure 4.5 shows the zonally integrated mass transport stream function, which is an indication of the global MOC, for the EOC (a) and LOL (b) experiments modelled by the LSG model (Butzin, pers. comm.). The figures show that in both experiments NADW formation ceases. While there is still some NADW production in LOL (maximum flux of about 5 Sv), NADW formation in EOC is virtually zero. The reduction/shutdown of NADW formation is caused by the open Panama Gateway connecting the Atlantic and the Pacific Oceans. In both cases the Southern Hemisphere displays a large cell of negative stream flow, which indicates enhanced formation of deep and bottom water masses (proto-AABW) in the Southern Ocean. The upper limb of this southern MOC cell is associated with enhanced southward transports of mass and heat in the upper levels. This feature is more pronounced in EOC than in LOL, which reflects the effect of the closed Drake Passage in EOC. There is a clear difference in the Southern Ocean (SO) region, between 50°S and 60°S. In the EOC experiment the MOC values are mainly negative, indicating a southward transport of water mass. A shallow positive cell in the near surface flow represents a northward flow of water masses with a return flow at about 500 m depth. The dominating feature is a negative circulation cell, which transports heat and water masses from the open Panama Gateway at intermediate depth to the south. On the other hand, in the LOL experiment, the area of positive values increases. After the opening of the DP, northward flow in the SO enhances and stretches in a positive circulation cell to the depth. The southward return flow diminishes and reaches only up to 50°S.

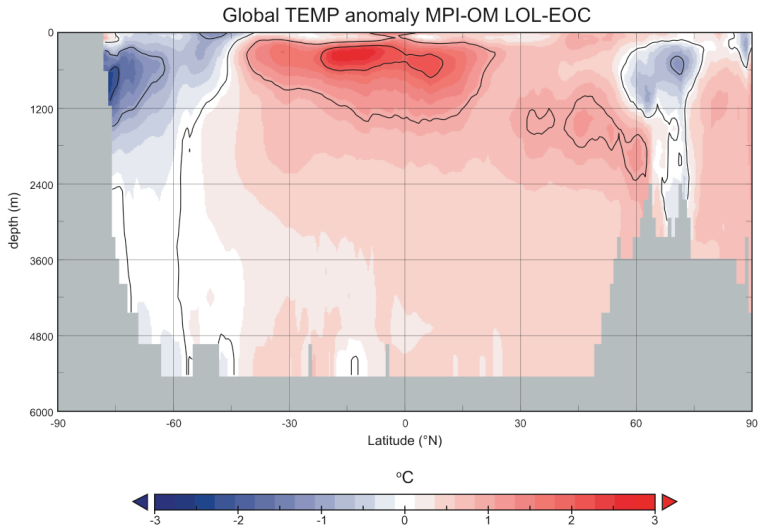

Figure 4.4: Zonal-mean ocean temperature difference between the LOL and the EOC experiments performed by MPI-OM.

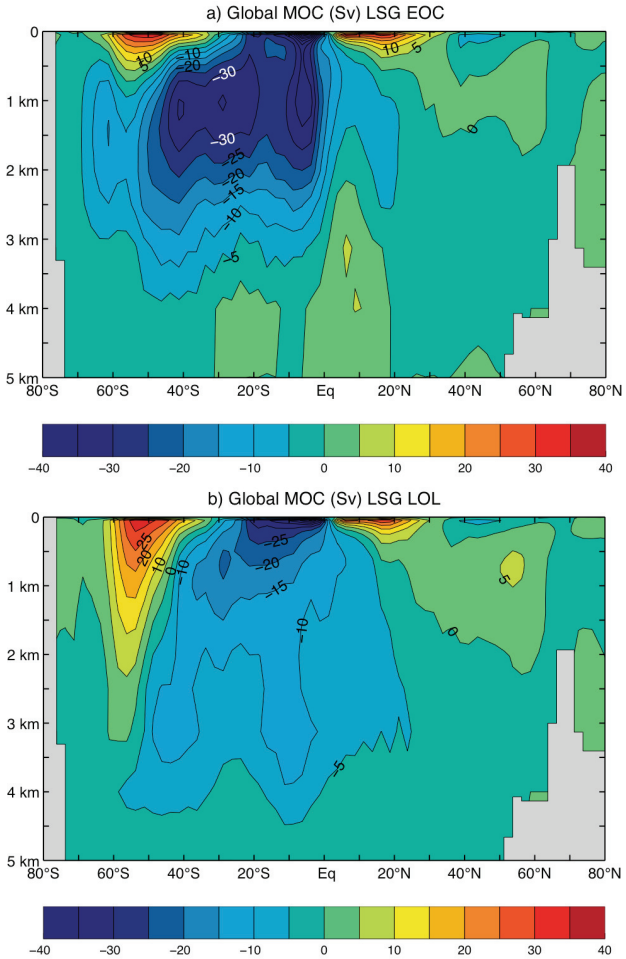

Figure 4.5: The Late Eocene (EOC, a) and Late Oligocene (LOL, b) meridional overturning circulation (MOC) modelled by LSG (Butzin, pers. comm.).

Figure 4.6 shows the annual mean sea surface temperature (SST) around Antarctica modelled by the MPI-OM in COSMOS for the EOC (a) and LOL (b) configurations and the anomalies between the two (LOL-EOC, c). With both configurations the SST exhibit positive absolute values with latitudinal dependence (panels a and b). Looking at the sea surface temperature (SST) anomalies between the two runs with open and with closed DP (LOL and EOC, respectively, Fig. 4.6c) two opposite areas are visible: a markedly negative in the Atlantic sector of the Southern Ocean and a positive, but with lower absolute values, near the coasts of South America. The pattern of the anomaly is caused by the different global ocean circulation in the two cases and is related to the ocean temperature patterns in the Southern Atlantic and in the Southern Pacific oceans. In none of the experiments sea-ice is detected. This is due to the warm SST, which, also in winter, is higher than the seawater freezing point (about -1.9°C).

The surface atmospheric temperature (SAT) anomalies between the LOL and the EOC COSMOS experiments are shown in Figure 4.7a. The opening of the gateway is associated with a mean decrease of the SAT of 0.4°C over the whole continent. This is related to the different SST field, as can be seen by comparing the pattern to Figure 4.6c, and it denotes the direct link between the ocean and the atmospheric temperatures. Figure 4.7b displays the net precipitation (P-E) anomalies between the two experiments. Values over the continent are very small but a slightly negative pattern is recognizable, meaning that the precipitation is lower in the LOL experiment. In the EOC experiment the warmer temperature produces higher moisture, especially over the ocean, and therefore also the precipitation is a little larger (0.1 m/y). The pattern of the P-E anomalies is clearly related to the ones of the SAT and of the SST, as can be seen comparing Figure 4.7b to Figure 4.7a and Figure 4.6. Finally, Figure 4.7c shows the 10 m wind velocity anomalies between the two COSMOS runs with open (LOL) and closed (EOC) DP. The anomalies are only positive, meaning that in the LOL experiment the ACC is fully established and has an impact on the above atmospheric circulation. It creates a temperature gradient in the atmosphere, which produces a vortex over Antarctica. This generates a barrier, which isolates the continent climatically. The highest anomalies in both strength and direction of the winds are found over the DP and in the Indo-Pacific sector. They explain the pattern of the SAT and of the P-E, due to the whirlwind around Antarctica produced by the ACC.

In Figure 4.8 the zonal mean u-velocity for the EOC (a) and LOL (b) COSMOS experiments is plotted, as well as the anomalies between the two (c). In both of the cases the highest velocities are found in the tropopause (ranging between the altitude of about 11 km and 17 km) in the Northern and Southern Hemispheres at a latitude of about 45°N(S). The highest velocity is 50 m/s between the 4^{th} and the 8^{th} model levels. The intensity of the jets depends on the temperature gradient between the atmospheric layers and between the Tropics and the Poles. The Northern Hemisphere jet is weaker than the Southern Hemisphere one because of the more complex topography, which obstructs the wind flow. Looking at the Southern Hemisphere, it can be seen that the jet stream is stronger in the LOL experiment, i.e. when the DP is open. This is due to the ocean and atmospheric temperature gradient between the Tropics and the South Pole. Indeed, when the DP is open (LOL configuration) there is a higher SST and SAT gradient in the southward direction, because of the reduced heat transport.

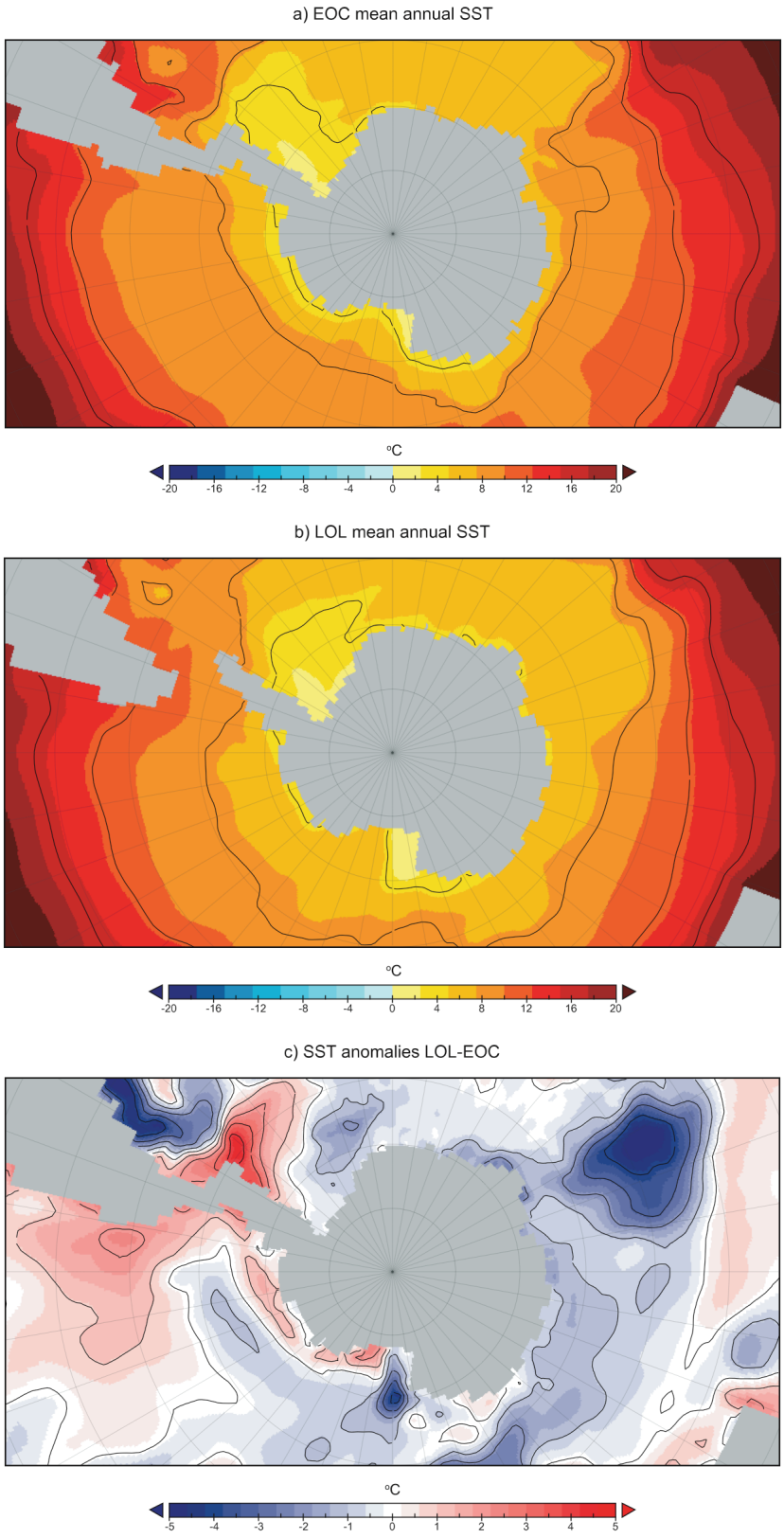

Figure 4.6: Annual mean sea surface temperature (SST) modelled by the MPI-OM for the EOC (a) and LOL (b) configurations and difference between the two (LOL-EOC, c).

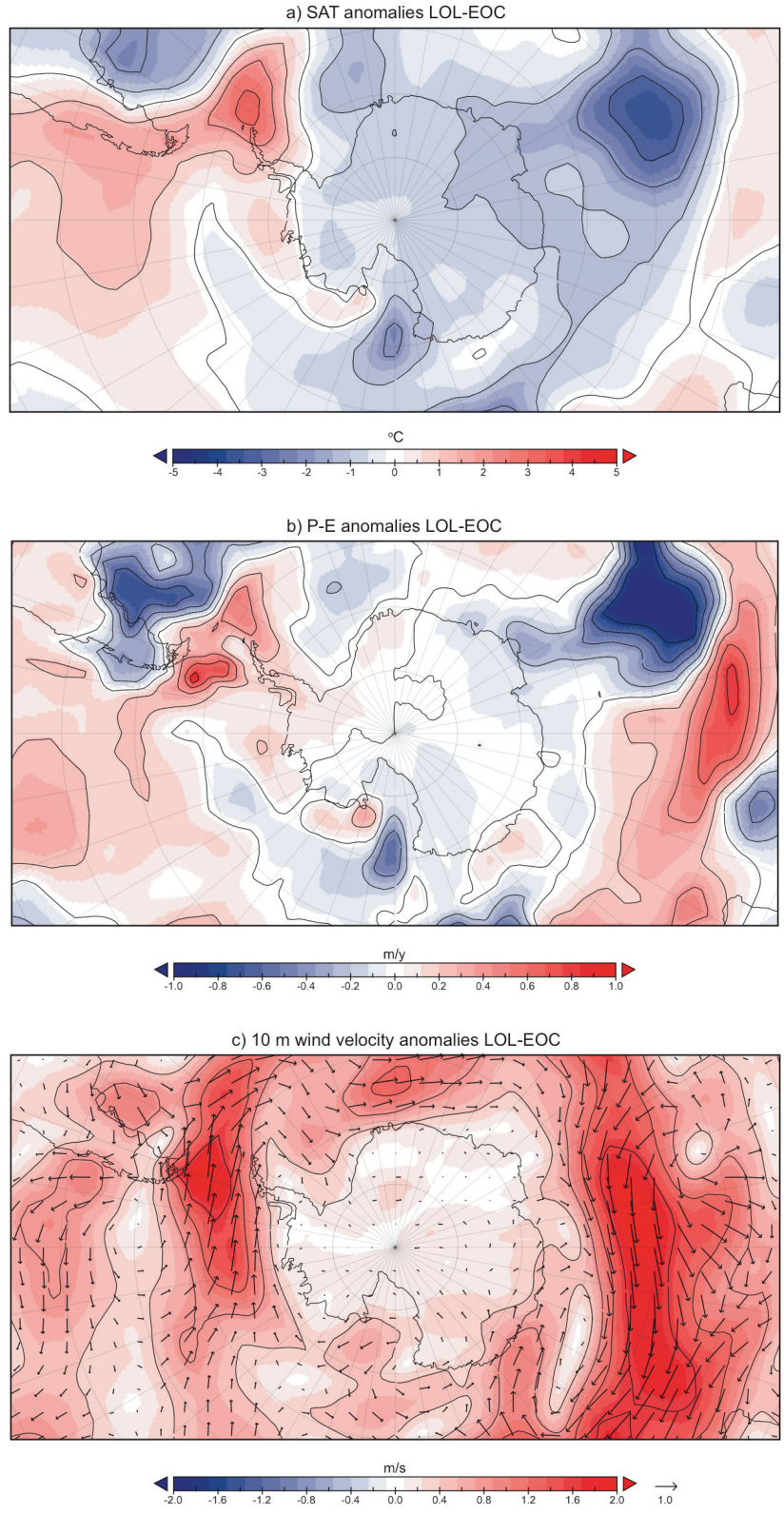

Figure 4.7: Annual mean surface atmospheric temperature (SAT, a), net precipitation (P-E, b) and 10 m wind velocity (c) anomalies between the two COSMOS experiments with open (LOL) and closed (EOC) Drake Passage.

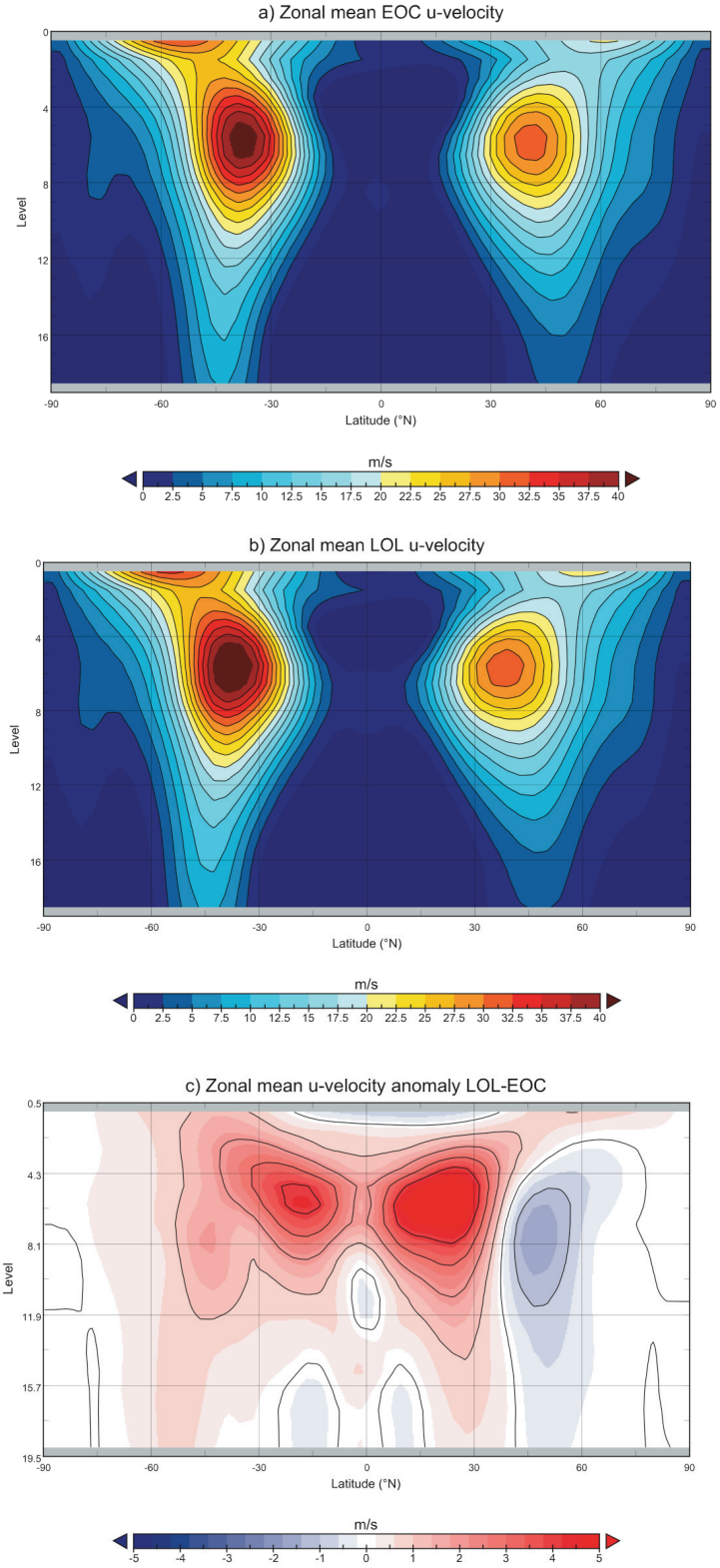

Figure 4.8: Zonal mean u-velocity for the EOC (a) and LOL (b) COSMOS experiments and anomalies between the two (c).

The AIS volume at the end of the EOC experiment is $7.7 \cdot 10^6$ km^3 and at the end of the LOL experiment is $9.26 \cdot 10^6$ km^3. The difference between the ice volume achieved in the two cases is therefore $1.56 \cdot 10^6$ km^3. The two distinct land configurations and the subsequent ocean circulations cause different climatic conditions even if other important constraints, such as the atmospheric carbon dioxide and the orbital configuration, are common in both experiments. The opening of the DP produces an additional growth of the AIS volume of about the 20% more than in the case of a climate state given with closed DP.

Figures 4.9 and 4.10 show the final AIS surface elevation (a) and ice thickness (b) for the two experiments EOC and LOL, respectively. In both cases ice develops only in East Antarctica and, even if in some locations it expands to the coast, it remains limited to the continent. The ice cap develops around the Gamburtsev Mountains and its flow to the western continent is constrained by the Transantarctic Mountains. The higher elevations of that region are not covered by ice. No ice cap overlays the islands of West Antarctica or the Antarctic Peninsula, which remain unaffected. Higher values of both surface elevation and ice thickness are found in the case of opened DP (LOL experiment), due to the colder temperatures over the continent. A bigger ice cap develops around the higher elevations in the inner continent, where the temperature is lower.

Figure 4.11 shows the differences in the Antarctic surface elevation (a) and ice thickness (b) between the LOL and the EOC experiments. An increase in area covered by ice sheets and of the ice thickness itself is detectable in the LOL experiment compared to the EOC. In equilibrium with the EOC climate Antarctica reaches a maximum surface elevation of 3290 m, whereas it reaches a maximum surface elevation of 3470 m in the LOL experiment. The modelling results exhibit the substantial difference between the two continental ice sheets originated by the climate states with open and closed DP. The anomalies are mostly positive for both the surface elevation and the ice thickness and more pronounced along the margins of the ice sheet, due to the difference in the extension of the ice-covered area and in the central sector where the ice sheet broadens from the Gamburtsev Mountains.

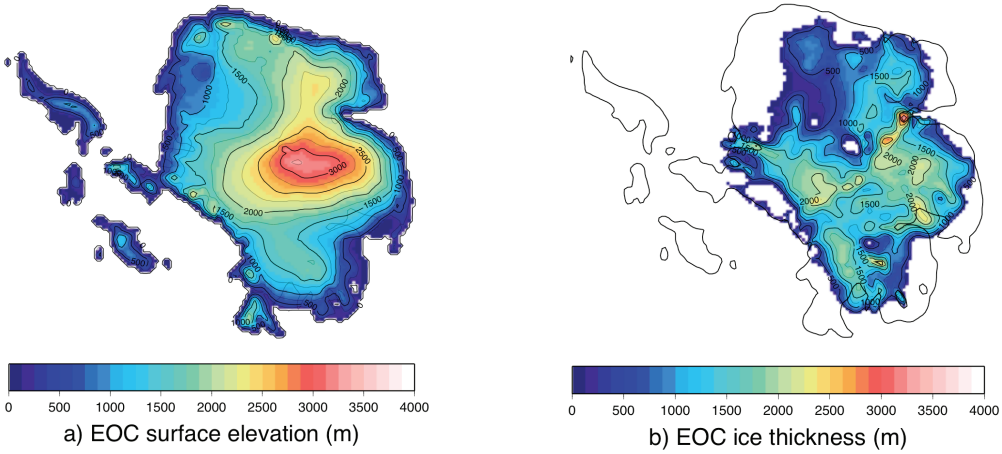

Figure 4.9: Antarctic surface elevation (a) and ice thickness modelled by the iteratively coupled COSMOS-ISM for the EOC experiment.

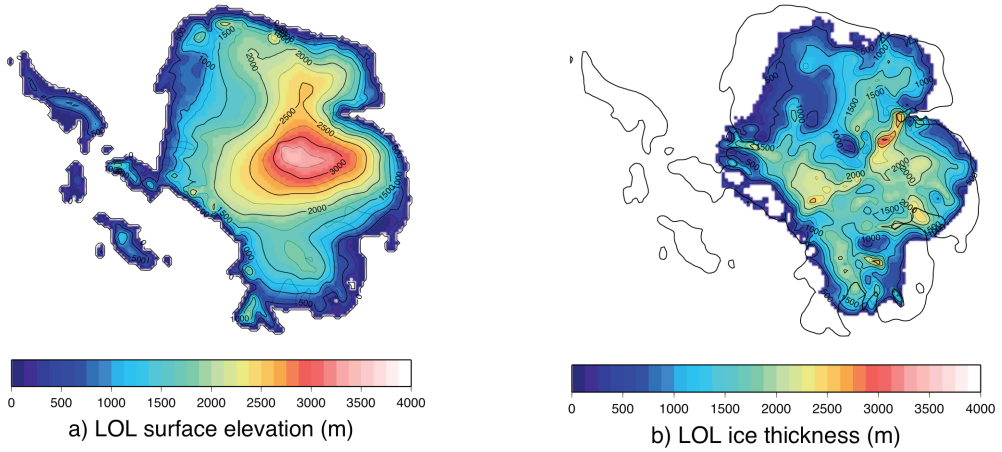

Figure 4.10: Antarctic surface elevation (a) and ice thickness modelled by the iteratively coupled COSMOS-ISM for the LOL experiment.

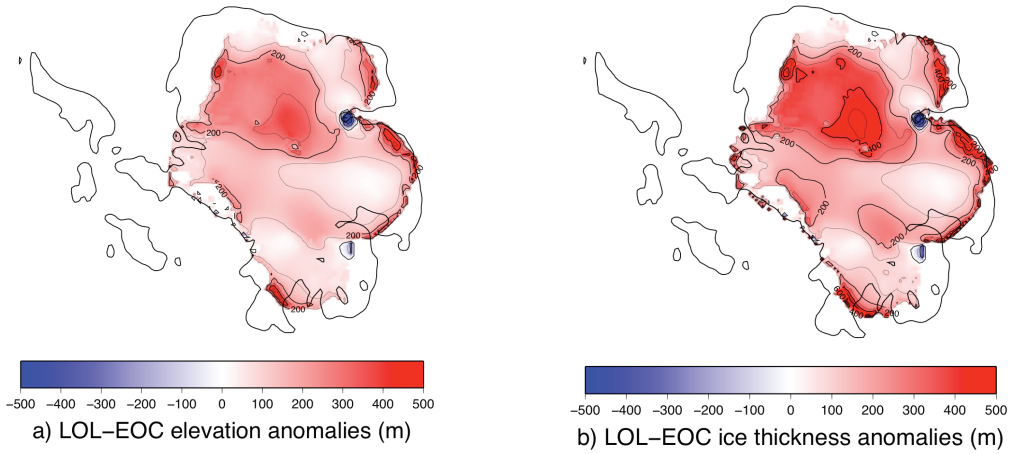

Figure 4.11: The Antarctic surface elevation (a) and ice thickness (b) anomalies at the equilibrium between the cases of Drake Passage open (LOL) and closed (EOC).

4.3 Summary

In this chapter the impact of the opening of the Drake Passage, between Antarctica and South America, and the subsequent establishment of the ACC on the formation of a continental ice sheet on Antarctica has been examined.

The analysis performed here was not directed at producing the exact climate states of the Late Eocene and of the Late Oligocene. Instead the interest was to explore the effect of different tectonic configurations, through their respective ocean circulations, on the evolution of the AIS. The major difference between these climate conditions, simulated via sequential model runs up to an equilibrium, is given by the different global topography, which in one case is similar to the Late Eocene (called EOC) and in the other to the Late Oligocene (called LOL). Result of the distinct land-sea distributions is the development of differing oceanic circulations and the consequent establishment of the ACC. Other climate bounds, like the orbital configuration and the atmospheric greenhouse gases concentration, are constant in the two experiments.

The AIS obtained, its covered area as well as its volume, are larger in case of LOL tectonic configuration than in case of EOC tectonic configuration. This is the result of a substantial change in the meteorological fields (surface temperature and precipitation) associated with the ocean flows. If the DP is open and the ACC fully established, the atmospheric circulation is affected too, and this results in a colder climate, which favours the growth of ice. In case of a closed DP, the precipitation is moderately higher due to the larger amount of air moisture from the ocean. However, the warmer temperature prevents the formation of an ice sheet of the same size as the one created when the DP is open.

The essence of this experiment is the demonstration of the interaction between the various climate sub-systems and the consecutive relationship between the processes linking them. Different tectonic configurations (land) produce different oceanic temperatures (ocean), which in turn cause distinct meteorological fields (atmosphere) and therefore force the AIS differently (cryosphere).

Chapter 5

Sensitivity of the Late Eocene Antarctica to atmospheric pCO_2

The hypothesis, stating that the AIS growth could be triggered by a climate response to declining pCO_2 in combination with a planetary orbital configuration that favoured accumulation of annual snow, is investigated in this chapter. The climate - ice sheet modelling approach is applied to examine the response of East Antarctica under Late Eocene global tectonic configurations and different atmospheric carbon dioxide (CO_2) concentrations. Four sensitivity experiments with different pCO_2 and using Late Eocene tectonic configuration and ocean temperature yield insights into the global climate and AIS behaviour under different pCO_2 levels.

5.1 Experimental set-up

This set of experiments is designed to study the origination of an AIS under different atmospheric pCO_2 concentrations and Late Eocene tectonic boundary conditions. Four sensitivity experiments have been performed using a fixed Late Eocene global tectonic configuration and a fixed advantageous orbital configuration yielding the coldest austral summers. The only difference between the experiments is given by the pCO_2 levels applied: $8\times CO_2$ (2240 ppm), $4\times CO_2$ (1120 ppm), $2\times CO_2$ (560 ppm) and $1\times CO_2$ (280 ppm). These specific carbon dioxide levels are motivated by estimates of the atmospheric CO_2 content obtained by proxy data (e.g., Zachos et al., 2008 and references therein). Alkenones record suggests that the pCO_2 could have been higher than 2000 ppm in the last phase of the Eocene and successively decreased to modern pre-industrial values.

The Late Eocene land-sea distribution, constructed from the modern one and common in all the sensitivity experiments, is shown in Figure 4.1a. The topography includes an ice-free Antarctic continent. The Antarctic bedrock elevation is isostatically relaxed after the removal of the ice sheet (Fig. 3.2), converted and included in COSMOS global orography. The surface background albedo of the ice-free Antarctica is set at the global mean value 0.3. All the remaining initial and boundary conditions for COSMOS are constructed from the modern ones on the different land-sea mask.

As summer temperature is the biggest limitation to ice sheet initiation, an orbital configuration producing the coldest Austral summer has been applied (minimum obliquity, maximum eccentricity, and aphelion corresponding to austral summer) in order to facilitate the coldest possible conditions and hence accumulation of snow on the continent. An advantageous orbital configuration has often been brought as precondition for widespread continental glaciation (see review in Coxall and Pearson, 2007).

Figure 5.1 shows schematically the modelling procedure applied to this experiment. The ocean model MPI-OM is initialized by a 10 ky spin-up run of the three-dimensional ocean model LSG, which uses the same EOC land-sea distribution as included in COSMOS (Fig. 4.1a) and present-day background climate. During the 50 years-long COSMOS runs, atmosphere and ocean exchange the heat and momentum fluxes every day of integration and the deep ocean temperature and salinity are restored to their initial values as explained in Chapter 3. The outcoming net precipitation and surface atmospheric temperature are averaged over the last 30 years and used to force the ISM. For each pCO_2 level, the ISM runs first for 10000 years (10 ky), i.e. for the first phase of ice growth, and for 100 ky, i.e. to reach a quasi steady state.

In Table 5.1 a summary of the experiments performed, with their denomination and schematic description, is given.

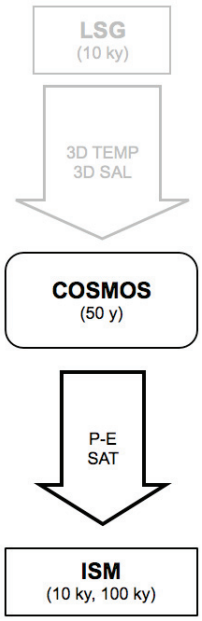

Figure 5.1: Flow-chart of the modelling procedure applied to the pCO_2 sensitivity experiments.

Table 5.1: Summary of the pCO_2 sensitivity experiments performed.

Name of the experiment	Description
EO_8CO2_cold	Experiment with: • EOC land-sea distribution (Fig. 4.1a); • ocean temperature and salinity L4-40 restored to LSG run with EOC land-sea distribution; • pCO_2 of 2240 ppm (8 times the pre-industrial level); • orbital configuration yielding the coldest austral summer.
EO_4CO2_cold	Experiment with: • EOC land-sea distribution (Fig. 4.1a); • ocean temperature and salinity L4-40 restored to LSG run with EOC land-sea distribution; • pCO_2 of 1120 ppm (4 times the pre-industrial level); • orbital configuration yielding the coldest austral summer.
EO_2CO2_cold	Experiment with: • EOC land-sea distribution (Fig. 4.1a); • ocean temperature and salinity L4-40 restored to LSG run with EOC land-sea distribution; • pCO_2 of 560 ppm (2 times the pre-industrial level); • orbital configuration yielding the coldest austral summer.
EO_1CO2_cold	Experiment with: • EOC land-sea distribution (Fig. 4.1a); • ocean temperature and salinity L4-40 restored to LSG run with EOC land-sea distribution; • pCO_2 of 280 ppm (the pre-industrial level); • orbital configuration yielding the coldest austral summer.

5.2 Results

5.2.1 Climate

Figure 5.2 shows the anomaly in the mean annual sea surface temperature (SST) modelled by the MPI-OM in COSMOS for the experiments with the highest pCO_2 (EO_8CO2_cold) and with the lowest pCO_2 (EO_1CO2_cold), whereas the absolute values for the different sensitivity experiments with the various atmospheric pCO_2 levels are plotted in Figure 5.3: $8\times CO_2$ (2240 ppm, a), $4\times CO_2$ (1120 ppm, b), $2\times CO_2$ (560 ppm, c) and $1\times CO_2$ (280 ppm, d). The anomalies (Fig. 5.2) are mostly positive, more evident along the coasts of West Antarctica, especially in the western Weddell Sea, and over the Southern Ocean at lower latitudes. The west-wind drift zone remains unaffected and experiences slight cooling in the Indian Ocean sector, possibly resulting from increased upwelling. The difference in the SST between the two extreme cases in these locations reaches up to 2 K. In all the four cases the absolute values of the SST (Fig. 5.3) are only positive. The coldest waters (between 273 K and 275 K) are located in the Weddell Sea and around the coasts of West Antarctica. Over the ocean surrounding the continent the SST presents a latitudinal dependence, decreasing southward from low latitudes. A small decrease in the values is visible with the decrease of the pCO_2 level, especially in the areas where the lowest temperatures are situated.

In none of the experiments sea ice is detected, not even in winter. This is a consequence of the warm SST, which in all cases is higher than the freezing point of seawater (about -1.9°C, or 271.25 K, in the Antarctic region).

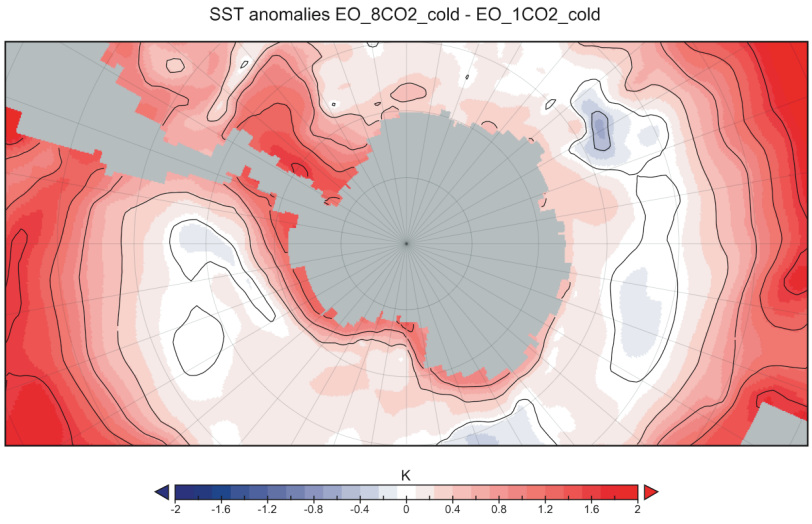

Figure 5.2: Annual mean sea surface temperature (SST) difference between the EO_8CO2_cold and the EO_1CO2_cold experiments modelled by MPI-OM in COSMOS.

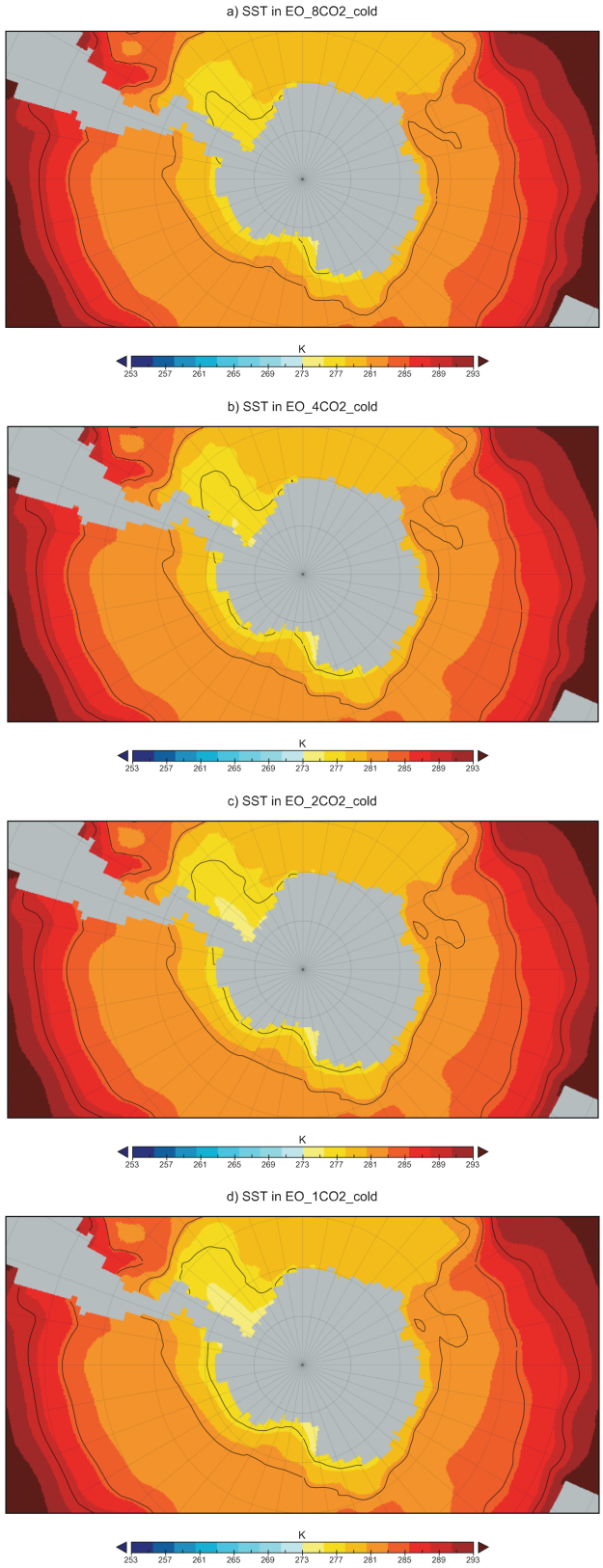

Figure 5.3: Annual-mean sea surface temperature (SST) modelled by MPI-OM in COSMOS for the different experiments with Late Eocene global tectonics and pCO_2 levels: $8\times CO_2$ (2240 ppm, a), $4\times CO_2$ (1120 ppm, b), $2\times CO_2$ (560 ppm, c) and $1\times CO_2$ (280 ppm, d).

The 30-year averaged annual-mean surface atmospheric temperature (SAT) over the Antarctic continent for the different experiments with different pCO_2 is shown in Figure 5.4. Lower pCO_2 levels are associated with lower SAT, especially in the interior of the continent. In all cases the lowest temperatures (lower than 260 K) are found in the vicinity of the Gamburtsev Mountains, at the highest elevations of the ice-free continent. The line of 273 K (0°C) expands with the pCO_2 decrease reaching the coasts of East Antarctica and extending over much of the Antarctic Peninsula. Over the ocean surrounding the continent, the SAT pattern mostly reflects the SST one (Fig. 5.2). Along the coasts, especially in the Weddell Sea, differences are most likely due to the cold winds from the continent. The annual mean surface atmospheric temperature (SAT) difference between the two extreme cases, the EO_8CO2_cold and the EO_1CO2_cold experiments is visible in Figure 5.5. The SAT anomalies present only positive values and are stronger over the continent than over the ocean surrounding it. The difference in the temperature with the pCO_2 level is also more marked in the inner areas, where values reach 5 K. In this case, different to what was found in Chapter 3, the amplification of the pCO_2 effect is not due to the ice-albedo feedback, as is this case no ice sheet or sea ice are present, but rather to the heat capacity of the continent.

The plots of the mean annual net precipitation (P-E) averaged over the last 30 years of model integration for the different experiments (Fig. 5.6) exhibit values between 0.2 m/y and 0.4 m/y water equivalent (WE) over most of the Antarctic continent, higher than the ones found for the control experiment in Chapter 3 (1 m/y WE). The precipitation increases along the coast and its pattern is very similar in the four cases. The annual mean net precipitation (P-E) difference between the two extreme EO_8CO2_cold and EO_1CO2_cold experiments is shown in Figure 5.7. The P-E anomalies present both positive and negative values. Slight positive anomalies are found over East Antarctica and the Antarctic Peninsula, whereas negative values interest mainly the areas above the ocean around the Antarctic coasts.

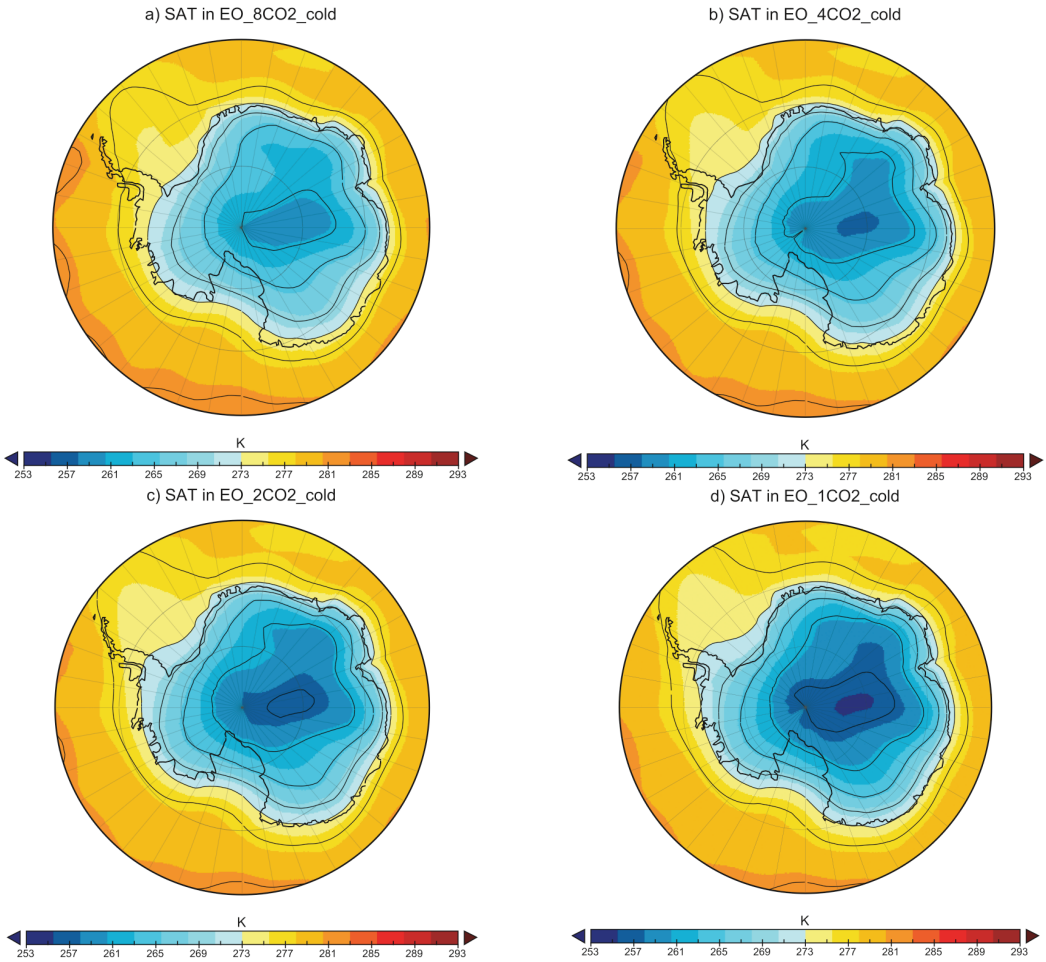

Figure 5.4: Annual mean surface atmospheric temperature (SAT) modelled by ECHAM5 in COSMOS for the different sensitivity experiments with Late Eocene global tectonics and pCO_2 levels: $8\times CO_2$ (2240 ppm, a), $4\times CO_2$ (1120 ppm, b), $2\times CO_2$ (560 ppm, c) and $1\times CO_2$ (280 ppm, d).

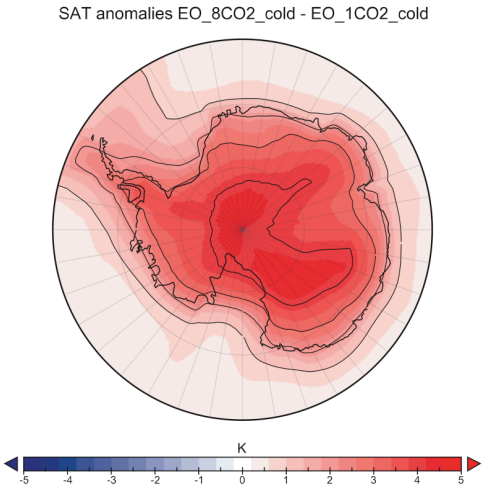

Figure 5.5: Annual mean surface atmospheric temperature (SAT) difference between the EO_8CO2_cold and the EO_1CO2_cold experiments modelled by ECHAM5 in COSMOS.

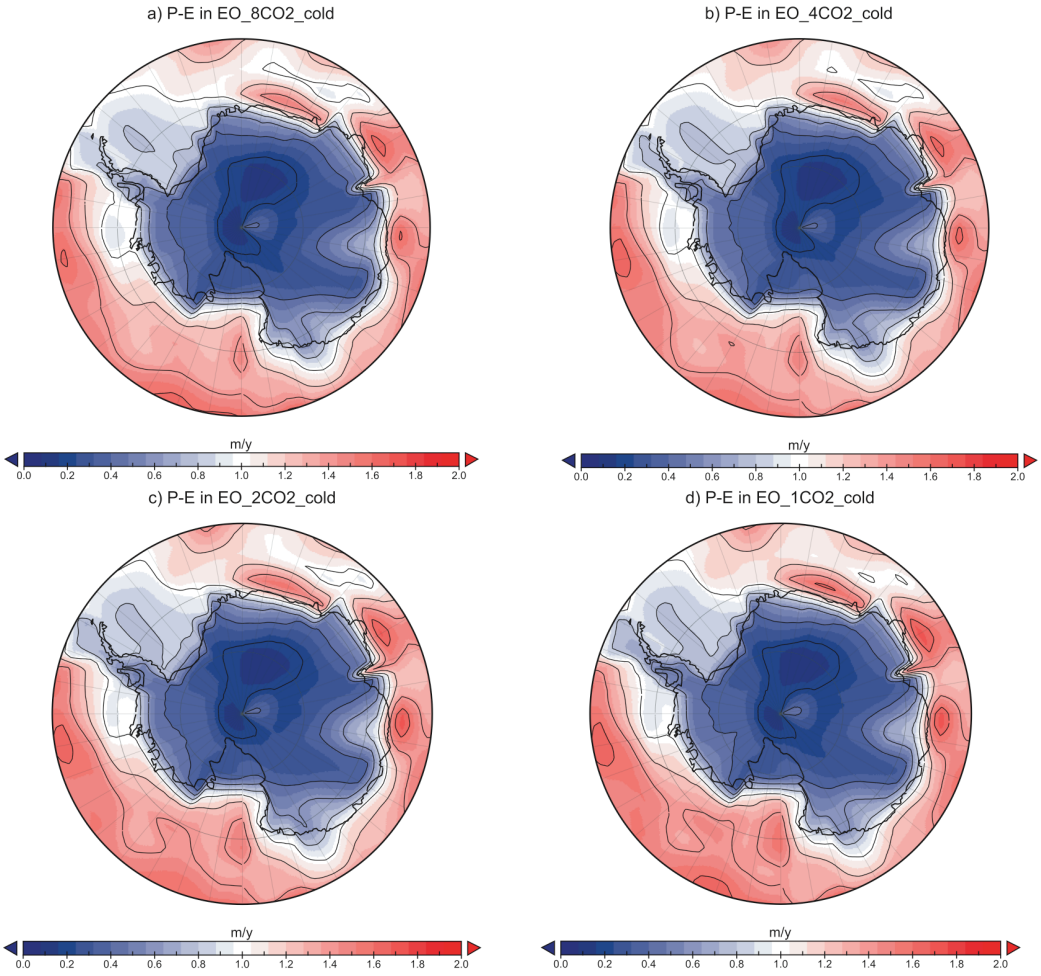

Figure 5.6: Annual mean net precipitation (P-E) modelled by ECHAM5 in COSMOS for the different sensitivity experiments with Late Eocene global tectonics and varying pCO_2 levels: $8\times CO_2$ (2240 ppm, a), $4\times CO_2$ (1120 ppm, b), $2\times CO_2$ (560 ppm, c) and $1\times CO_2$ (280 ppm, d).

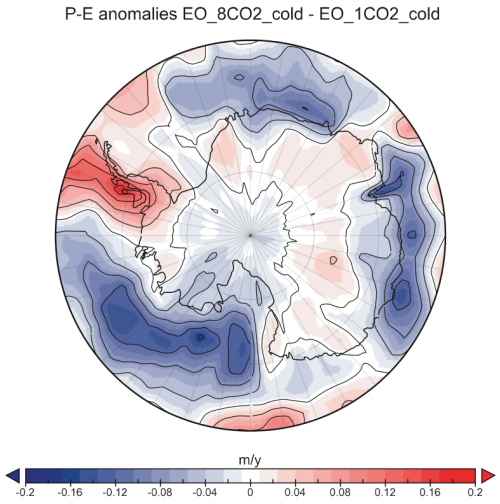

Figure 5.7: Annual mean net precipitation (P-E) difference between the EO_8CO2_cold and the EO_1CO2_cold experiments modelled by ECHAM5 in COSMOS.

In Figure 5.8a the global and Antarctic (between 60°S and the South Pole) annual-mean SAT for different carbon dioxide concentrations is shown. In both the cases, the SAT increases of 0.45 K with doubling of the pCO_2 level. The SAT difference between the two extreme cases of carbon dioxide concentrations of $8\times CO_2$ (2240 ppm) and of $1\times CO_2$ (280 ppm) is about 3 K averaged over the whole continent. As found in Chapter 3, the reason for this low climate sensitivity is the limiting effect due to restoring of the deep ocean to constant hydrography (salinity and temperature). This fixes the heat flux to the mixed layer, which is free to react to the atmospheric forcings and, therefore, to the different pCO_2 levels. It has been shown (Fig. 3.12) that the coupled climate-ice sheet model underestimates the global climate sensitivity by a factor of about 3, and by a factor of about 4 in the Antarctic region. This has to be kept in mind for a more realistic interpretation of the climate sensitivity found in this experiment. The zonal mean SAT over Antarctica for the different CO_2-experiments (Fig. 5.8b) emphasizes two important points. First, the strong SAT dependence on the latitude is clearly visible. The SAT decreases steadily about 20 K from the latitude of 60°S to the South Pole. Secondly, it shows the high polar sensitivity to the pCO_2 level. The difference in the SAT between the experiments is more pronounced poleward in the inner continent. At the South Pole the difference in the SAT between the extreme cases of 280 ppm and 2240 ppm is about 5 degrees, i.e. two degrees more than the mean difference calculated above.

In Figure 5.9a the global and Antarctic P-E for the different carbon dioxide levels is shown. In both the cases the net precipitation remains almost constant (around 1.65 m/y WE in the first case and 0.7 m/y WE in the Antarctic region, between 60°S and 90°S). This is a consequence of the fact that neither the total precipitation nor the evaporation vary markedly with the varying atmospheric CO_2 (not shown). In fact, the ocean temperature controls the evaporation, but the change in the SST consequent to the change in the pCO_2 level is quite small. Therefore no prominent change in the evaporation is resulting and, accordingly, also no substantial change in the precipitation. In Figure 5.9b the zonal mean P-E over Antarctica for the different experiments is displayed. The plot shows the poleward decrease of the precipitation for all the experiments. P-E declines from 1.4 m/y over the ocean surrounding Antarctica to 0.2 m/y in the interior of the continent. The decrease of P-E presents the same pattern for all the experiments, with small differences only on the coasts. The stepwise structure of the decrease is an artefact of the interpolation process.

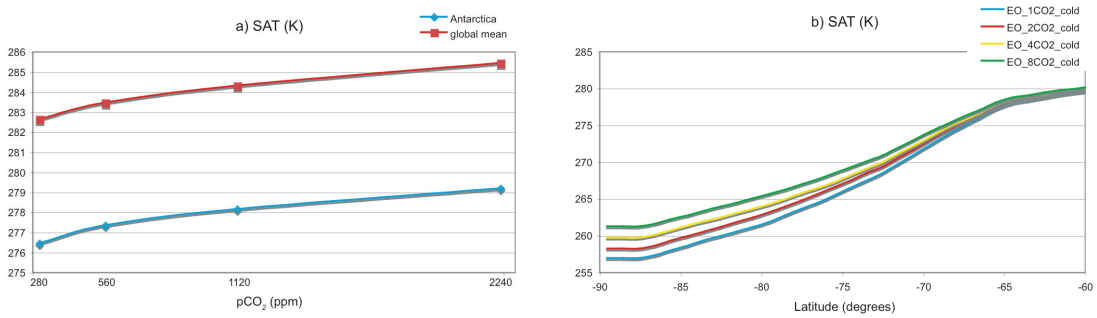

Figure 5.8: a: The global (in red) and Antarctic (in blue) annual-mean SAT modelled by ECHAM5 in COSMOS for the different experiments with various pCO_2 levels. **b:** The zonally-averaged annual mean SAT over Antarctica for the different COSMOS experiments.

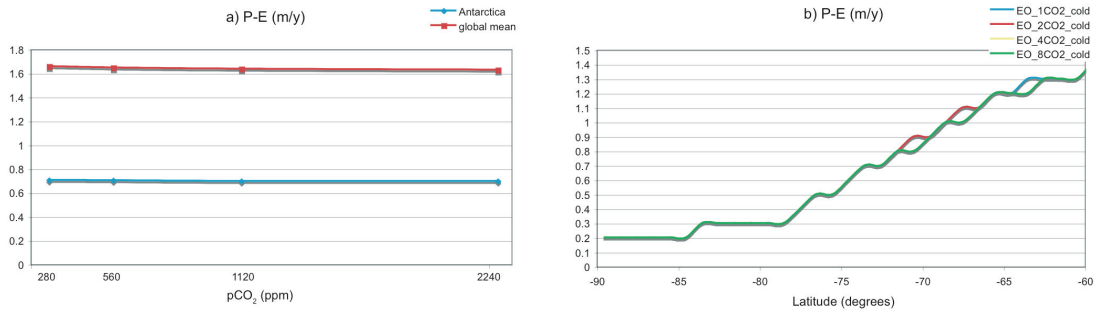

Figure 5.9: a: The global (in red) and Antarctic (in blue) annual mean P-E for the different COSMOS experiments with varying CO_2. **b:** The zonally-averaged annual mean P-E over Antarctica for the different COSMOS experiments.

Consequent to the difference in the SST and SAT for the various pCO_2, is also a change in the surface wind pattern. Figure 5.10 shows the annual mean 10 m wind difference between the two extreme cases of $8\times CO_2$ (2240 ppm) and $1\times CO_2$ (280 ppm) whereas the absolute values for the four different experiments are plotted in Figure 5.12. In all the experiments the highest wind velocities (around 8 m/s to 9 m/s) are found over the ocean surrounding the Antarctic continent, especially in the Indian sector, in the west wind drift zone. On the other hand, the lowest velocities are located along the coasts of Antarctica, where an inversion of the wind direction is also visible. Lower wind speed is also recognizable for lower pCO_2 levels in the East drift zone. The anomalies between the two extreme cases are only positive and up to 2 m/s. Regionally, the temperature gradient increases (Fig. 5.4 and Fig. 5.5) and, as a consequence, there is also an increase in the wind velocity (up to 2 m/s) and an enlargement of the wind belt itself.

For the various pCO_2 also a change in the u-velocity pattern is visible. In Figure 5.11 the zonal mean u-velocity difference between the two extreme cases with $8\times CO_2$ (2240 ppm) and $1\times CO_2$ (280 ppm) is plotted, whereas the absolute values for the four different experiments are shown in Figure 5.13. In all cases (Fig. 5.13) the highest velocities (over 50 m/s) are found in the tropopause at a latitude of about 45°N(S) in both the hemispheres. The anomalies (Fig. 5.11) show positive values (over 5 m/s) in the same areas, meaning that the u-velocity is higher for higher pCO_2 levels. Indeed, as

shown above (e.g., Fig. 5.5), higher pCO_2 values result in higher SAT. Therefore, the temperature gradient trough the atmosphere levels increases and the jet stream gets stronger.

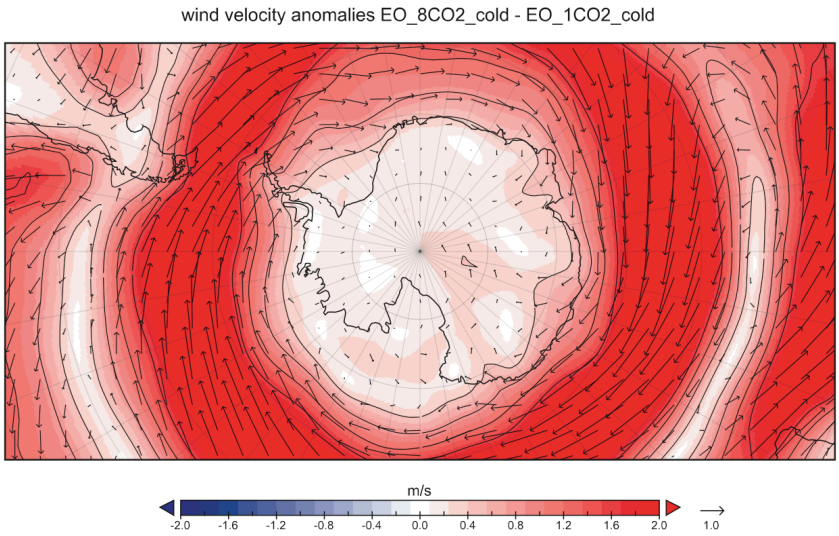

Figure 5.10: Annual mean 10 m wind velocity difference between the EO_8CO2_cold and the EO_1CO2_cold experiments modelled by ECHAM5 in COSMOS.

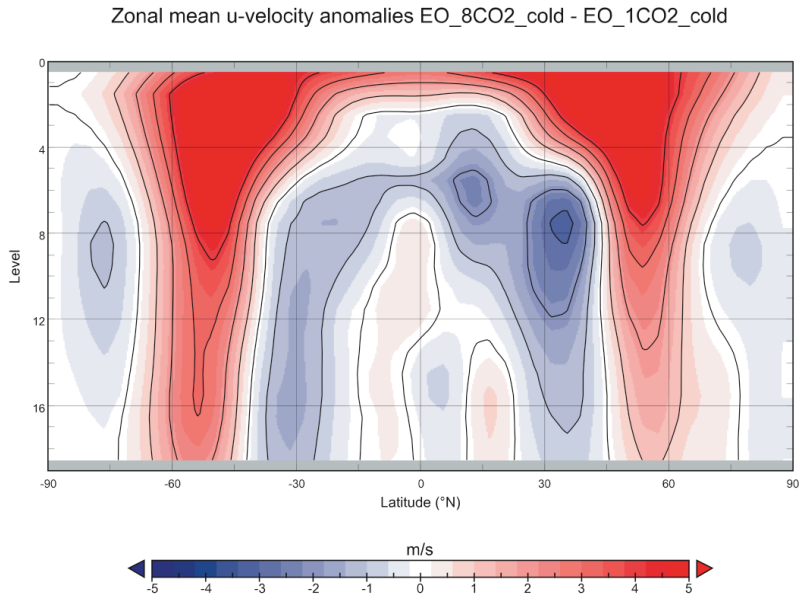

Figure 5.11: Zonal mean u-velocity difference between the EO_8CO2_cold and the EO_1CO2_cold experiments modelled by ECHAM5 in COSMOS.

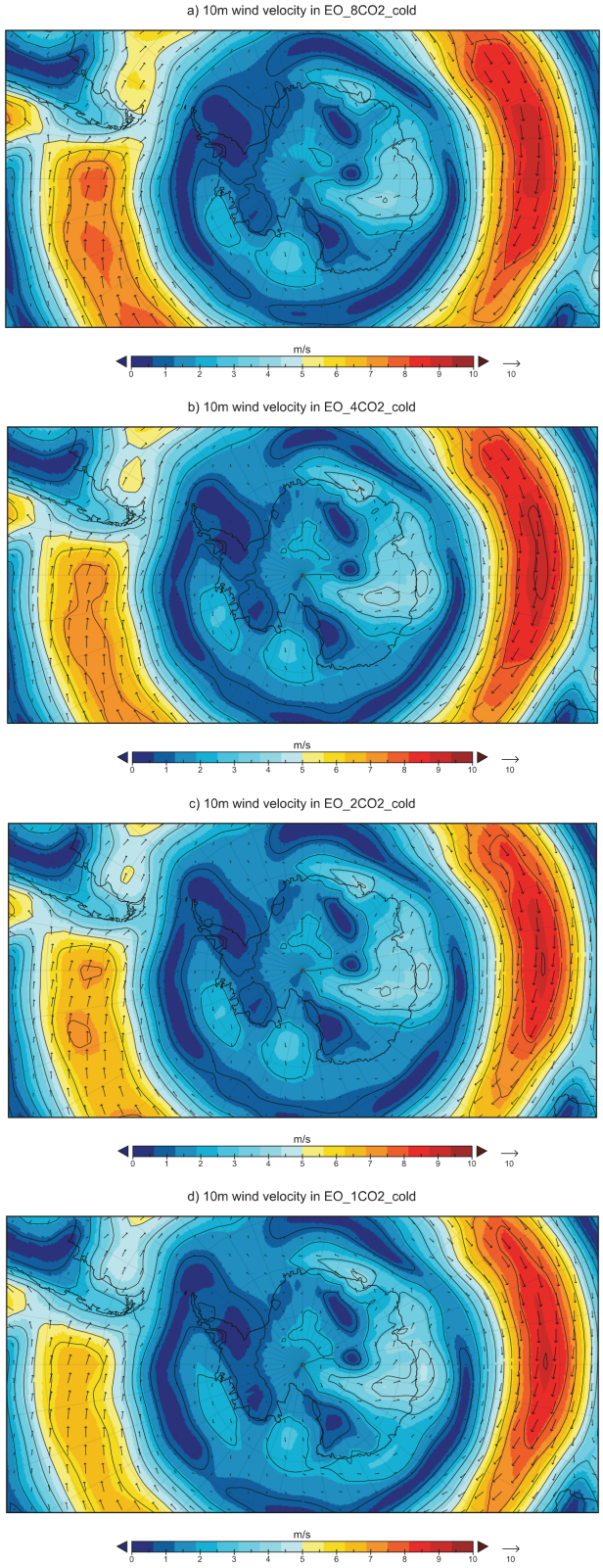

Figure 5.12: Mean annual 10 m wind velocity modelled by ECHAM5 in COSMOS for the different experiments with Late Eocene global tectonics and varying pCO_2 levels: $8\times CO_2$ (2240 ppm, a), $4\times CO_2$ (1120 ppm, b), $2\times CO_2$ (560 ppm, c) and $1\times CO_2$ (280 ppm, d).

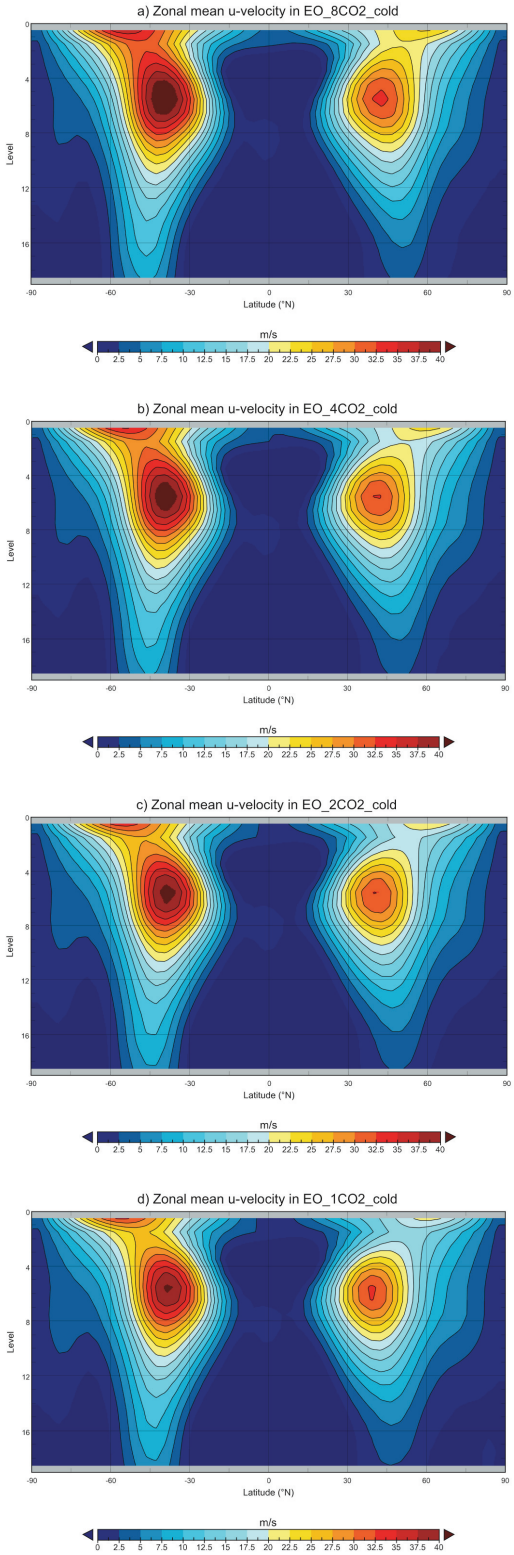

Figure 5.13: Zonal mean u-velocity modelled by ECHAM5 in COSMOS for the different experiments with Late Eocene global tectonics and varying pCO_2 levels: $8\times CO_2$ (2240 ppm, a), $4\times CO_2$ (1120 ppm, b), $2\times CO_2$ (560 ppm, c) and $1\times CO_2$ (280 ppm, d).

5.2.2 Initial phase of AIS growth

The Antarctic ice volume calculated by the ISM in the four experiments after 10 ky is shown in Figure 5.14. The plots show the evolution of the ice volume during the first 10 ky of model integration driven by invariant GCM climate forcings (SAT and P−E) obtained with the COSMOS experiments and discussed in the previous section.

Even during the first (kilo-)years of AIS initiation, the difference between the four cases is clearly visible. Under the same set-up, the smaller the amount of carbon dioxide in the atmosphere, the lower is the atmospheric temperature that forces the ISM. This results in a steeper inclination of the curve and in a larger ice volume in the first phase of the AIS growth.

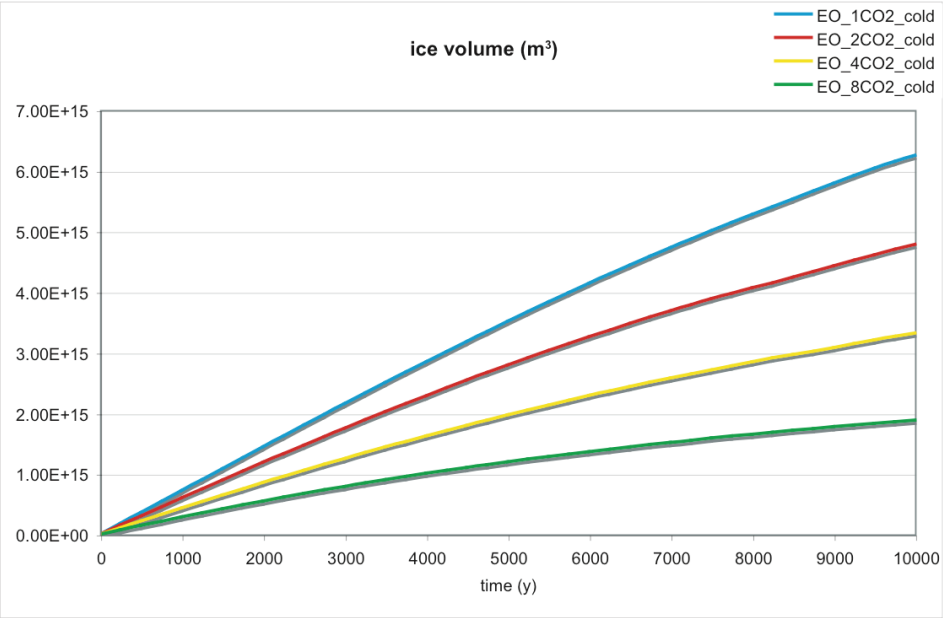

Figure 5.14: The Antarctic ice volume along the four experiments with Late Eocene global tectonics and varying pCO_2 levels $8\times CO_2$ (2240 ppm), $4\times CO_2$ (1120 ppm), $2\times CO_2$ (560 ppm) and $1\times CO_2$ (280 ppm). The different atmospheric CO_2 levels yield different progressions of the ice volume in the course of the ISM run for 10 ky.

In Table 5.2, the ice volume, the mean ice thickness and the mean surface elevation acquired after 10 ky of model integration are summarized. The difference in the ice volume achieved in the four cases is between $1.44\cdot10^6$ km and $1.47\cdot10^6$ km^3.

Table 5.2 AIS volume, mean ice thickness and surface elevation achieved after 10 ky of ISM integration for the different experiments.

Experiment	AIS volume after 10 ky (10^6 km^3)	Mean ice thickness (m)	Mean surface elevation (m)
EO_8CO2_cold	1.88	59.18	327.20
EO_4CO2_cold	3.32	104.34	363.02
EO_2CO2_cold	4.78	150.27	389.97
EO_1CO2_cold	6.25	196.53	435.04

Figures 5.15, 5.16, 5.17 and 5.18 show the Antarctic surface elevation (a) and ice thickness (b) after 10 ky of ISM integration, initiated with no ice and forced by constant climates from the different experiments.

In general the increase of the ice-covered area and of the ice thickness is evident with the decrease in the atmospheric carbon dioxide. The ice starts to grow in the inner-eastern part of the Antarctic continent favoured by the cold temperatures due to the extreme cold austral summer orbit (summer cooling). With this orbit, quite extensive higher-elevated areas remain below freezing in summer, allowing ice sheets to nucleate and expand.

At 8×CO_2 (Fig. 5.15) a small ice cap forms in East Antarctica near the Gamburtsev Mountains. The maximum ice thickness reaches 1500 m in that area and the surface elevation, given by the sum of the bedrock elevation and the ice thickness, sets at about 2750 m. Nevertheless most of the continent remains ice-free or with ice thickness lower than 250 m.

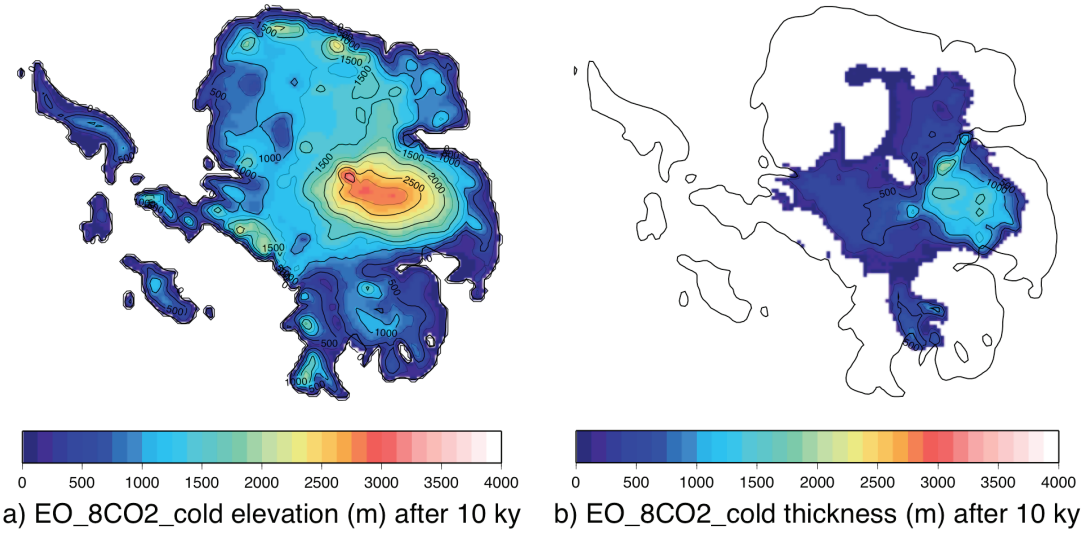

Figure 5.15: The Antarctic surface elevation (a) and ice thickness (b) after 10 ky of ISM integration for the experiment EO_8CO2_cold.

At 4×CO_2 (Fig. 5.16) the small ice cap expands and covers more than half of East

Antarctica. The majority of the continental ice presents a general thickness lower than 500 m, but the total elevation now reaches 3000 m.

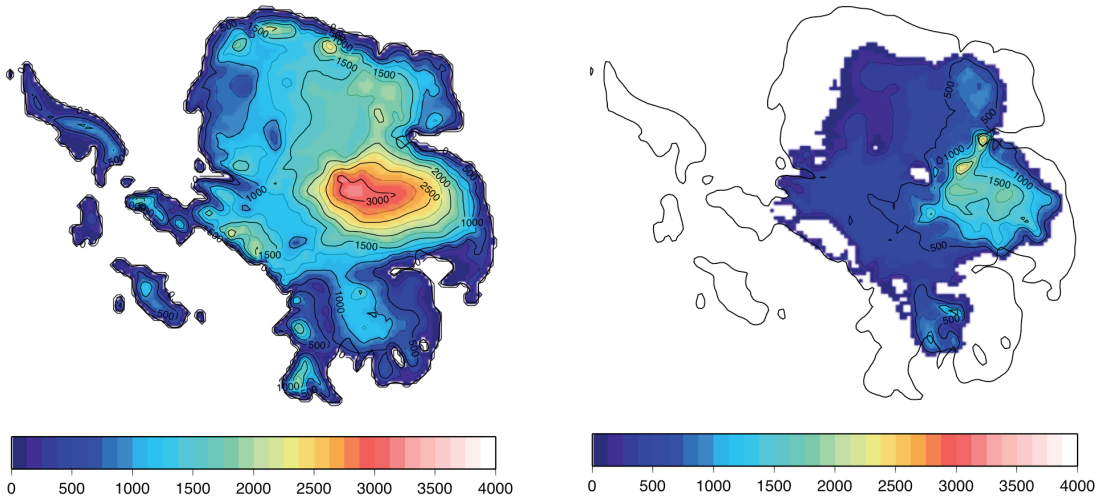

Figure 5.16: The Antarctic surface elevation (a) and ice thickness (b) after 10 ky of ISM integration for the experiment EO_4CO2_cold.

At the CO_2 level of $2\times CO_2$ (Fig. 5.17) ice covers most of the eastern region. The initial ice cap forms a sheet with mean thickness of 1500 m and overtaking 2000 m in its highest point. Other two main caps are noticeable corresponding approximately to the regions between Dronning Maud Land and Prydz Bay and the Wilkes Basin (see Fig. 1.1 for the locations).

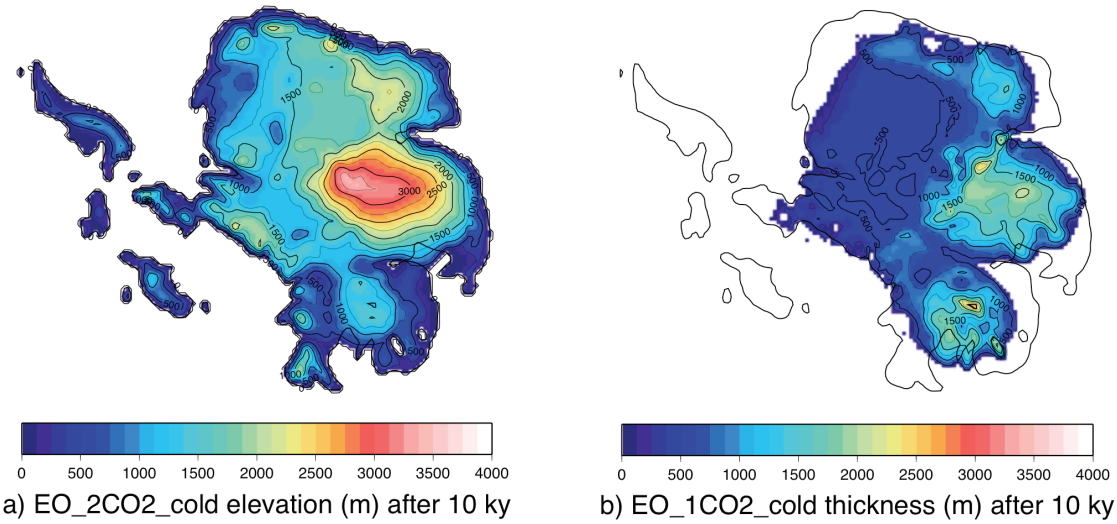

Figure 5.17: The Antarctic surface elevation (a) and ice thickness (b) after 10 ky of ISM integration for the experiment EO_2CO2_cold.

Finally, the largest ice sheet is obtained with pre-industrial carbon dioxide level ($1\times CO_2$, Fig. 5.18). Ice covers almost completely East Antarctica. Three nuclei of ice

are clearly visible, the most massive one was also present in the $8\times CO_2$ experiment. The prominent elevation of the Gamburtsev Mountains reaches 4000 m and the peaks of Dronning Maud Land are higher than 2000 m. Moreover in large parts of the covered area, the ice thickness remains under 500 m. Even if reaching the coast at several points, none of the ice sheets expands outside the continental borders and none involves the islands constituting West Antarctica and the Antarctic Peninsula.

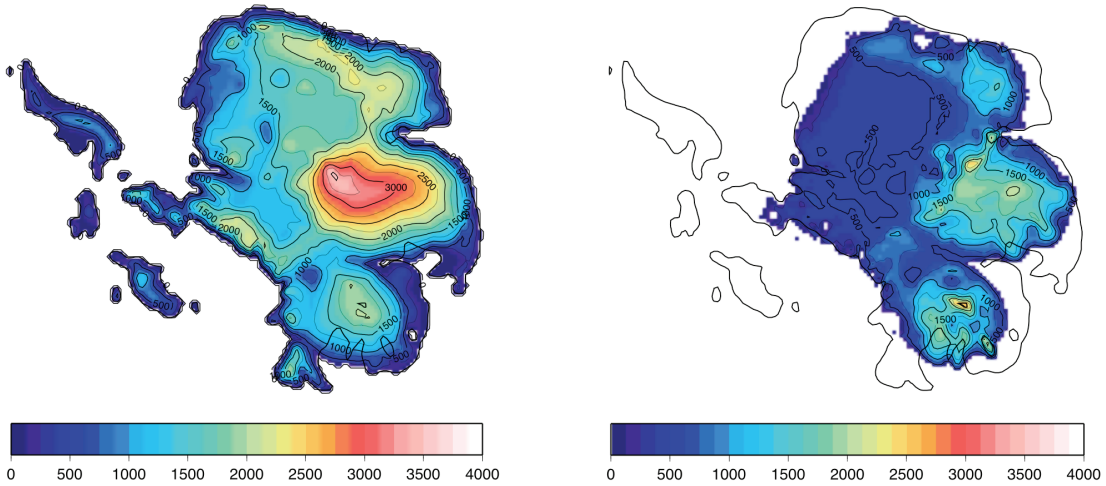

Figure 5.18: The Antarctic surface elevation (a) and ice thickness (b) after 10 ky of ISM integration with climate frocings from the experiment EO_1CO2_cold.

5.2.3 AIS steady-state with invariant climate

In order to estimate the quasi-equilibrium response of the ISM alone, longer runs (100 ky) have been performed with the ISM driven by invariant GCM climates with by different pCO_2 levels, discussed in Section 5.2.1. The Antarctic ice volume in the course of the four experiments is shown in Figure 5.19.

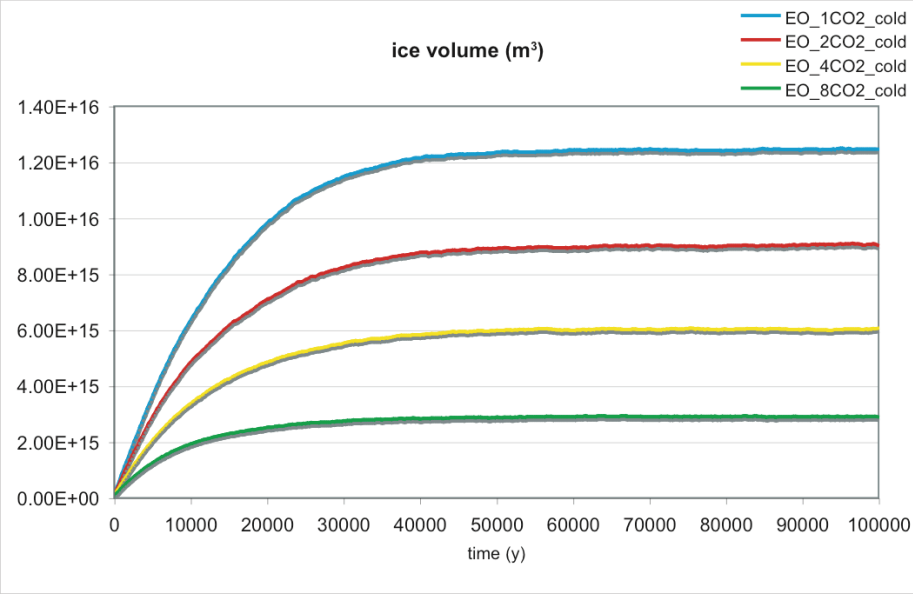

Figure 5.19: The Antarctic ice volume along the four experiments with 8×CO_2 (2240 ppm), 4×CO_2 (1120 ppm), 2×CO_2 (560 ppm) and 1×CO_2 (280 ppm). The different atmospheric CO_2 levels yield different progressions of the ice volume in the course of the ISM run for 100 ky.

Steady-state is reached after approximately 50 ky, achieving very different values of ice volumes, mean ice thickness and mean surface elevation (Tab. 5.3). Under unchanged climatic boundary conditions, the lower the concentration of carbon dioxide in the atmosphere, the larger is the ice volume formed at the steady-state. The steady-state ice volume is $2.87 \cdot 10^6$ km^3 in the case of an atmospheric CO_2 level of 2240 ppm, $6.02 \cdot 10^6$ km^3 in the case of 1120 ppm, $9.01 \cdot 10^6$ km^3 for 560 ppm and $12.40 \cdot 10^6$ km^3 for 280 ppm. Therefore, after 100 ky, the AIS reaches an ice volume that is approximately between one and a half (for 8×CO_2) and two times (for 1×CO_2) the value achieved in the first 10 ky.

Table 5.3: AIS volume, mean ice thickness and surface elevation achieved after 100 ky of ISM integration for the different experiments.

Experiment	AIS volume after 100 ky (10^6 km^3)	Mean ice thickness (m)	Mean surface elevation (m)
EO_8CO2_cold	2.87	90.26	354.80
EO_4CO2_cold	6.02	189.38	416.85
EO_2CO2_cold	9.01	283.12	481.97
EO_1CO2_cold	12.40	390.98	555.95

At 8×CO_2 (Fig. 5.20) the small ice cap found in East Antarctica after 100 ky extends further to its stable state in western direction, compared to Figure 5.15, after 10 ky. But it still remains confined in the inner eastern region.

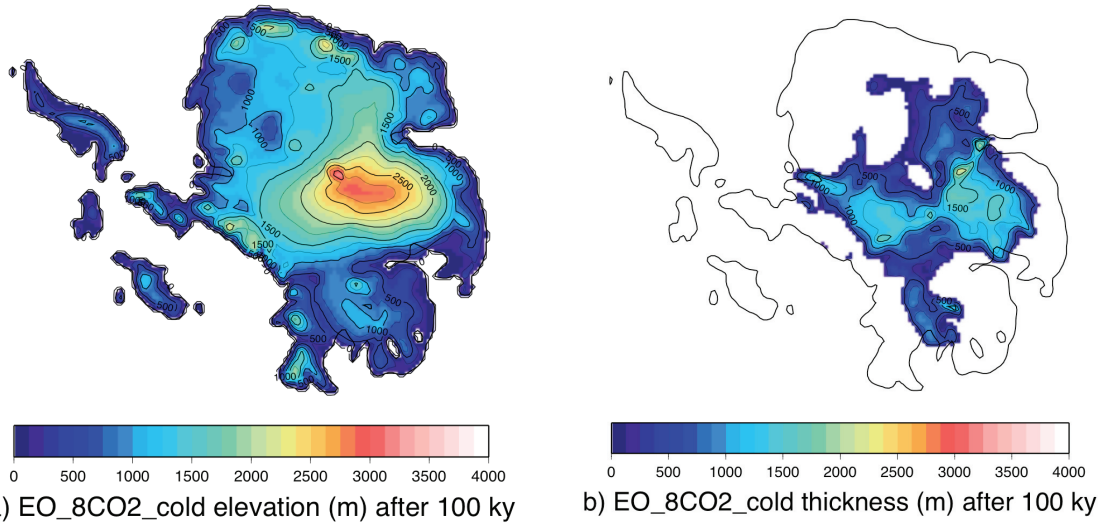

Figure 5.20: The Antarctic surface elevation (a) and ice thickness (b) after 100 ky of model integration for the experiment EO_8CO2_cold.

At 4×CO_2 (Fig. 5.21) the ice cap expands in space and altitude covering the major part of the eastern continent, but with reduced height.

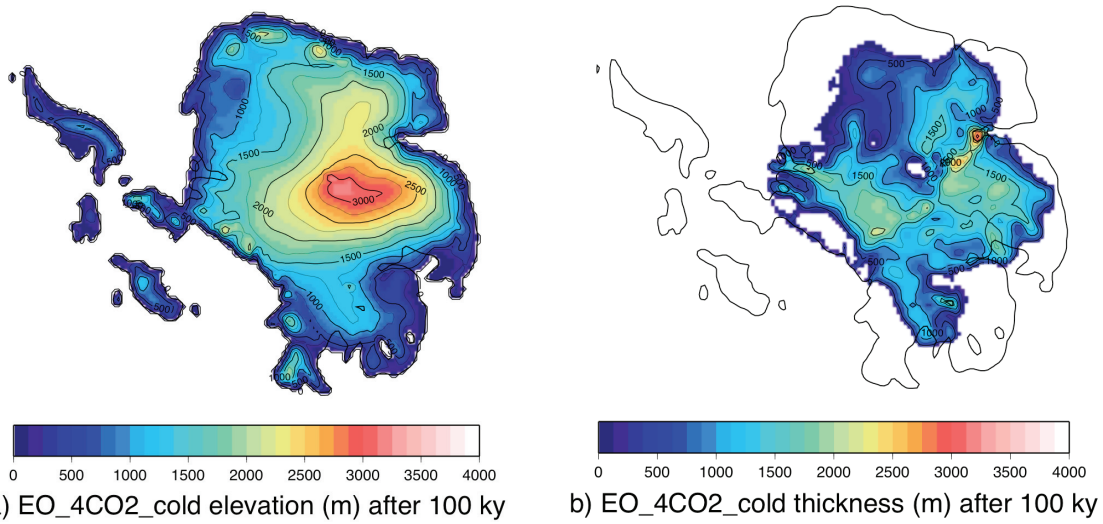

Figure 5.21: The Antarctic surface elevation (a) and ice thickness (b) after 100 ky of model integration for the experiment EO_4CO2_cold.

At steady-state reached and CO_2 level of 2×CO_2 (Fig. 5.22) ice covers almost totally east Antarctica, the highest dome surpassing 3000 m.

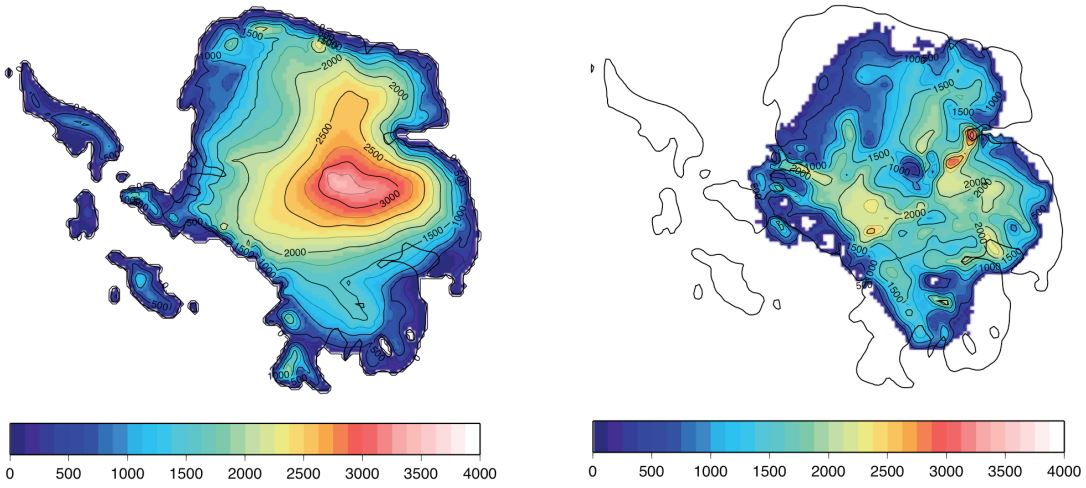

Figure 5.22: The Antarctic surface elevation (a) and ice thickness (b) after 100 ky of model integration for the experiment EO_2CO2_cold.

Lastly, the ice sheet obtained with pre-industrial pCO_2 ($1\times CO_2$, Fig. 5.23) covers almost completely East Antarctica and has a dome shape like the present-day one. The ice volume achieved in this case is about half of the modern value. The "missing" ice volume, with respect to today's AIS, concerns the coasts of east Antarctica and the entire west Antarctica and Antarctic Peninsula.

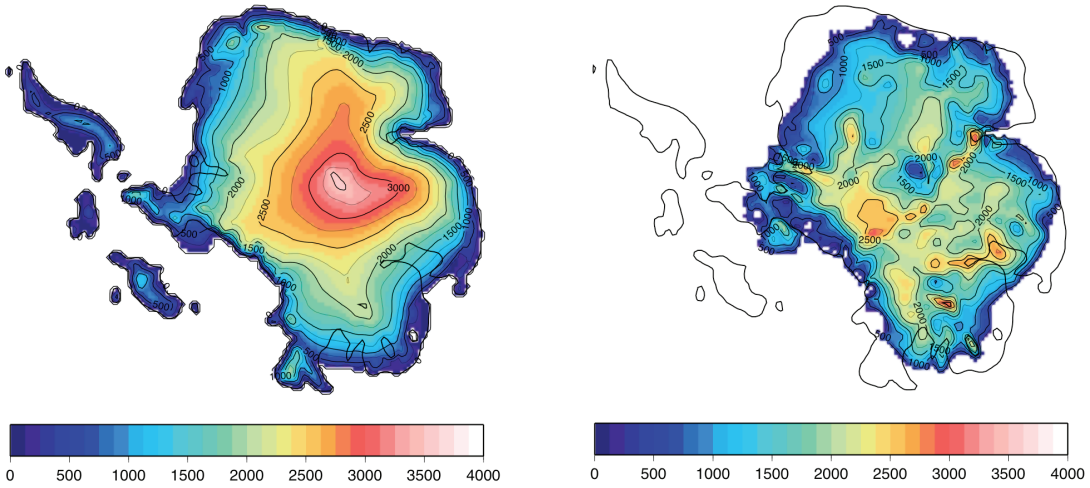

Figure 5.23: The Antarctic surface elevation (a) and ice thickness (b) after 100 ky of model integration for the experiment EO_1CO2_cold.

5.3 Summary

In this chapter the sensitivity of the Late Eocene Antarctica to different pCO_2 levels combined with an advantageous orbital configuration has been tested.

In summarizing the main findings it is worth to emphasise that this experiment was not aimed at reproducing accurately the climate of the Late Eocene and the subsequent Antarctic glaciation due to a decrease in the atmospheric carbon dioxide concentration. The intent is rather to investigate the growth of the AIS in response to distinct climate scenarios. These simulated climate states have a common set of initial and boundary conditions except for the atmospheric CO_2 level. Importantly, they all have the same Late Eocene tectonic configuration. This pseudo paleo-topography is responsible for an initialization of the world oceans yielding initial ocean temperature and salinity same for all the four experiments. An orbital configuration producing the coldest austral summer has also been applied to all the cases, in order to create favourable conditions for ice-sheet growth. Individual climate scenarios have been simulated with the above describing common boundary conditions, but with different pCO_2, namely $8\times CO_2$ (2240 ppm), $4\times CO_2$ (1120 ppm), $2\times CO_2$ (560 ppm) and $1\times CO_2$ (280 ppm).

It has been found that lower atmospheric pCO_2 is associated with lower SAT over Antarctica while P-E seems to remain constant. As a consequence, an increment in the ice sheet extension and volume has been detected. Under the same climate constraints, the smaller the amount of carbon dioxide in the atmosphere, the larger is the ice volume achieved in the first phase of the AIS growth (i.e. after 10 ky). This denotes the substantial sensitivity of the global climate and its components (atmosphere, ocean and cryosphere) to the carbon dioxide in the atmosphere not only for modern climate, as discussed in the third chapter, but also in a paleo-context. However, as found in Chapter 3, the climate sensitivity is low due to the limiting effect of the ocean salinity and temperature restoring. The coupled climate-ice sheet model underestimates the global climate sensitivity by a factor of about 3 and by a factor of about 4 in the Antarctic region. Consequently, also the climate sensitivities found in this experiment are underrated by about the same order.

The ice volume built up in 10 ky rises of nearly the same quota (about $1.46\cdot10^6$ km) each time the pCO_2 is cut to half. This could suggest a linear inverse relationship between the atmospheric pCO_2 and the ice sheet response, which should be taken as representative for such sensitivity experiments only and not as general rule, since potential non-linear feedbacks are not investigated in this analysis.

When the ISM is run for 100 ky to reach a quasi-equilibrium, the steady-state ice sheet volume increases between about one and a half (in the case of a carbon dioxide level of 2240 ppm) and two times (in the case of 280 ppm) the value reached after 10 ky. The AIS volume obtained with pre-industrial CO_2 is about half of the observed present value. Nevertheless it should be kept in mind that in these experiments the AIS is still not in equilibrium with the rest of the climate system, since the ISM is driven by invariant climate forcings.

Chapter 6

Sensitivity of Antarctica to the orbital configuration

In this section the significance of the orbital insolation forcing on the origin of an early AIS is investigated. The experiments assess if a convenient set of orbital parameters (obliquity, eccentricity and precession), permitting a cold austral summer, serves as pre-condition for the initial growth of the AIS. Four different experiments are conducted with the land-sea distributions as used in the previous chapters. For each configuration, two distinct orbital setups were used: the modern one and one yielding the smallest Antarctic summer insolation.

6.1 Experimental set-up

This set of experiments intends to study the early formation of the AIS under different land and orbital configurations. Two sets of two experiments each investigate the effect on the AIS of an advantageous orbital configuration with distinct tectonic distributions.

The Late Eocene (EOC) and the Late Oligocene (LOL) tectonic configurations are the same used for the previous experiments and shown in Fig.4.1. In both cases the topography used to force the climate model COSMOS includes an ice-free Antarctica, isostatically relaxed after the removal of the ice sheet (Fig. 3.2). The surface background albedo of the ice-free Antarctica is fixed to the global mean value 0.3. The atmospheric carbon dioxide concentration is set to its pre-industrial level (280 ppm) in both cases. The other initial and boundary conditions for the two settings are constructed from the modern ones on the different land-sea masks. In the two cases, the ocean model MPI-OM in COSMOS is initialized by two 10-ky spin-up runs of the ocean model LSG, run with the respective land-sea distributions.

Hereafter, in each COSMOS-experiment a modern astronomical orbit and a "cold" orbit are applied. The first uses present-day parameters yielding an "intermediate" orbit (see Section 1.1.3), the latter produces the coldest possible Antarctic summers. Cooler summers are believed of encouraging the start of an ice sheet, and in general of an ice age (e.g. Milankovitch, 1941), by melting less of the previous winter's ice and snow. The "modern" orbit uses obliquity (obl) of 23.44°, eccentricity (ecc) of 0.0167 and precession (P) of 283°, whereas the "cold" orbit has minimum obliquity (obl=22°), maximum eccentricity (ecc=0.05), and aphelion corresponding to austral summer (P = 270°).

In Figure 6.1 the annual mean (solid lines) and the January (dashed lines) incoming solar short-wave (SW) radiation at the top of the atmosphere (TOA), calculated using Berger and Loutre (1991), are shown for the two orbits used in the experiments: the modern (red) and the "cold" (blue). In the first case (annual mean, solid lines), the difference between the two orbits is principally visible in the Polar Regions, where the difference in the incoming radiation reaches the maximum value of 10.8 Wm^{-2} and is an effect of the obliquity of the ecliptic. Lower obliquity causes Polar Regions to receive less seasonally contrasting solar radiation, as well as reduced annual mean solar radiation, producing conditions more favourable to glaciation. Like changes in precession and eccentricity, changes in tilt influence the relative strength of the seasons, but the effects of the tilt cycle are particularly pronounced in the high latitudes. The January (austral summer) difference in insolation (dashed lines) is primarily due to the precession of Earth's orbit.

The scheme of the modelling procedure applied to these experiments is illustrated in Figure 6.2. The ocean model MPI-OM is initialized by a 10 ky spin-up run of the three-dimensional ocean model LSG, which uses the same EOC and LOL land-sea distributions as included in COSMOS (Fig. 4.1) and present-day background climate. During the 50 years-long COSMOS runs, atmosphere and ocean exchange the heat and momentum fluxes every day of integration and the sub-surface and deep ocean temperature and salinity are restored to their initial values as explained in Chapter 2.

The outcoming net precipitation and surface atmospheric temperature are averaged over the last 30 years and used to force the ISM. In each experiment, the ISM runs for 10000 years (10 ky), i.e. for the first phase of the AIS growth.

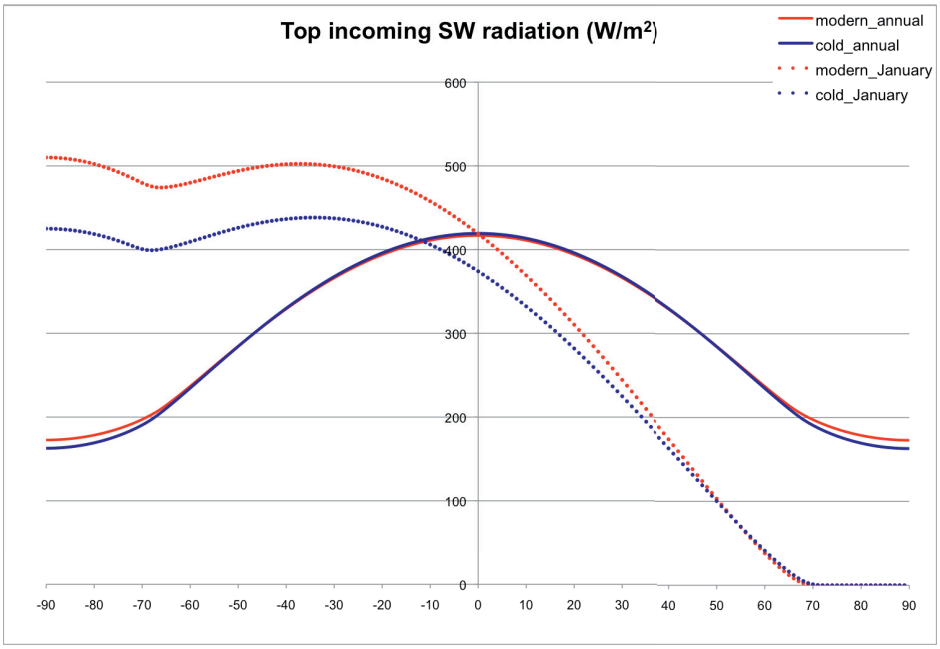

Figure 6.1: Annual mean (solid lines) and January (dashed lines) incoming solar radiation at the top of the atmosphere calculated using Berger and Loutre (1991) for the two different orbits used in the experiments: the modern (red) and the "cold" (blue).

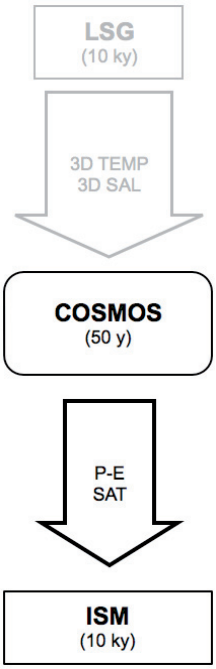

Figure 6.2: Flow-chart of the modelling procedure applied to this set of experiments.

Table 6.1 gives a summary of the set-ups of the four sensitivity experiments performed, with their denomination and schematic description.

Table 6.1: Summary of the experiments performed in this chapter.

Name of the experiment	Description
EOC	Experiment with: • EOC land-sea distribution (Fig. 4.1a); • ocean temperature and salinity L4-40 restored to LSG run with EOC land-sea distribution; • pCO_2 of 280 ppm (the pre-industrial level); • modern orbital configuration.
EOC_cold	Experiment with: • EOC land-sea distribution (Fig. 4.1a); • ocean temperature and salinity L4-40 restored to LSG run with EOC land-sea distribution; • pCO_2 of 280 ppm (the pre-industrial level); • orbital configuration yielding the lowest austral summer insolation.
LOL	Experiment with: • LOL land-sea distribution (Fig. 4.1b); • ocean temperature and salinity L4-40 restored to LSG run with LOL land-sea distribution; • pCO_2 of 280 ppm (the pre-industrial level); • modern orbital configuration.
LOL_cold	Experiment with: • LOL land-sea distribution (Fig. 4.1b); • ocean temperature and salinity L4-40 restored to LSG run with LOL land-sea distribution; • pCO_2 of 280 ppm (the pre-industrial level); • orbital configuration yielding the lowest austral summer insolation.

6.2 Results

The ocean surface and mixed layer can react to changes in atmospheric forcings during the COSMOS runs, and therefore, to the change in solar radiation reaching the Earth. The annual mean anomalies between the sea surface temperature (SST) obtained with the “cold” and with the modern orbit for the different land-sea distributions EOC and LOL are plotted in Figure 6.3. In general the anomalies are small, remaining in a range of 1 K. The most evident negative differences are located in the Weddell Sea and along the coasts of West Antarctica. Here the ocean temperature in the cold-orbit experiment is a little lower than in the modern-orbit experiment. In the EOC case (a) the negative anomalies between the SST obtained with the two orbits is more evident than in the LOL case (b). A potential reason could be the enhanced ocean mixing on the LOL case, which would lead to a reduced temperature response to the insolation anomaly.

In none of the experiments sea ice is detected, not even in the coldest modelled condition, winter of the LOL_cold experiment. This is a consequence of the warm SST, which in no case is lower than the freezing point of seawater. The minimum value of SST is actually found in the Weddell Sea in July of the LOL_cold experiment, corresponding to 271.35 K (or -1.8°C). Therefore, it is reasonable to expect this area to be more subject than others to potential sea ice formation for an additional lowering of the ocean temperature.

In Figure 6.4 the mean annual surface atmospheric temperature (SAT) anomalies between different experiments are plotted. In Figure 6.4a and b the anomalies are calculated between the temperature obtained with the "cold" orbit and with the "modern" orbit for both of the topographic configurations, EOC and LOL. The SAT anomalies are negative, showing that the SAT obtained with a "cold" orbit is lower than the one obtained with the "modern" orbit. In both cases the maximum anomaly in the temperature field reaches -3 K in the inner continent. The difference in the mean annual SAT over the Antarctic region (between -60°S and -90°S) is 0.17 K for EOC and 0.09 K for LOL, whereas the difference in the summer SAT is 0.99 K for EOC and 0.36 K for LOL. The anomalies are more pronounced in the case of EOC configuration (a). Negative values affect the whole continent, but are more pronounced in the interior than on the coast. With the LOL configuration (b) the highest differences are located over West Antarctica. The values are still negative but smaller than in the EOC configuration. Figure 6.4c illustrates the anomalies between the SAT calculated with the LOL and with EOC set-ups applying the modern orbit (compare to Figure 4.7a). A mean decrease of the SAT in the Antarctic region (0.4 K) is associated to the opening of the Drake Passage (DP) and to the changed oceanic circulation. Still, an area of positive anomaly is observable over the DP itself (about 2.5 K). Finally, in Figure 6.4d the anomaly between the SAT calculated with the LOL and with EOC set-ups applying the "cold" orbit are plotted showing areas of both positive and negative anomalies. However, the mean anomaly over the whole Antarctic region is slightly negative (0.07 K). The low value seems to denote an interaction of the insolation and tectonic forcings.

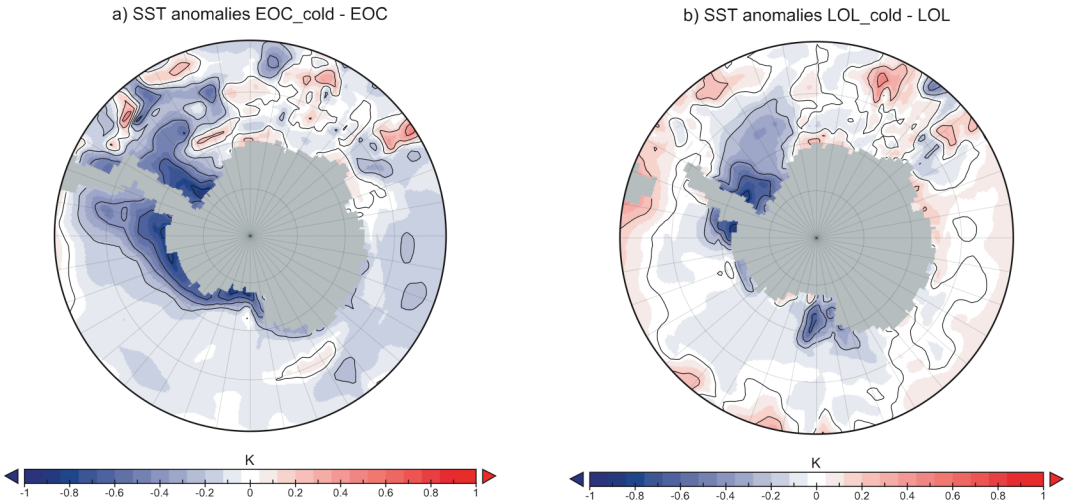

Figure 6.3: Annual mean sea surface temperature (SST) anomalies between the experiments EOC_cold and EOC (a) and between LOL_cold and LOL (b) modelled with ECHAM5 in COSMOS.

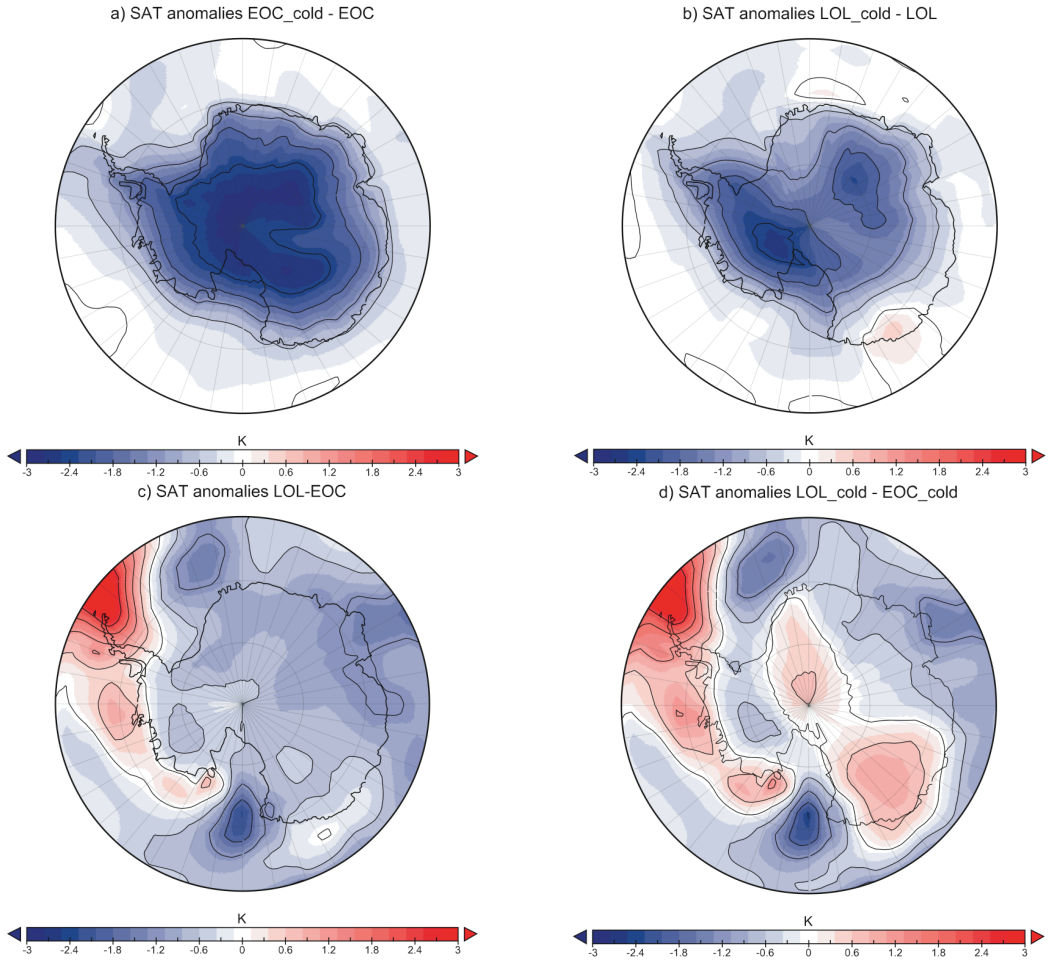

Figure 6.4: Annual mean surface atmospheric temperature (SAT) anomalies between the experiments EOC_cold and EOC (a), between LOL_cold and LOL (b), between LOL and EOC (c) and between LOL_cold and EOC_cold (d) modelled with ECHAM5 in COSMOS.

In Figure 6.5 the mean annual net precipitation (P-E) anomalies for the different tectonic configurations are shown. The anomalies are calculated between the precipitation fields obtained with the "cold" orbit and with the modern orbit. The pattern of the anomalies is variegate, but in both cases the P-E anomalies are mostly negative over the Antarctic continent and become positive over the ocean surrounding it. The negative anomalies are more pronounced in the case of Late Oligocene land-sea distribution (LOL, b), especially over West Antarctica and the Antarctic Peninsula. The negative values in the EOC configuration are more extended over East Antarctica.

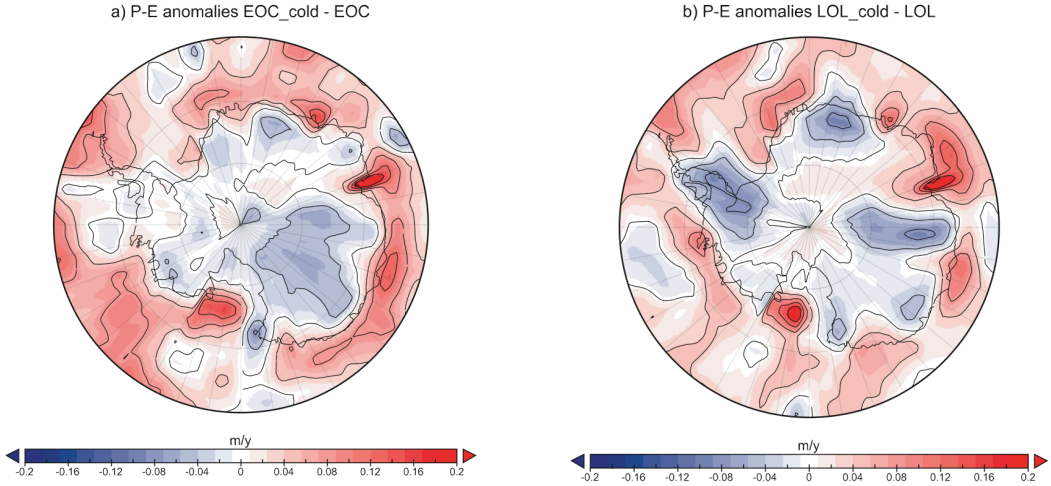

Figure 6.5: Annual mean net precipitation (P-E) anomalies between the experiments EOC_cold and EOC (a) and between LOL_cold and LOL (b) modelled with ECHAM5 in COSMOS.

The change in the surface wind pattern is shown in Figure 6.6. The anomalies are calculated between the 10 m wind speed modelled with ECHAM5 in COSMOS applying the "cold" and the modern orbital configuration for the EOC (a) and the LOL (b) set-ups. In both pairs of experiments the differences are predominantly positive, but relatively small (less than 1.5 m/s) and close to zero over the interior of the Antarctic continent. The difference in the atmospheric flow is slightly more pronounced in the EOC set-up, as compared to the LOL. The increase in surface wind speed is likely caused by the enhanced meridional temperature gradient.

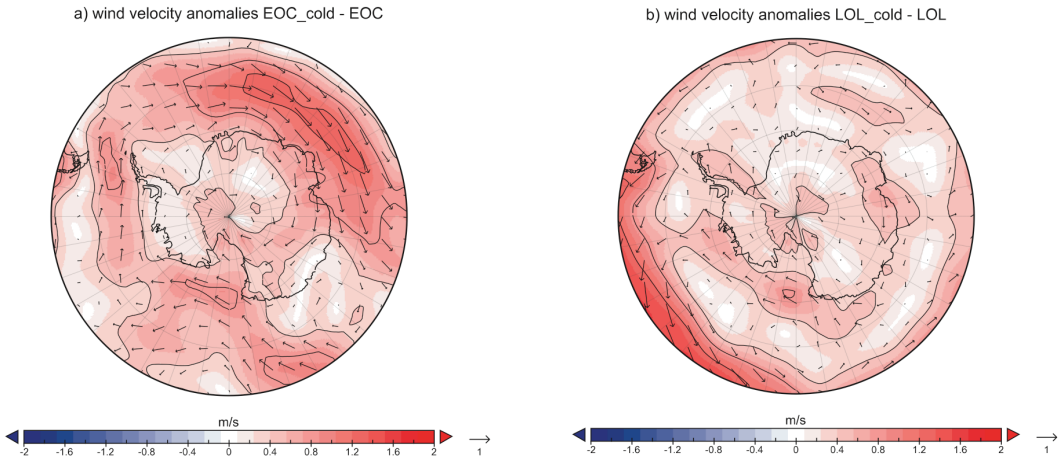

Figure 6.6: Annual mean 10 m wind velocity anomalies between the experiments EOC_cold and EOC (a) and between LOL_cold and LOL (b) modelled with ECHAM5 in COSMOS.

In Figure 6.7 the zonal mean u-velocity for the EOC (a), LOL (b), EOC_cold (c) and LOL_cold (d) COSMOS experiments is plotted. In all the cases the highest velocities (around 50 m/s) are found in the tropopause in the Northern and Southern Hemispheres at about 45°N(S). The intensity of the jets in the Southern Hemisphere is higher in the experiments applying the modern orbit with respect to the corresponding experiments applying the "cold" orbit. This derives from the temperature gradients between the atmospheric layers. In fact, it has been shown above that the lower insolation reaching the Southern Hemisphere, related to the "cold" orbit, results in lower SAT. Therefore, the vertical gradient of temperature is also lower in this case and this causes weaker jets.

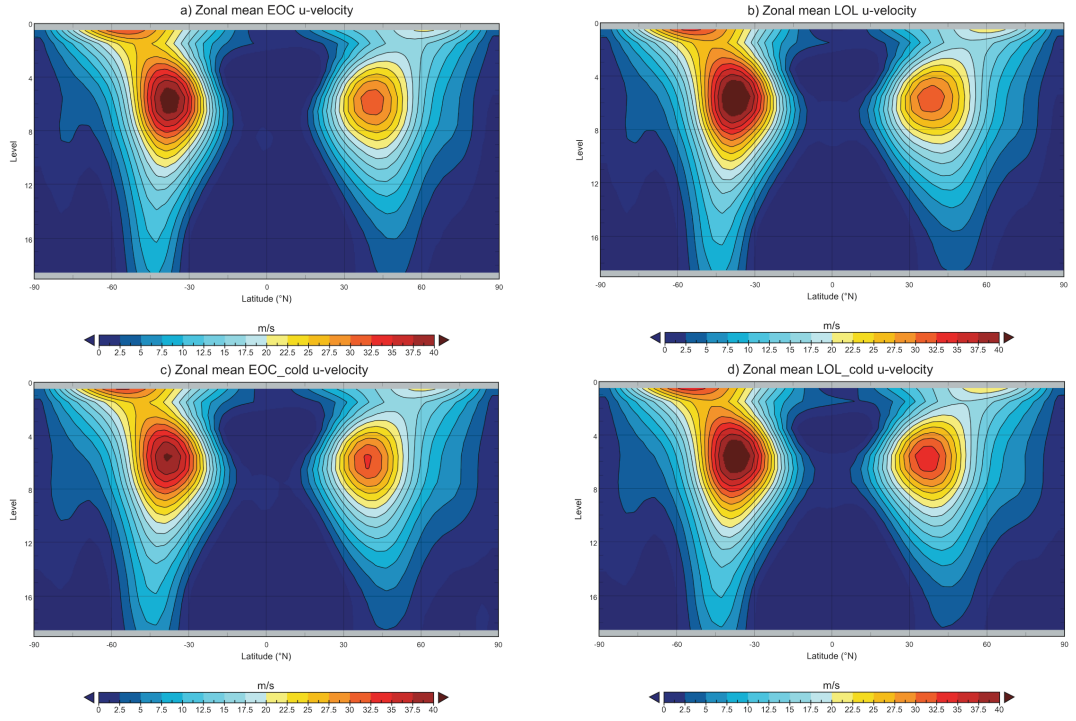

Figure 6.7: Zonal mean u-velocity for the EOC (a), LOL (b), EOC_cold (c) and LOL_cold (d) COSMOS experiments.

Figure 6.8 shows the AIS volume computed by the ISM along the four experiments, the two with Late Eocene tectonics (EOC and EOC_cold, solid lines) and the two with Late Oligocene tectonics (LOL and LOL_cold, dashed lines). The plot displays the progression of the ice volume during the first 10 ky of glacial inception modelled by the ISM driven by constant EOC and LOL climates with different orbital configurations, the modern (modern orbit, in red) and the one providing the coldest austral summers (cold orbit, in blue). The plot shows that differences in the trend are distinctly recognizable after about 4 ky of model integration and become more evident at the end of the experiment, after 10 ky. For each tectonic configuration and under the same internal climatic constraints (tectonic configuration, ocean temperature and carbon dioxide concentration), the orbital configuration varies the amount of solar radiation that reaches the Antarctic region and therefore affects the temperature field. Lower temperatures, achieved with the cold orbit, favour the ice growth, which reaches higher values in both land configurations. In the case of the EOC experiments the difference in the ice volume achieved between the two orbits is $1.1 \cdot 10^6$ km^3, whereas it is $0.73 \cdot 10^6$ km^3 for the LOL configuration. Finally, it is also visible that the trend of the AIS volume is the same in the two "cold" experiments. This appears to be a coincidence due to the fact that only the first phase of ice sheet growth is analyzed (the first 10 ky). If longer ISM runs would be considered, the trends may diverge. There is an interaction of the insolation and tectonic effects: the stronger ocean circulation in the LOL configuration increases the effective heat capacity of the ocean. Higher mixing of the ocean results in larger amount of energy needed to warm the water up.

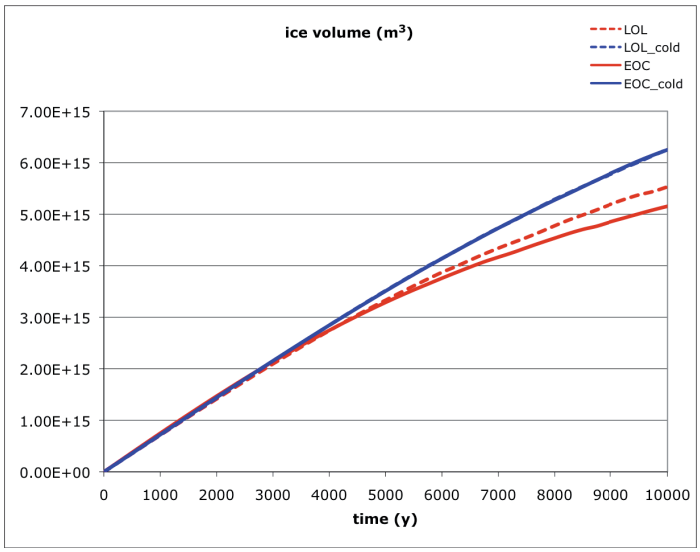

Figure 6.8: The AIS volume computed by the ISM for the four experiments, the two with late Eocene tectonics (EOC and EOC_cold, solid lines) and the two with Late Oligocene tectonics (LOL and LOL_cold, dashed lines).

The two plots in Figure 6.9 show the AIS thickness anomalies (in m) between the two EOC (a) and the two LOL (b) experiments after 10 ky, whereas Figures 6.10, 6.11, 6.12 and 6.13 show the absolute values of AIS surface elevation (a) and ice

thickness (b) for the four different experiments: EOC, EOC_cold, LOL and LOL_cold. The anomalies (Fig. 6.9) are mostly positive in both cases. This demonstrates that a larger amount of ice grows in the colder conditions provided by the astronomical configuration with minimum obliquity and maximum eccentricity, with respect to the current one. The anomaly in the ice thickness is more pronounced with the EOC set-up. In the LOL case the climate is colder due to the ocean temperature provided by the paleo-topography including open DP and the fully established Antarctic Circumpolar Current (ACC), as demonstrated in Chapter 4. Negative anomalies are also visible in both plots, indicating that in some areas the modern insolation seems to produce ice with higher elevation. This is most likely due to the difference in the atmospheric precipitation and circulation over the continent, which is driven by changes in the surface temperature caused by the orbitally-constrained insolation itself. In all experiments (Fig. 6.10, 6.11, 6.12 and 6.13) ice caps develop in East Antarctica and remain restricted to the continent. The coasts of East Antarctica also remain ice-free. Thicker ice sheets are found in correspondence of the most elevated areas of the Gamburtsev Mountains. Finally, in no experiment ice develops on the archipelago of West Antarctica and of the Antarctic Peninsula.

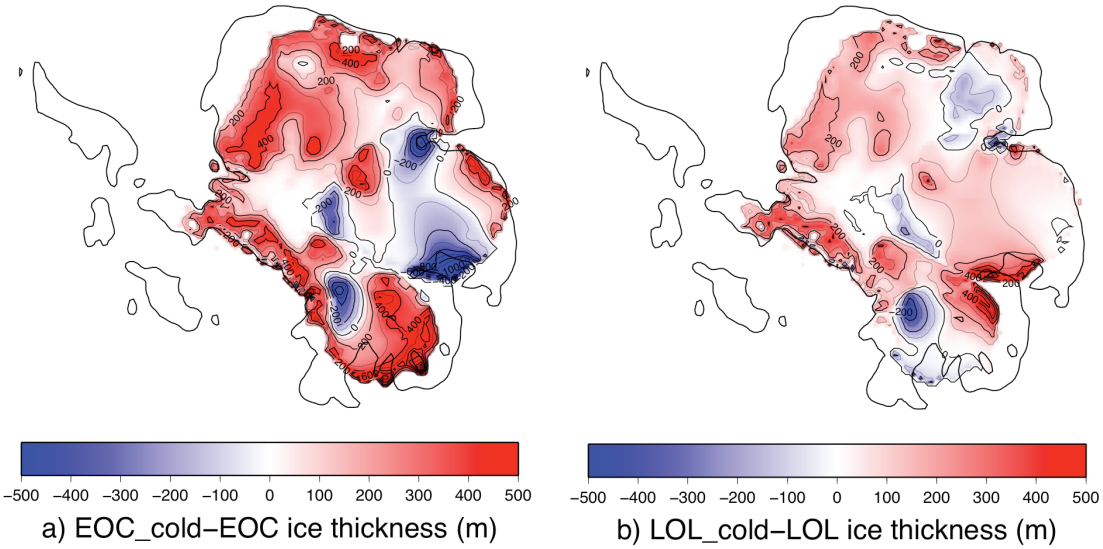

Figure 6.9: The Antarctic ice thickness anomalies after 10 ky of ISM integration between the model results with "cold" and modern orbital configurations and Late Eocene (EOC, a) or Late Oligocene (LOL, b) boundary conditions.

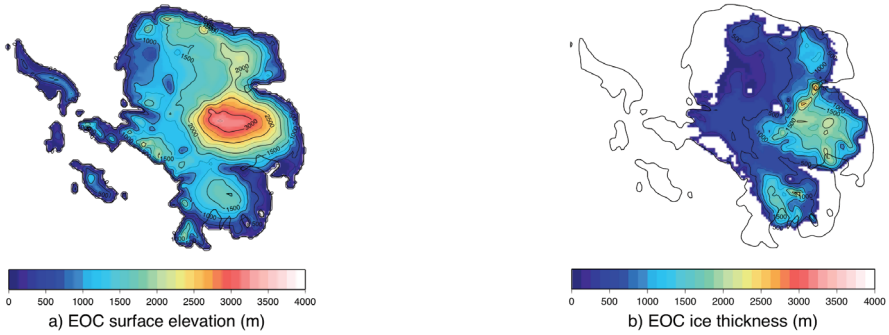

Figure 6.10: AIS surface elevation (a) and ice thickness (b) after 10 ky of ISM integration for the EOC experiment.

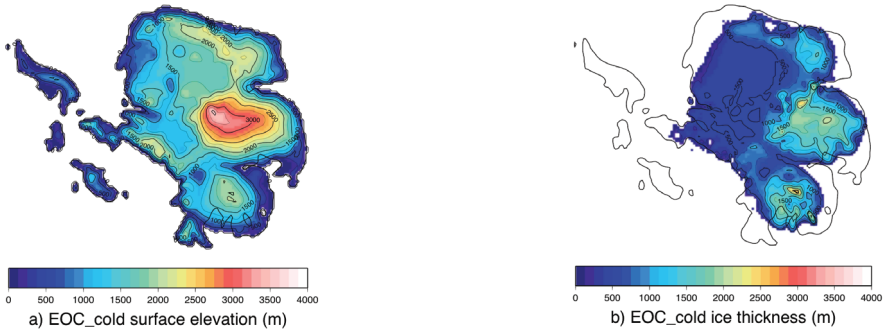

Figure 6.11: AIS surface elevation (a) and ice thickness (b) after 10 ky of ISM integration for the EOC_cold experiment.

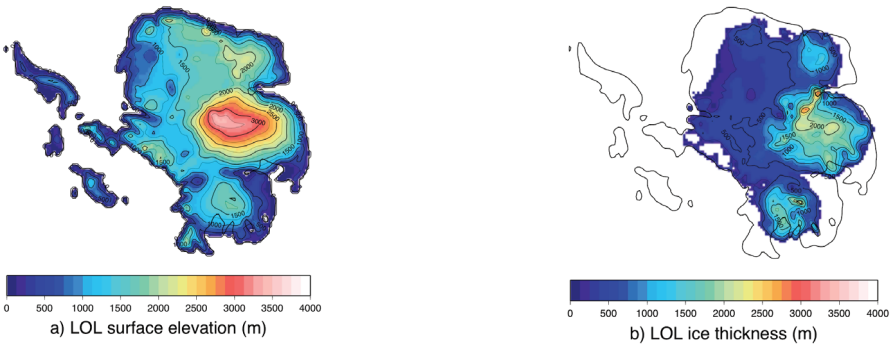

Figure 6.12: AIS surface elevation (a) and ice thickness (b) after 10 ky of ISM integration for the LOL experiment.

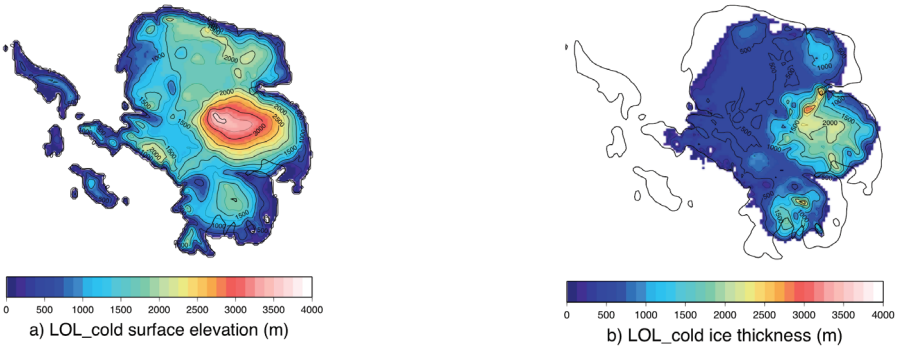

Figure 6.13: AIS surface elevation (a) and ice thickness (b) after 10 ky of ISM integration for the LOL_cold experiment.

6.3 Summary

This chapter was dedicated to a set of sensitivity experiments quantifying the importance of a favourable orbital configuration on the first phase of AIS growth, using two specific tectonic set-ups. The goal was not to fully investigate the role that the cyclicity of the Earth's orbital configuration could have had in triggering the long-term glaciation and the consequent oscillations in the AIS extent and volume. Alternatively, the attention is focused on the measure of the AIS sensitivity to specific orbital settings and state to which magnitude an orbit yielding the coldest austral summer temperatures could favour the first phase of the ice sheet development.

The two tectonic configurations used are the ones corresponding approximately to the Late Eocene (EOC), and to the Late Oligocene (LOL), already applied in the previous experiments. With respect to these settings, four different climate states, two for each configuration, have been simulated. Each pair of climates, namely the EOC and the LOL climates simulated with COSMOS, was determined by the respective global ocean temperatures and by different orbital positions. One experiment applied the modern orbit and one used the orbit with lowest obliquity, highest eccentricity and aphelion corresponding to the austral summer, hence advantaging the ice sheet initiation by reducing the summer temperature.

The results show that for each couple of climate runs, the "cold" astronomical orbit helps the formation of the AIS by decreasing the surface atmospheric temperature (SAT) and preventing the summer melting of snow. Accordingly, the AIS created with this condition is more massive in volume and occupies a larger area as well. The SAT anomaly over the continent, calculated by subtracting the temperature obtained with the modern orbit from the one obtained with the "cold" orbit for both the EOC and LOL configurations, are strictly negative. The ice thickness anomalies show also local positive values, due to changes in the atmospheric circulation and precipitation. The anomalies in the AIS thickness and volume are more significant for the EOC experiments than for the LOL. This derives from the fact that, under the same astronomical conditions, the climate simulated for the LOL experiment is cooler than the one simulated for the EOC, as shown in the set of experiments illustrated in Chapter 4. This suggests that the astronomical configuration has less influence in the initial stage of AIS expansion. Lastly, the deviations in the ice volume between the two orbits computed for the EOC and LOL experiments exhibit values, $1.1 \cdot 10^6$ km^3 and $0.73 \cdot 10^6$ km^3 respectively, which are of a lower order of magnitude than the changes caused by the decrease in atmospheric CO_2 concentration and by the opening of the Drake Passage.

Chapter 7
Discussion

In this study a coupled climate - ice sheet model has been developed to investigate the sensitivity of Antarctica to the main potential climate forcings that could have driven its glaciation at the Eocene-Oligocene (E-O) transition, about 35 Ma ago. The model consists of an Earth System Model comprising General Circulation Models for the atmosphere and ocean including sea ice as well as a three-dimensional ice sheet model for Antarctica.

Various sensitivity experiments show that the Antarctic continent reacts in a comparable way with respect to the two dominant potential forcings, i.e. the opening of the Drake Passage and the decrease in atmospheric carbon dioxide concentration, whereas a favourable orbital configuration seems to have less impact on an early ice sheet development.

As in all numerical modelling studies, the results must be considered in view of the assumptions, which sensitivity experiments require. Nevertheless they contribute in advancing the knowledge of the processes, which occurred along the Eocene-Oligocene transition.

The Eocene-Oligocene (E-O) transition represents the largest global cooling event of the Cenozoic Era and has been associated with cooling of low-, middle-, and high-latitudes (e.g., Lear et al., 2008). The Antarctic region has been profoundly affected by the global climate change of the Cenozoic. Therefore, a better understanding of past changes in this region is crucial, but the reason of this climate development is widely debated (e.g., Zachos et al., 2008; Merico et al., 2008). The two most widely held explanations for the fundamental climatic shift and initiation of the E-O Antarctic glaciation are a cooling of Antarctica due to: (1) changes in ocean circulation controlling poleward heat transport (e.g., Mikolajewicz et al., 1993); or (2) a gradually forced threshold response to declining atmospheric carbon dioxide levels (e.g., DeConto and Pollard, 2003). While new drill sites and proxy records are important for exploring these hypotheses, computer models play a valuable role in allowing exploration of Antarctic climate evolution through sensitivity studies.

This study focuses on the performance and interpretation of different sets of sensitivity experiments. It does not aim at precisely modelling the Antarctic glacial inception as it could have occurred at the E-O transition, but rather at analysing the Antarctic response to the reputed principal drivers of its evolution. In the introduction of this thesis the scientific questions targeted by this research have been set and they can now be discussed in view of the results.

1. *Is it possible to achieve a complete model representation of the Antarctic climate system, including the ocean, the atmosphere and the Antarctic cryosphere?*

The determination of responses in the Antarctic Ice Sheet (AIS) to climatic forcing is of great importance for the study of its sensitivity. In Chapter 3 the validation of the modelling procedure for present-day climate as well as a model description of the Antarctic climate including the global ocean, atmosphere and the Antarctic cryosphere has been described. The applied models, specifically Huybrechts (1993) ice sheet model (ISM) for the Antarctic cryosphere and the Earth System Model COSMOS (composed of the AGCM ECHAM5 and the OGCM MPI-OM), are capable to simulate the present-day AIS and global ocean and atmosphere. The iterative modelling procedure applied ensures that the various model components adapt to the new boundary conditions.

In numerical modelling, the quality of model output depends on the quality of model input. The most important data used as boundary and forcing conditions in an ice-sheet model are the subglacial bedrock topography and the surface mass balance. For present-day ice sheets, the quality of these model inputs depends on field data, which is absent in some areas. Airborne radar and seismic surveying provide the only viable methods of acquiring information on the ice-sheet base at a continental scale. Their big limitation, critical in Antarctica, is that large portions of ice sheet remain un-surveyed. Thus, the subglacial bedrock topography in these regions has to be estimated often from just a few measurements, and is subject to potential errors. Mass balance of large ice masses is also very difficult to establish accurately over a wide area. Antarctica gains ice mass through accumulation of snow. Snowfall occurs close to the ice-sheet margin in contrast to the interior, where accumulation is associated with solid precipitation directly from water vapour (e.g., Monaghan and Bromwich, 2008). Ice loss in Antarctica occurs through iceberg calving and sub-ice-shelf melting (Jacobs et al., 1992). Satellite observations and direct measurements, provide estimates of mass

balance across a wide area, and have been used to assess Antarctic mass balance (Vaughan et al., 1999; Arthern et al., 2006). However such analysis provides only an estimate of the current situation, which is unfortunately not sufficient to model past or future scenarios. For this reason it is recommendable to provide the ice sheet models with forcing fields from a GCM. In this set-up it is possible to explore the AIS behaviour in a self-consistent way.

The time scales at which the different climate subsystems (ocean, atmosphere and cryosphere) react to each other are very different, varying between days and thousands of years. This complication must be taken into account for modelling the interactions between them. The biggest obstacle for the solution of this problem is represented by the computation time needed to simulate each process on the different time scales. In this study this problem has been solved by the isolation of the climate subsystems and modelling the processes acting on them separately. The modelled subsystems have then been connected with each other using an asynchronous coupling procedure.

The ocean general circulation model (OGCM) MPI-OM in COSMOS is initialized by 10 ky spin-up runs of the OGCM LSG. This strategy has been used in all experiments. In addition to a present-day control run with modern bathymetry, two LSG paleo-runs with ocean gateway changes similar to the Late Eocene and to the Late Oligocene have been performed. These experiments use present-day atmospheric forcings and create a background climate, considered as zeroth-order approximation of the real Late Eocene and Late Oligocene paleoclimates (Lohmann and Lorenz, 2000; Butzin et al., 2005). This is a reasonable procedure to produce an adequate initialization of the global ocean for the different time slices of interest. The resulting thermohaline fields are used to initialize MPI-OM. During the coupled runs subsurface and deepwater temperatures and salinities in MPI-OM are restored to their initial values. As a consequence, the surface layer can freely adapt to atmospheric changes while the deep ocean stays close to the equilibrium. Various sensitivity experiments to different relaxation constants ($8 \cdot 10^{-4}$ and $5 \cdot 10^{-1}$) and for different model levels (L4-40, L15-40) show that the combination with three-dimensional restoring between the levels 4 and 40 and using the restoring constant $f=8 \cdot 10^{-4}$ yields the most reasonable results, i.e. smaller sea surface temperature (SST) and sea surface salinity (SSS) adjustment.

The modern subsurface horizontal ocean flow modelled by the MPI-OM in COSMOS, i.e. coupled with ECHAM5, has been compared with a control run performed with the stand-alone MPI-OM forced by prescribed present-day climatology. The principal characteristics of the modern global oceanic circulation are present in both model outputs, even though disagreement in the representation of the ocean currents in some areas is recognizable. Plausible reason for these dissimilarities could be that the run performed with MPI-OM in COSMOS is too short and the global ocean cannot reach quasi-equilibrium. A practical solution in this direction could be the execution of the spin-up run directly with the fully-coupled AOGCM COSMOS. This would lead, in the first place, to the direct inclusion of the atmospheric response and, in the second place, to avoid the use of the relaxation of the ocean temperature and salinity to the initial values, which could also be the reason of the discrepancy. Alternatively, the restoring process itself could be enhanced in order to clarify both kind and extent of the changes in the ocean circulation that this procedure implies. Nevertheless, the sensitivity analysis of this thesis is conducted with the confidence that these

dissimilarities have small consequences on the final results, although they must be taken into consideration for their interpretation.

This procedure has the advantage of speeding up the computing time, avoiding longer spin-up runs with the coupled AOGCM. Another significant benefit is the possibility to decompose the processes acting on the various climate subsystems and to perform focused sensitivity experiments. On the other hand, limitation of this modelling approach is the fact that the deep ocean is relaxed to a fixed climate state and cannot freely react to atmospheric changes during the COSMOS runs, as the real ocean surface does. However, this would take hundreds of years of model integration, taking long computation time. As a consequence, some processes cannot be adequately represented (e.g., the deepening or shallowing of the ocean mixing layer or the possible ocean amplification of insolation effects). Furthermore, in the LSG spin-up runs no atmospheric response is incorporated. Because the present-day background climate used in the paleo-experiments does not represent truthfully the Late Eocene and the Late Oligocene climates, also no direct feedback between the deep ocean and the AIS is considered.

In all the experiments the climate model COSMOS, composed of MPI-OM and of the atmospheric model ECHAM coupled by the OASIS3 coupler, has been run for an integration time (50 years) long enough to let the global atmosphere adapt to changes in the boundary conditions (normally in maximum 5-10 years) and return consistent meteorological fields. The resulting modelled surface atmospheric temperature (SAT) and net precipitation (P-E) have been used to force the ISM in an iterative coupling procedure. The ISM has also been run to steady state, which is normally reached after integrating 50 ky. Hence, both the models are run to their steady state at each iteration. This assures that they adapt to the changed boundary conditions, i.e. the meteorological fields in the case of the ISM and the Antarctic orography in the case of COSMOS. Therefore the steady state obtained is representative of the climate at the discrete time span.

Using this methodology, the modern conditions of the AIS have been modelled and the results show good agreement with radar survey data (BEDMAP dataset, Lythe et al., 2001). However, the final modelled AIS volume is 12% lower ($0.31 \cdot 10^6$ km^3) than its observed modern value of $2.54 \cdot 10^7$ km^3 (Lythe et al., 2001). Pronounced differences occur mainly in the western AIS (WAIS) and at the coasts of the East AIS (EAIS). Those anomalies are due to the difference in the representation of the meteorological fields, as the horizontal resolution of the climate model is about 10 times coarser than the one of the ice sheet model. This affects in particular West Antarctica and the Antarctic Peninsula. On the other hand differences could also be caused by the dataset used to compare the model results. The BEDMAP dataset (Lythe et al., 2001) quantifies elevation and ice thickness well in many areas of the Antarctic continent, however, there are many large data gaps. Furthermore, also where coverage is good, radar transects are often separated by several kilometres and interpolation of data remains necessary. This may cause high errors (around 200 m) in the estimation of the ice thickness (Lythe et al., 2001).

The inclusion of the AIS in COSMOS represents an important advancement in the representation of the Antarctic surface topography in general circulation models. The

surface elevation modelled with the iterative procedure between COSMOS and the ISM is more detailed than the standard ice sheet included in COSMOS. This permits a better simulation of the atmospheric processes over Antarctica and therefore a better study of its behaviour in consequence of climate changes. The iterative modelling approach produces differences with respect to the stand-alone version of the ISM in the WAIS only, whereas it gives consistent results with regard to the EAIS. Although the stand-alone version of the ISM simulates more precisely the present AIS, the forcing fields are calculated through empirical parameterizations based on modern climate observations taken over Antarctica (Huybrechts, 1993) and, therefore, do not apply in the context of paleo-climate.

The methodology has been further examined by doubling the atmospheric pCO_2 and quantifying the impact on the global climate and on the AIS. The ice sheet-climate model is able to react to changes in the climate constraints. An increase of 1.2 K in global surface atmospheric temperature is a consequence of a doubling the atmospheric pCO_2. With respect to the last IPCC assessment (2007), this experiment's result is about 40% lower than the best estimate (3 K) of the climate sensitivity and near its lower bound (1.5 K). The climate sensitivity has also been compared with the one given by the ECHAM5/MPIOM model simulation derived from the World Climate Research Programme's Coupled Model Intercomparison Project multi-model data set (CMIP3). With respect to the CMIP3 model run, the iteratively coupled climate-ice sheet model underestimates the global climate sensitivity by a factor of about 3 and of about 4 in Antarctica. This is due to the fact that the doubling in the CO_2 concentration concerns mostly the atmosphere, while the deep ocean is not much affected due to the restoring of the temperature to the initial values. The lower climate sensitivity resulting from this modelling approach represents a limitation to the detailed study of the Antarctic response in the paleo-experiments. Therefore it must be taken into account when investigating the Antarctic and climate sensitivity in a greenhouse world.

The climate-ice sheet model is also effective in diagnosing the amplification of the temperature rise on higher latitudes, as it has also been found by Masson-Delmotte et al. (2006). The final AIS volume is reduced by about the 3.6% ($0.08 \cdot 10^6$ km^3) with respect to the present-day modelled AIS, the reduction affecting especially the margins of East Antarctica and in the WAIS. This is an expected result, since these areas are very sensitive to changes in climate conditions due to their exposition to the ocean and their lower ice thicknesses than the interior of the AIS.

2. *To what amount does the opening of the Drake Passage and the consequent establishment of the Antarctic Circumpolar Current change the oceanic circulation? How does this affect the evolution of the Antarctic Ice Sheet?*

The fourth chapter of this thesis has examined the possible relation between the opening of the Drake Passage (DP), the consequent establishment of the Antarctic Circumpolar Current (ACC) and its climatic effects on Antarctica. The iterative modelling procedure between COSMOS and the ISM, validated in Chapter 3, has been applied with the Late Eocene and Late Oligocene tectonic configurations. The experiments performed were not aimed at the accurate reconstruction of the climate of these two periods, but at assessing the different evolution of the AIS caused by different tectonic configurations and their respective ocean circulations.

In line with the ocean modelling study of Mikolajewicz et al. (1993), the results show a stronger ACC when the DP is open with respect to the configuration with closed DP. A reduced southward heat transport is detected for the Late Oligocene configuration, which leads to an average cooling of the Southern Ocean deep waters by up to -1 K. Similar result (mean decrease of -0.5 K) was found by Nong et al. (2000) using the NCAR CSM Ocean Model.

In none of the experiments, with closed DP (Late Eocene) and with open DP (Late Oligocene), sea ice is present around Antarctica and in the surrounding ocean in any season. This derives from the fact that in both cases the SST is higher than the freezing point of seawater (about -1.9°C). Unfortunately, no proxy data is available for reconstructing past sea ice distribution in the Antarctic region and, therefore, for attesting the robustness of this finding. However, based on temperature reconstructions from deep-sea drilling projects, Kennett (1977) suggested the first sea ice to have developed only after the E-O transition. Once the surface and deep ocean temperature had cooled enough to allow substantial Antarctic sea ice to form, a thermohaline oceanic circulation in the sense of the present day system was initiated.

The establishment of the ACC affects the atmospheric circulation over Antarctica. An increase in the wind speed over and around the continent is detected when the ACC is established. The resulting temperature decrease affects both the atmosphere and the ocean. The mean surface atmospheric temperature (SAT) over the Antarctic continent and the surrounding ocean (i.e. between the South Pole and 60°S) is 0.4 K lower when the DP is open than in the experiment with a closed DP. This value is much lower than the one given by Toggweiler and Bjornsson (2000) for the same latitudes (3 K). This derives, on one hand, from the underestimated climate sensitivity of the climate-ice sheet model due to the restoring of the ocean temperature and salinity to the initial values. On the other hand, the study of Toggweiler and Bjornsson on the effect of the opening of the DP has been performed with a water-planet model which does not include a realistic global continental configuration, but in which land is limited to two polar opposite islands connected by a thin barrier.

The AIS obtained when the DP is open is larger and more massive than in the case of a closed DP. The AIS volume achieved in the first scenario is 20% ($1.56 \cdot 10^6$ km^3) larger than in the second one. If the temperature difference between both scenarios were even larger, as proposed by Toggweiler and Bjornsson (2000), then the difference in Antarctic ice volume would also be larger than 20%.

This experiment confirms the inter-connection between the climate sub-systems (ocean, atmosphere and cryosphere) and the continuous relationship between the processes acting on them.

3. *How sensitive was the Late Eocene Antarctica to the atmospheric carbon dioxide concentration?*

This question has been addressed in Chapter 5 by representing the possible Late Eocene climatic conditions under different atmospheric CO_2 concentrations (pCO_2) and by investigating the genesis of the AIS under these different scenarios. This experiment was not directed to exactly simulate the late Eocene global climate and consequent glaciation due to a progressive reduction in the atmospheric carbon dioxide

concentration, but rather to investigate the AIS establishment in climate scenarios given by different pCO_2, conditions.

Proxy data studies (e.g., Pagani et al., 2005) indicate a general decrease in pCO_2 along the Eocene-Oligocene transition. However, the method to derived paleo-pCO_2 from proxy records is difficult, resulting in large uncertainties of the values. Therefore a wide range of values is given for the Late Eocene pCO_2. Several values have been considered in this study ranging from the pre-industrial to 8 times the pre-industrial value: $1\times CO_2$ (280 ppm), $2\times CO_2$ (560 ppm), $4\times CO_2$ (1120 ppm) and $8\times CO_2$ (2240 ppm).

The resulting Late Eocene climate in general shows lower atmospheric temperature values for lower pCO_2 levels. The value of the SAT over Antarctica and the surrounding ocean is 0.45 K lower each time the pCO_2 is reduced by 50%. This relatively low climate sensitivity has the same origin as the present-day climate's response to a doubling of the pCO_2 (Chapter 3). Also in this case the reduced response of the global climate can be explained by the relaxation of the ocean temperature to its initial values calculated with the LSG model. Indeed, as described in Chapter 3, the coupled climate-ice sheet model underestimates the global climate sensitivity by a factor of about 3 and by a factor of about 4 in the Antarctic region. This has to be considered to get a more realistic interpretation of the climate sensitivity found for the Late Eocene.

Under the same Late Eocene boundary conditions, lower SAT over Antarctica results in larger ice sheet volume and extension. After 10 ky of model integration, i.e. in the initial phase of ice sheet growth, the AIS volume increases by about $1.45\cdot10^6$ km^3 each time the pCO_2 is reduced by half, which seems to indicate a linear correspondence. DeConto and Pollard (2003) performed a similar experiment with a coupled climate-ice sheet model obtaining a higher sensitivity of the AIS volume to the pCO_2 level. Their results show a wider range in ice volume after 10 ky, from $0.2\cdot10^6$ km^3 ($8\times CO_2$) to $10.7\cdot10^6$ km^3 ($1\times CO_2$). This follows from the fact that in their climate model no realistic ocean component simulating the Late Eocene global circulation is included, but rather a non-dynamical 50-m slab ocean model, which can more easily react to changes in the atmosphere.

Previous modelling studies (Pollard and DeConto, 2005 and Langebroek et al., 2009) suggest the initiation of the AIS when the pCO_2 decreases below a critical threshold and do not relate linearly in these two processes. However these studies use a different modelling approach where the pCO_2 decreases during the model simulation. Furthermore, they disagree on both the degree of the AIS sensitivity and the critical glaciation value of the atmospheric pCO_2. So the relative importance of pCO_2 concerning the volume of the AIS still needs to be debated.

4. *How much can a favourable orbital configuration promote the initial AIS growth?*

The development of the AIS could have been supported by a specific orbital configuration (Coxall et al., 2005). To quantify influence of the insolation forcing on the AIS development two pairs of sensitivity experiments have been performed using the two tectonic configurations analogous to the Late Eocene and to the Late Oligocene,

respectively. Two different climates for each configuration have been performed, applying the modern orbit and also an orbit giving the smallest Antarctic summer insolation (called "cold" orbit).

The surface atmospheric temperature (SAT) over the Antarctic region is lower when the "cold" orbit is applied for both tectonic configurations. The difference in the mean annual SAT is 0.17 K for the Late Eocene and 0.09 K for the Late Oligocene, whereas the difference in the summer SAT is 0.99 K for the Late Eocene and 0.36 K for the Late Oligocene. This is due to the fact that with the "cold" orbit less solar radiation reaches the southern polar latitudes and the temperature is therefore lower than with the current orbit. The difference between the SAT for the two simulated orbits is higher within the two Late Eocene experiments. There is an interaction between the tectonic and the insolation forcings: in the Late Oligocene experiments, with the fully established ACC, the heat capacity of the ocean increases and, therefore, more energy is needed to heat it up.

As a consequence of the decrease in SAT, the "cold" astronomical orbit favours the glacial inception and the AIS originated under this condition is larger. In the case of Late Eocene climate, the "cold" astronomical orbit contributes to an increase in AIS volume of about 20% ($1.1 \cdot 10^6$ km^3), while the increase is 13% ($0.73 \cdot 10^6$ km^3) in the case of Late Oligocene configuration. Also these different values are due to the fact that in the latter case the ocean heat capacity is higher than in the Late Eocene, due to the different circulation and the fully established ACC.

7.1 Comparing the different factors

As already mentioned, this study does not simulate the Eocene-Oligocene (E-O) climatic transition explicitly, but concentrates on sensitivity experiments analysing the important processes that can be considered as necessary for the Antarctic glaciation. These processes are: (1) the opening of the Drake Passage (DP) and consequent establishment of the Antarctic Circumpolar Current (ACC) leading to the climatic isolation of the Antarctic continent; (2) the decrease in atmospheric pCO_2 level and relative SAT; (3) a favourable orbital configuration yielding cold austral summers and therefore minimizing melting of ice.

Although the experiments are different from each other, their results can be compared in order to give an idea on the relative importance that each mechanism could have had in the first phase of the Antarctic glaciation. As shown in Chapter 4, the opening of the DP alone causes changes in the global ocean circulation and, most importantly, the establishment of the ACC. This current substantially reduces the poleward heat flux from lower latitudes and contributes to the climatic isolation of the Antarctic continent. Therefore it decreases the Antarctic temperature by 0.4 K and this contributes to an increase in the AIS volume of $1.56 \cdot 10^6$ km^3. The sensitivity study explained in Chapter 5 relates a halving of the pCO_2 level with a decrease in Antarctic SAT of 0.45 K and, consequently, with an increase in AIS of $1.45 \cdot 10^6$ km^3 in the first

phase of the glaciation. Finally, a favourable orbital configuration decreases the Antarctic SAT by 0.17 K for the Late Eocene and 0.09 K for the Late Oligocene. This results in AIS growth of $1.1 \cdot 10^6$ km^3 and $0.73 \cdot 10^6$ km^3, respectively.

Therefore, reviewing the climate sensitivity given for the different forcings suggests that the first two processes (opening of DP and low pCO_2) seem to have a comparable effect on Antarctic SAT. The difference given by the insolation computed for both of the tectonic set-ups seem to be of minor importance. The obtained secondary importance of the orbital configuration is consistent with the conclusions of Langebroek et al. (2009), who suggest that orbital forcing is only important for glacial inception of Antarctica if the pCO_2 level is close to the threshold value, but do not represent a precondition.

As final remark, it must be mentioned that in none of the experiments performed in this study a climate state with an ice-free Antarctic continent has been reached. The geological record (see recent review in Coxall and Pearson, 2007) support the hypothesis that the major climatic changes, which acted along the E-O transition, brought to global cooling, especially at high latitudes, and rapid growth of the first semi-permanent ice-sheet on Antarctica only starting from the Early Oligocene. This implies that the Late Eocene Antarctic environment was temperate and ice-free. However, this climate regime has not been achieved in the sensitivity experiments conducted in this research. A greenhouse climate, like during the Eocene, could have most likely been realized by applying all the extreme boundary constraints yielding the warmest conditions: Late Eocene land-sea distribution, high atmospheric carbon dioxide concentration and orbital configuration providing the highest values of insolation in the Southern Hemisphere. Nevertheless, this type of climatic condition has not been investigated, but rather a sensitivity study isolating the various important factors has been preferred. Furthermore, even if this kind of climate would have been considered, it would have probably not been obtained. Indeed, it has been demonstrated in Chapter 3 that the relaxation of the ocean temperature and salinity to the initial values modelled with the LSG ocean model reduces the climate sensitivity of the coupled climate-ice sheet model itself. This derives from the fact that the LSG spin-up runs, which initialize the MPI-OM in the various COSMOS experiments, in all cases apply a present-day background climate.

Chapter 8
Conclusions and outlook

This study shows that the climate-ice sheet model used proofs to be a useful tool for investigating the Antarctic Ice Sheet (AIS) response to global climate under various scenarios. The modelling results indicate that the AIS is highly sensitive to different global land-sea distributions, atmospheric greenhouse gases and orbital forcings.
However, there are some aspects in the modelling strategy which should be improved in future research. Nevertheless, this modelling approach could be helpful to examine the scientific challenges of understanding the Antarctic and global climate evolution along the whole Cenozoic.

8.1 General conclusions

The modelling experiments illustrated in this study are helpful to understand the sensitivity of the Antarctic continent to the major changes, which occurred during the Eocene-Oligocene (E-O) transition. The causal mechanism for this fundamental shift is controversial, the most popular explanations being that glaciation was caused either (1) by cooling of Antarctica due to plate tectonic reorganisation and related changes in ocean circulation (e.g., Kennett, 1977; Barker, 2001); or (2) by a response to declining atmospheric pCO_2 favoured by the Earth's orbital configuration (e.g., DeConto and Pollard, 2003). Models and proxy records are being interpreted very differently to bring support to both theories. In this study no transient model run from a greenhouse to an icehouse climate has been considered, but rather several sets of sensitivity experiments have investigated the response of the Antarctic continent to changes in the global climate conditions. General conclusions can now be drawn, based on the results of the analysis. They are:

1. A complete representation of the Antarctic climate system, including the ocean, the atmosphere and the Antarctic cryosphere, has been obtained. This has been possible by a new modelling approach, involving four numerical models in a coupled modelling system. The iterative coupling procedure applied in this study accounts for the different time scales at which the climate subsystems (ocean, atmosphere and cryosphere) evolve.

2. The opening of the Drake Passage is followed by a change in the global ocean circulation and in the establishment of the Antarctic Circumpolar Current. The reorganization of the oceanic flow results in a decrease of the water and air temperatures in the Southern Ocean region and in an increase of the atmospheric vortex around the continent. These changes cooperate in decreasing the Antarctic surface atmospheric temperature (SAT) by approximately 0.4 K. Subsequent to this is the development of an AIS which has a volume of $1.56 \cdot 10^6$ km^3 larger than the one obtained with closed Drake Passage.

3. The development of the AIS under Late Eocene climate boundary conditions has been found sensitive to the concentration of atmospheric carbon dioxide. The results show that reducing the atmospheric pCO_2 level by 50% would decrease the Antarctic surface atmospheric temperatures by 0.45 K. This leads to an increase of the AIS volume of about $1.45 \cdot 10^6$ km^3 after 10 ky.

4. Under the same Late Eocene and Late Oligocene climate boundary conditions the development of an early AIS is supported by a favourable orbital configuration. An astronomical set-up yielding the lowest austral summer insolation decreases the Antarctic SAT by 0.17 K for the Late Eocene continental configuration and by 0.09 K for the Late Oligocene with respect to a modern orbit. The smaller decrease in temperature suggests that the orbital forcing does not seem to be critical for the early development of the AIS.

5. The modelling results achieved with the sensitivity experiments performed in this study support the idea that the two main processes (i.e. the opening of the

Drake Passage and the decrease in atmospheric pCO_2 favoured by the Earth's orbital configuration) could have had comparable importance in creating the conditions for an Antarctic glaciation.

8.2 Outlook

The improved resolution of proxy records can provide better constraints for modelling E-O climate change scenarios and permit to test hypotheses on climate change mechanisms that incorporate many factors. Model output force to crosscheck data-based interpretations and seek new ways of constraining key processes. The new iterative numerical method developed in this study provides results that can be used to separately test the proposed hypotheses. However, the model set-up can still be improved.

First of all the spin-up runs for the three tectonic settings (Present Day, Late Eocene and Late Oligocene) could be performed with the fully-coupled COSMOS, instead of with the LSG ocean model only. This would considerably rise the computing times to about 4 months for 1000 to 2000 years of model integration, but it would assure that the atmospheric response is included in the ocean start-up and that the outcoming climates are representative of the period examined with higher approximation. Furthermore the restoring of the ocean temperature and salinity to the initial values would be avoided, reducing the probability to have discrepancies between the modelled and the actual global oceanic circulation.

In parallel, the temperature and salinity restoring process in MPI-OM should be elaborated with an in-depth sensitivity analysis using different relaxation factors for different levels. This would clarify if this were the ultimate cause of changes in the oceanic circulation and, in this case, in explaining the reason and the way in which the circulation is modified when applying this procedure.

Moreover, it is recommended to investigate the model behaviour with different resolutions for both the climate and the ice-sheet model. The model resolutions used in this study are T31GR30 for the climate model (which corresponds to about 400 km for the atmosphere and the ocean) and 40 km for the ice sheet model. These resolutions can be increased to T63GR15 (about 200 km) for the climate model and 20 km for the ice sheet model. This would also substantially increase the computation time, but could allow a more detailed study of the different feedbacks between the global climate and the AIS, especially the WAIS at the relatively narrow Antarctic Peninsula.

The iterative modelling procedure between the climate and the ISM could be improved by performing a higher number of iterations using a shorter integration time of the ISM. A better estimation of the timing of the response of the AIS to the climate forcings could be achieved by integrating the ISM for 1 ky or 10 ky at each iteration. This would significantly raise the number of the iterations as well as the time of the computations, but it would help in investigating more directly the response of the ice sheet to changes in the climate boundary conditions.

Additionally it would be very interesting to conduct experiments investigating the reaction of AIS growth and volume under different initial bedrock scenarios. The initial

condition for paleoclimate studies is an ice-free bedrock elevation resulting from the isostatically adjusted Antarctic orography (Lythe et al., 2001). This is a commonly used strategy in Antarctic modelling studies, since little is known about the bedrock configuration in the past eras. However, due to their high elevations and polar location, regions such the Gamburtsev Mountains, the Transantarctic Mountains and the Dronning Maud Land could have served as nucleation points for glacial onset, as suggested by modelling experiments (DeConto and Pollard, 2003) and sediment evidence (Barker et al., 2007). Nevertheless the uplift history of some of those mountainous areas (i.e. the Gamburtsev Mountains) is not yet well known. A new bedrock topography for E-O has recently been published by Wilson and Luyendyk (2009), estimating an increase of the total Antarctic landmass by 10-20% with respect to the ice-free isostatically adjusted present-day bedrock topography. This would probably result in a larger initial AIS. Experiments with different bedrock settings would help to clarify the role of the topography in the initial phase of the development of the East Antarctic Ice Sheet.

The study of the influence of the decrease in atmospheric pCO_2 could be advanced with experiments where the carbon dioxide concentration is reduced during the model iterations. In this study equilibrium sensitivity experiments have been performed in order to find a link between the pCO_2 level and the ice sheet establishment. By decreasing the pCO_2 during the iterations the possibility of a glaciation threshold value could be investigated.

The orbital-induced response of the AIS needs supplementary investigation as well. Variations in the sediment records are dominated by Milankovitch frequencies (Naish et al., 2001). In this research, extreme values of orbital parameters showed that the Earth's orbital configuration serves only as a support for the formation of the AIS, rather than a necessary precondition. Further sensitivity studies with different orbital configurations and long-term simulation with varying orbital parameters could yield more insight into the pace of the ice-sheet evolution given by the cyclicity of the orbital frequencies.

The modelling approach used to study the sensitivity of Antarctica to the climate forcings, which could have acted along the E-O transition, could be applied to different periods in the Cenozoic (for example the Middle Miocene) and investigate evolution and oscillations in the volume and extent of the ice-sheet. In this respect, links between the Southern and Northern Hemisphere glaciation could also be investigated and the timing as well as the drivers of the bipolar glaciation addressed.

In general, future application of new and existing proxies, recovery of additional high-quality sediment archives from the oceans and continents and more complex models that integrate chemical and biological processes across the E-O transition will no doubt yield exciting results and should rapidly advance the field of palaeoclimatology. In this context this study brings a new modeling approach as well as new insights in the sensitivity of the Antarctic climate. Both aspects being fundamental for the comprehension of the mechanisms, which drive climate changes.

Appendixes

A.1 The atmospheric general circulation model ECHAM5

A summary of the main components of the AGCM ECHAM5 is given in the following. A detailed description of the model components can be found in Roeckner et al. (2003).

The atmosphere general circulation model ECHAM5 has been developed from the operational forecast model of the European Centre for Medium-Range Weather Forecasts (ECMWF) and a parameterisation package developed in at the Max Planck Institute for Meteorology (MPI-M) in Hamburg. ECHAM5 has a spectral dynamical core that solves the equations for vorticity, divergence, temperature and the logarithm of surface pressure in terms of spherical harmonics with a triangular truncation.

A flux-form semi-Lagrangian scheme (Lin and Rood, 1996) is used for passive tracer advection, i.e., for the water components (vapour, liquid, solid) and for chemical substances. This scheme satisfies the fundamental requirements of mass conservation, consistency with the discretization of the continuity equation and preservation of linear tracer correlations.

The integration of the general circulation requires heating/cooling rates within the atmosphere and energy fluxes at the surface and at the top of the atmosphere (TOA) related to the radiative transfer of solar shortwave and terrestrial longwave radiation. These forcing fields depend on the composition of the atmosphere, of the gaseous, the particulate as well as the condensed constituents, the orbital position of the Earth, the local solar zenith angle, as well as the thermal structure from the surface to the top of the atmosphere. At each radiation time step the transfer calculation is executed at all grid points of the Gaussian grid used in the AGCM.

The scheme used in ECHAM5 for calculating radiative transfer of solar energy within the atmosphere (Fouquart and Bonnel, 1980) includes Rayleigh scattering, absorption by water vapour and ozone and CO_2+N_2O+CO+CH_4+O_2 as uniformly mixed gases. Aerosols and cloud particles are effective through absorption and scattering. The computation of transmissivities and reflectivities across a vertical column is split into two separate calculations for the cloud-free part and the cloudy part. The scheme has four spectral bands, one for visible and UV range, and three for the near infrared. For the shortwave part of the spectrum, the single scattering properties are determined on the basis of Mie calculations using idealized size distributions for both cloud droplets and spherical ice crystals (Rockel et al., 1991) and the results are averaged over the relatively wide spectral ranges of the GCM. No subgrid-scale variability of cloud is taken into account in the radiation code, i.e. clouds are treated as plane-parallel homogeneous layers.

Terrestrial infrared radiation redistributes energy within the atmosphere depending on the composition of the atmosphere with regard to the active gases, aerosols and cloud

particles, and cools the atmosphere to space to balance the solar irradiation. The solution of the transfer differs from that in the shortwave by the presence of emitting sources within the atmosphere and the presence of a diffuse external source, the Earth surface, compared to the solar beam. Scattering is neglected.

The stratiform cloud scheme consists of prognostic equations for the water phases, bulk cloud microphysics, and a statistical cloud cover scheme with prognostic equations for the distribution moments. The microphysics scheme includes phase changes between the water components and precipitation processes. Moreover, evaporation of rain and melting of snow are considered as well as sedimentation of cloud ice.

A mass flux scheme is employed for shallow, mid-level and deep convection (Tiedtke, 1989). The scheme is based on steady state equations for mass, heat, moisture, cloud water and momentum for an ensemble of updrafts and downdrafts including turbulent and organized entrainment and detrainment. Turbulent entrainment and detrainment rates are specified differently for the three types of cumulus convection. Organized entrainment and detrainment are related to cloud activity itself.

The subgrid-scale orography parameterization (Lott and Miller, 1997; Lott, 1999) takes into account the main mechanisms of interaction between subgrid-scale orography and the atmospheric flow: momentum transfer from the Earth to the atmosphere accomplished by orographic gravity waves and the drag exerted by the subgrid-scale mountain when the air flow is blocked at low levels.

The parametrization for the momentum flux deposition from a gravity wave spectrum is based on the Doppler spread theory of propagation and dissipation of a gravity wave spectrum (Hines, 1997). The forcing mechanisms generating the gravity waves are located in the troposphere and include convective activity, shear instability, frontal systems or transient flow over topography. In the middle atmosphere, the gravity waves propagate predominantly upward from their source regions and form a broad background spectrum of waves. The quantity of interest is the deposition of the horizontal momentum transferred by the vertically propagating gravity waves. The momentum flux deposition is obtained as a function of the input gravity wave spectrum, the buoyancy frequency and the horizontal wind.

The surface temperature is obtained from the surface energy balance equation using an implicit coupling scheme that is unconditionally stable and allows to synchronously calculate the respective prognostic variables and surface fluxes (Schulz et al., 2001). The surface temperature is used as boundary condition to determine the vertical profile within the 5-layer soil model assuming vanishing heat fluxes at the bottom (10m). Surface runoff and drainage are obtained from a scheme taking into account the heterogeneous distribution of field capacities within a grid-cell (Dümenil and Todini, 1992). An hydrological discharge model is applied (Hagemann and Dümenil-Gates, 2001). A simple scheme is used for calculating the water temperature, ice thickness and ice temperature of lakes. The albedo of snow and ice is assumed to be a linear function of surface temperature, ranging between a minimum value $T_s=T_0$ at the melting-point and a maximum value for "cold" temperature $T_s \leq T_0-T_d$.

The turbulent surface fluxes for momentum, heat and moisture are obtained from bulk transfer relationships involving the difference of the respective model variable (wind components, potential temperature, humidity) between the surface and the lowest

model level, the wind velocity at that level and the transfer coefficients. The latter are obtained by integrating the flux-profile relationships between the surface and the lowest model level. Approximate analytical expressions in terms of roughness length and bulk Richardson number are employed for momentum and heat, respectively. Over land, the roughness length is a function of subgrid-scale orography and vegetation. Over sea, the aerodynamic roughness depends on friction velocity whereas the roughness length for heat transfer has to be adjusted owing to the fact that the transfer coefficient is largely independent of wind speed. In unstable conditions, an interpolation is used between the free convection limit and the neutral approximation.

The horizontal diffusion is formulated in spectral space. The treatment of horizontal diffusion differs from that of the other processes in that it does not involve a physical model of subgrid-scale processes, but rather a numerically convenient form of scale selective diffusion with coefficients determined empirically to ensure a realistic behaviour of the resolved scales.

A.2 The ocean general circulation model MPI-OM

A summary of the OGCM MPI-OM is given in the following. A detailed description of the model components can be found in the technical report by Wetzel et al. under http://www.mpimet.mpg.de/.

The Max-Planck-Institute Ocean Model (MPI-OM) is a z-coordinate global GCM based on the primitive equations for a hydrostatic Boussinesq fluid with a free surface (Marsland et al., 2003). Scalar and vector variables are formulated on an orthogonal curvilinear C-grid (Arakawa and Lamb, 1977).

Diffusion is implemented following Griffies (1998). Horizontal tracer mixing by unresolved eddies is parameterized following Gent et al. (1995). For the vertical eddy viscosity and diffusion the Richardson-number dependent scheme of Pacanowski and Philander (1981) is applied with additional wind mixing parameterization. A bottom boundary layer slope convection scheme allows for an improved representation of the flow of statically unstable dense water over sills. The effect of ocean currents on surface wind stress is taken into account following Luo et al. (2005).

Momentum advection of tracers is by a mixed scheme that employs a weighted average of both central-difference and upstream methods. The weights are chosen according to the ratio of the second spatial derivative over the first spatial derivative of the advected quantity.

The motions associated with the vertically integrated velocity field (barotropic part) are solved implicitly which damps the external gravity wave mode and thus allows the use of a longer time-step in the integrations.

Time stepping in MPI-OM is based on the idea of operator splitting, as described by e.g. Press et al. (1988). The prognostic variables are updated successively in several subroutines. Prescribed forcing is read in at the start of each time-step after which the sea ice dynamics equations are solved by means of functional iteration with under

relaxation. Then the sea ice thermodynamics are implemented. The ocean momentum equation is first solved partially for the friction terms and then the advection terms. This results in a partially updated momentum equation, which is decomposed into baroclinic, and barotropic subsystems, solved separately. The prognostic equation for the free surface is solved implicitly, which allows for the model's barotropic time-step to equal the baroclinic time-step.

The embedded sea ice model consists of sea ice dynamics following Hibler (1979) and zero-dimensional thermodynamics following Semtner (1976). For more details on MPI-OM and the embedded sea ice model see Marsland et al. (2003) and Jungclaus et al. (2006).

Thermodynamics of sea ice involves the determination of the local growth or melt rate at the base of the sea ice and the local melt rate at the surface. To allow for the prognostic treatment of the subgridscale fractional sea ice cover the surface heat balance is solved separately for the ice covered and ice free areas. That is, the net atmospheric heat flux is weighted according to the open water heat flux and heat flux over sea ice (or sea ice and snow). To complete the sea ice thermodynamic evolution a heat balance equation must also be applied at the ocean/sea ice and ocean/atmosphere interfaces.

Realization of the sea ice thermohaline coupling to the ocean model requires consideration of salt and fresh water exchanges during sea ice growth and melt. Sea ice is assumed to have a constant salinity independent of its age. The ocean model's upper layer salinity is changed by a certain amount due to the surface fresh water flux (modified by snow fall which accumulates on top of the sea ice) and due to sea ice growth or melt.

A.3 Ocean temperature and salinity adjustment

Several sensitivity experiments have been performed with MPI-OM using different constants of relaxation for different model levels. In the following the results for the Late Eocene and Late Oligocene configurations applying a three-dimensional restoring of temperature and salinity with a relaxation constant of 0.5 between the levels 15 and 40 are shown.

Figure A.1 shows the annual mean sea surface temperature (SST) adjustment of the MPI-OM ocean model to the LSG input after 20 years of model integration for the tectonic configurations Late Eocene (EOC, a) and Late Oligocene (LOL, b). In general, in the case of the EOC configuration, the world ocean surface temperature undergoes a strong warming with respect to the initial temperature (modelled by the LSG ocean model) up to 4 K. On the other side, the North Atlantic experiences a temperature decrease up to about -4 K, which interests also the area of the (open) Panama Gateway. In the case of the LOL configuration (Fig. A.1b) an overall cooling of more than 5 K of the global SST is evident, especially in the Pacific equatorial region. The coastal regions of North America, South Africa and Australia present a warming up to 3 K. Other regions of the North and South Pacific Ocean and the South Indian Ocean show the same kind of surface cooling.

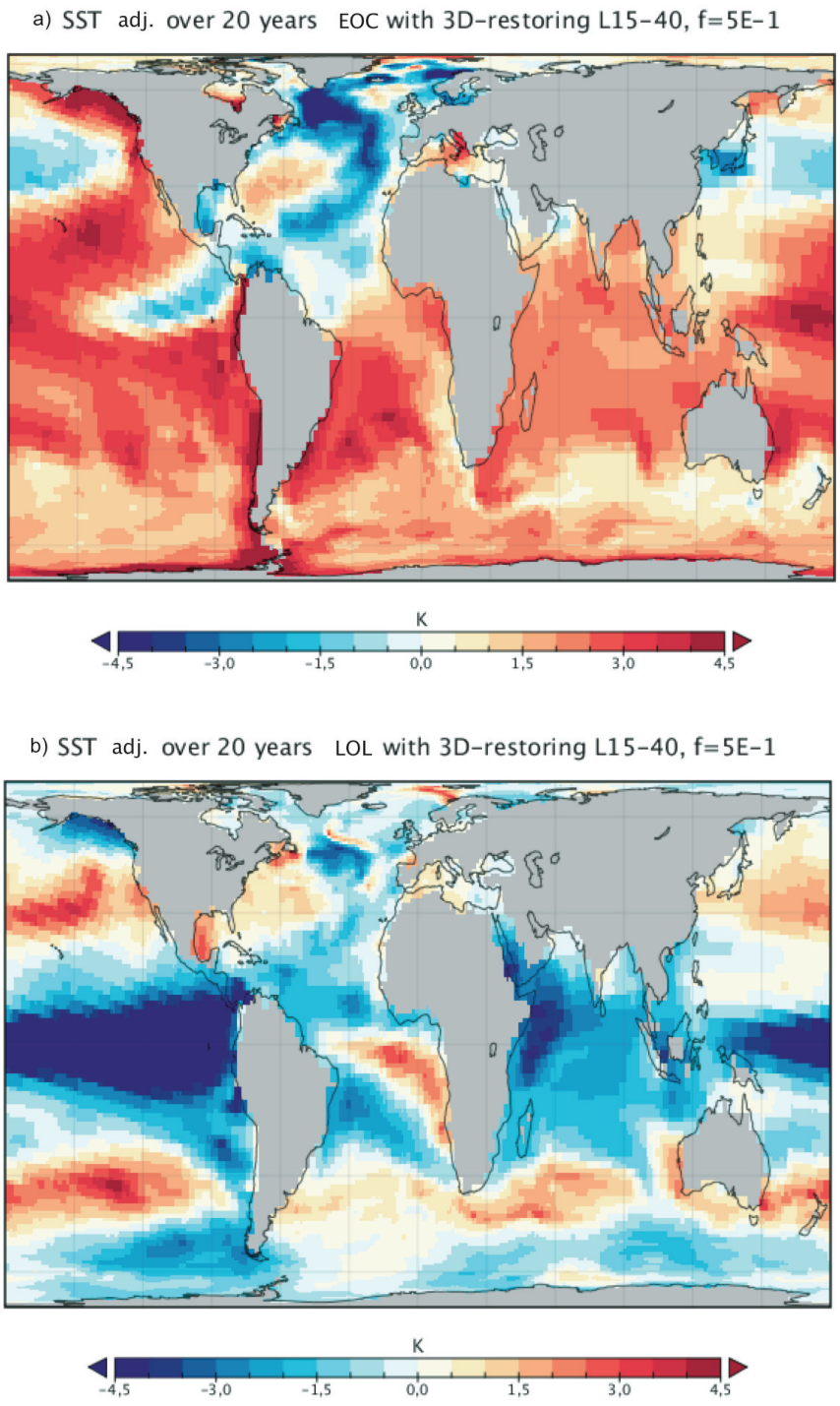

Figure A1: Annual mean sea surface temperature (SST) adjustment of the MPI-OM ocean model to the LSG input for the tectonic configurations Late Eocene (EOC, a) and Late Oligocene (LOL, b) using a 3-dimensional restoring between the model levels (L) 15 and 40 and a relaxation constant (f) of 0.5 (Butzin, pers. comm.).

In Figure A.2 the annual mean sea surface salinity (SSS) adjustment of the MPI-OM ocean model to the LSG input after 20 years of model integration for the tectonic configurations Late Eocene (EOC, a) and Late Oligocene (LOL, b) is shown. An increase in the salinity up to 2 PSU is detectable with the EOC configuration in the equatorial regions, specifically in the Pacific and Atlantic Oceans in correspondence of the Panama Gateway and in the northern Indian Ocean. Differently, a decrease of over 2 PSU in the surface salinity is visible in the North Atlantic and in the Arctic Ocean. With the LOL configuration, a relevant increase in the salinity is recognizable in the central Pacific and Indian Oceans. The remaining global ocean is characterized by zones of negative anomalies near zones of positive anomalies.

Therefore, the salient results of this sensitivity study are: (1) in the EOC experiments the SST undergoes a stronger drift than in the LOL experiments; (2) in both the EOC and the LOL experiments the adjustment in the SST as well as in the SSS with the restoring constant $f=5\cdot10^{-1}$ is stronger than with the restoring constant $f=8\cdot10^{-4}$.

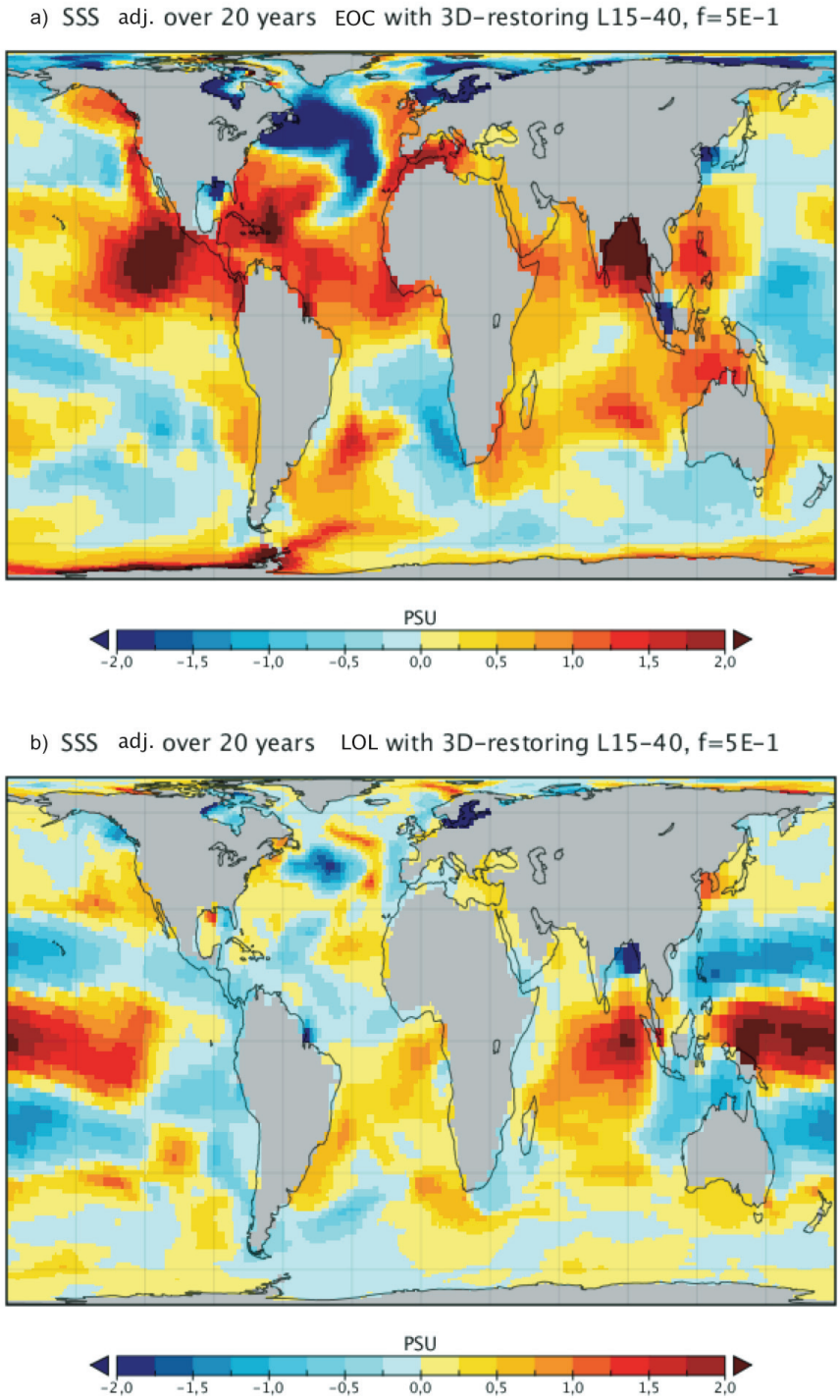

Figure A2: Annual mean sea surface salinity (SSS) adjustment of the MPI-OM ocean model to the LSG input for the tectonic configurations Late Eocene (EOC, a) and Late Oligocene (LOL, b) using a 3-dimensional restoring between the model levels 15 and 40 and a relaxation constant of 0.5 (Butzin, pers. comm.)

References

Ambach, W. (1988). Interpretation of the Positive-Degree-Days Factor by Heat Balance Characteristics - West Greenland. Nordic Hydrology, 19, 217-224.

Antonov, J. I., Locarnini, R. A., Boyer, T. P., Mishonov, A. V., Garcia, H. E. (2006). World Ocean Atlas 2005, Volume 2: Salinity. S. Levitus, Ed. NOAA Atlas NESDIS 62, U.S. Government Printing Office, Washington, D.C., 182 pp.

Arakawa, A. and Lamb, V. R. (1977). Computational design of the basic dynamical processes of the UCLA general circulation model. Methods Comput. Phys., 17, 173-265.

Arthern, R. J., Winebrenner, D. P., Vaughan, D. G. (2006). Antarctic snow accumulation mapped using polarization of 4.3-cm wavelength microwave emission. J. Geophys. Res., 111, D06107.

Bamber, J. L., Rive, R. E. M., Vermeersen, B. L. A., LeBrocq, A. M. (2009). Reassessment of the Potential Sea-Level Rise from a Collapse of the West Antarctic Ice Sheet. Science, 324, 901-903.

Barker, P. F. (2001). Scotia Sea regional tectonic evolution: implications for mantle flow and palaeocirculation. Earth-Science Reviews, 55, 1-39.

Barker, P. F., Diekmann, B. Escutia, C. (2007). Onset of Cenozoic Antarctic glaciation. Deep Sea Research Part II: Topical Studies in Oceanography, 54, 2293-2307.

Barker, P. F. and Burrell, J. (1977). The Opening Of Drake Passage. Marine Geology, 25, 15-34.

Barnola, J.-M., Raynaud, D., Korotkevich, Y. S., Lorius, C. (1987). Vostok ice core provides 160,000-year record of atmospheric CO_2. Nature, 329, 408-414.

Barrett, P. J. (2007). Cenozoic climate and sea level history from glacimarine strata off the Victoria Land Coast, Cape Roberts Project, Antarctica, In: M. J. Hambrey, P. Christoffersen, N. F. Glasser, and B. Hubbart (Eds). Glacial Processes and Products, International Association of Sedimentologists Special Publication, Vol. 39, pp. 259-287.

Bennett, M. R. (2003). Ice streams as the arteries of an ice sheet: Their mechanics, stability and significance. Earth Sci. Rev., 61, 309-339.

Berger, A. (1976) Obliquity and precession for the last 5,000,000 years. Astronomy and Astrophysics, 51, 127-135.

Berger, A. and Loutre, M. (1991), Insolation values for the climate of the last 10 million years, Quaternary Sci. Rev., 10(4), 297-317.

Berner, R. A. (1997). The carbon cycle and CO_2 over Phanerozoic time: the role of land plants. Philosophical Transactions of the Royal Society Series B, 353, 75-82.

Berner, R. A. (1992). Palaeo-CO_2 and climate; discussion. Nature, 358, 114.

Berner, R. A. (1990). Atmospheric carbon dioxide levels over Phanerozoic time. Science, 249, 1382-1386.

Berner, R. A. and Kothavala, Z. (2001). GEOCARB III. A revised model of atmospheric CO_2 over Phanerozoic time. American Journal of Science, 291, 182-204.

Boucot, A. J. and Gray, J. (2001). A critique of Phanerozoic climatic models involving changes in the CO_2 content of the atmosphere. Earth-Science Reviews, 56, 1-159.

Bretagnon, P. and Francou, G. (1988). Planetary theories in rectangular and spherical variables - VSOP 87 solutions . Astronomy and Astrophysics, 202, 309-315.

Bromwich, D. H. (1988). Snowfall in High Southern Latitudes. Rev. Geophys. 26, 149-168.

Butzin, M., Prange, M., Lohmann, G. (2005). Radiocarbon simulations for the glacial ocean: The effects of wind stress, Southern Ocean sea ice and Heinrich events. Earth and Planetary Science Letters, 235, 45-61.

Comiso, J. C. (2010). Variability and trends of the global sea ice cover, 205-246, in: D.N. Thomas and G. S. Dieckmann (eds.), Sea Ice, Wiley-Blackwell, 2nd edition.

Coxall, H. K., Wilson, P. A. , Pälike H., Lear, C.H. Backman, J. (2005). Rapid stepwise onset of Antarctic glaciation and deeper calcite compensation in the Pacific Ocean. Nature, 433, 53-57.

Coxall, H.K. and Pearson, P.N. (2007). The Eocene-Oligocene transition, in: Williams, M., et al., eds., Deep-time perspectives on climate change: Marrying the signal from computer models and biological proxies. Geological Society (London), Micropalaeontological Society (in press).

Croll, J. (1867a). On the change in the obliquity of the eliptic, its influence on the climate of the polar regions and on the level of the sea . Philosophical Magazine, 33, 426-445.

Croll, J. (1867b). On the eccentricity of the earth's orbit, and its physical relations to the glacial epoch . Philosophical Magazine, 33, 119-131.

Crowell, J. C. and North, G. R. (1991). Palaeoclimatology . No. 18 in Oxford Monographs on Geology and Geophysics. Oxford University Press, New York.

Crowley, T. J. (2000). Carbon dioxide and Phanerozoic climate: An overview. In Huber, B. T., MacLeod, K. G. and Wing, S. L., (eds.), Warm Climates in Earth History, Cambridge University Press, 425-444.

DeConto, R. M. and Pollard, D. (2003). A coupled climate-ice sheet modeling approach to the Early Cenozoic history of the Antarctic ice sheet. Palaeogeography, Palaeoclimatology, Palaeoecology, 198, 39-52.

Dümenil, L. and Todini, E. (1992) A rainfall-runoff scheme for use in the Hamburg climate model. In: Advances in Theoretical Hydrology, A Tribute to James Dooge, edited by Kane, J. O., European Geophysical Society Series on Hydrological Sciences, pp. 129-157. Elsevier, Amsterdam.

Exon, N.F., Kennett, J.P., Malone, M.J., et al. (2001) Proceedings of the Ocean Drilling

Program, Initial Reports Volume 189. Available online at: http://www-odp.tamu.edu/publications/189_IR/189TOC.HTM

Fouquart, Y. and Bonnel, B. (1980) Computations of solar heating of the Earth's atmosphere: A new parameterization. Beitr. Phys. Atmos., 53, 35-62.

Fortuin, J. P. F. and Oerlemans, J. (1990). Parameterization of the annual surface temperature and mass balance of Antarctica. Annals of Glaciology, 14, 78-84.

Fox, A.J. and Cooper, A.P.R. (1994). Measured properties of the Antarctic Ice Sheet derived from the SCAR Antarctic Digital Database. Pol. Rec., 30, 201-206.

Gale, A. S., Huggett, J. M., Pälike, H., Laurie, E., Haliwood, E. A. and Hardebol, J. (2006). Correlation of Eocene - Oligocene marine and continental records: orbital cyclicity, magnetostratigraphy and sequence stratigraphy of the Solent Group, Isle of Wight, UK. Journal of the Geological Society of London, 163, 4010415.

Gent, P., Willebrand, J., McDougall, T. J., McWilliams, J. C. (1995). Parameterizing eddy-induced tracer transport in ocean circulation models. J. Phys. Oceanogr., 25, 463-474.

Giovinetto, M. B., Waters, N., Bentley, C.R. (1990). Dependence of Antarctic surface mass balance on temperature, elevation and distance to open ocean. Journal of Geophysical Research, 95, 3517-353.

Goodess, C. M., Palutikof, J. P., Davies, T. D. (1992). The nature and causes of climate change. Belhaven Press, London.

Griffies, S. M. (1998). The Gent-McWilliams skew flux. J. Phys. Oceanogr., 28, 831-841.

Grosfeld, K. and Gerdes, R. (1998). Circulation beneath the Filchner Ice Shelf, Antarctica, and its sensitivity to changes in the oceanic environment: a case-study. Annals Of Glaciology, 27, 99-104.

Hagemann S. and Dümenil-Gates, L. (2001). Validation of the hydrological cycle of ECMWF and NCEP reanalyses using the MPI hydrological discharge model. J. Geophys. Res., 106, 1503- 1510.

Hagemann, S. and Dümenil, L. (1998). A parametrization of the lateral waterflow for the global scale. Climate Dynamics, 14, 17-31.

Hibler, W. D. (1979). A dynamic thermodynamic sea ice model. J. Phys. Oceanogr., 9, 815-846.

Hines, C. O. (1997a). Doppler spread parameterization of gravity wave momentum deposition in the middle atmosphere. Part I: Basic formulation . J. Atmos. Solar Terr. Phys., 59, 371-386.

Hines, C. O. (1997b). Doppler spread parameterization of gravity wave momentum deposition in the midd le atmosphere. Part II: Broad and quasi monochromatic spectra and implementation. J. Atmos. Solar Terr. Phys., 59, 387-400.

Hoskins, B.J. and Simmons, A.J. (1975). A multi-layer spectral model and the semi implicit method. Q. J. Roy. Meteor. Soc., 101, 637-655.

Hönisch, B. and Hemming, N. G. (2004). Ground-truthing the boron isotope-paleo-pH proxy in planktonic foraminifera shells: Partial dissolution and shell size effects Paleoceanography, 19, PA001026.

Huybrechts, P. (2002). Sea-level changes at the LGM from ice - Dynamic reconstructions of the Greenland and Antarctic Ice Sheets during the glacial cycles. Quaternary Sci. Rev., 21, 203-231.

Huybrechts, P. (1993). Glaciological modelling of the late Cenozoic East Antarctic Ice Sheet: Stability or dynamism? Geografiska Annaler, 75A, 221-238.

Imbrie, J., Hays, J. D., McIntyre, A., Mix, A. C., Morley, J. J., Pisias, N. G., Prell, W. L., Shackleton, N. J. (1984). The orbital theory of Pleistocene climate: Support from a revised chronology of the marine $\delta^{18}O$ record. In Berger, A., Imbrie, J., Hays, J., Kukla, G. J. and Saltzman, E., (eds.), Milankovitch and Climate, Boston, Reidel, 269-305.

IPCC (2007). Climate Change 2007: The Physical Science Basis. Contribution of Working Group I to the Fourth Assessment Report of the Intergovernmental Panel on Climate Change. In: S. Solomon, D. Qin, M. Manning, Z. Chen, M. Marquis, K. B. Averyt, M. Tignor, and H. L. Miller (Eds). Cambridge University Press, Cambridge, UK, 996 pp.

Jacobs, S. S., Hellmer, H. H., Doake, C. S. M., Jenkins, A., Frohlich, R. M. (1992). Melting of ice shelves and the mass balance of Antarctica. J. Glaciol., 38, 375-387.

Jovane, L., Florindo, F., Sprovieri, M., Pälike, H. (2006). Astronomic calibration of the late Eocene/early Oligocene Massignano section (central Italy). Geochemistry, Geophysics, Geosystems, 7, GC001195.

Jungclaus, J. H., N. Keenlyside, Botzet, M., Haak, H., Luo, J. J., Latif, M., Marotzke, J., Mikolajewicz, U., Roeckner, E. (2006). Ocean Circulation and Tropical Variability in the Coupled Model ECHAM5/MPI-OM. Journal of Climate, 19, 3952-3972.

Kållberg, P., Berrisford, P., Hoskins, B., Simmmons, A., Uppala, S., Lamy-Thépaut, S., Hine, R. (2005). ERA-40 Atlas. Reading, ECMWF.

Kennett, J. P. (1978). The Development Of Planktonic Biogeography In The Southern Ocean During The Cenozoic. Marine Micropaleontology, 3, 301-345.

Kennett, J. P. (1977). Cenozoic Evolution of Antarctic Glaciation, the Circum-Antarctic Ocean, and Their Impact on Global Paleoceanography. Journal of Geophysical Research 82, 3843-3860.

Langebroek, P. M., Paul, A., Schulz, M. (2009). Constraining atmospheric CO_2 content during the Middle Miocene Antarctic glaciation using an ice sheet-climate model. Clim. Past., 4, 859-895.

Laskar, J., P. Robutel, P., Joutel, F., Gastineau, M., Correia, A. C. M., Levrard B., (2004). A long-term numerical solution for the insolation quantities of the Earth. A&A, 428, 261-285.

Laskar, J., F. Joutel, Boudin, F. (1993). Orbital, precessional and insolation quantities for the Earth from -20Myr to +10Myr. Astron. Astrophys., 270, 522-533.

Lawver, L. A., and Gahagan, L. M. (1998). Opening of Drake Passage and its impact on Cenozoic ocean circulation. In: T. J. Crowley, and K. C. Burke (Eds). Tectonic Boundary Conditions for Climate Reconstructions. Oxford University Press, New York, pp. 212-223.

Lear, C. H., Bailey, T. R., Pearson, P. N., Coxall, H. K., Rosenthal, Y. (2008). Cooling and ice growth across the Eocene-Oligocene transition. Geology, 36, 251-254.

Lin, S. J. and Rood, R. B. (1996). Multidimensional flux form semi-Lagrangian transport. Mon. Wea. Rev., 124, 2046-2068.

Liu, Z., Pagani, M., Zinniker, D., DeConto, R., Huber, M., Brinkhuis, H., Shah, S. R., Leckie, R. M., Pearson, A. (2009). Global Cooling During the Eocene-Oligocene Climate Transition. Science, 323, 1187-1190.

Locarnini, R. A., Mishonov, A. V., Antonov, J. I., Boyer, T. P., Garcia, H. E. (2006). World Ocean Atlas 2005, Volume 1: Temperature. S. Levitus, Ed. NOAA Atlas NESDIS 61, U.S. Gov. Printing Office, Washington, D.C., 182 pp.

Lohmann, G. and Lorenz, S. (2000). On the hydrological cycle under paleoclimatic conditions as derived from AGCM simulations. J. Geophys. Res., 105, 17417-17436.

Lott, F., (1999) Alleviation of stationary biases in a GCM through a mountain drag parameterization scheme and a simple representation of mountain lift forces. Mon. Wea. Rev., 127, 788-801.

Lott, F. and Miller, M.J. (1997). A new subgrid-scale orographic drag parameterization: Ist formulation and testing. Q. J. Roy. Meteor. Soc., 123, 101-127.

Lythe, M. B., Vaughan, D. G. and the BEDMAP Consortium (2001). BEDMAP- A new ice thickness and subglacial topographic model of Antarctica. Journal of Geophysical Research, 106, 11335 - 11351.

Luo, J.-J., Masson, S., Roeckner, E., Madec, G., Yamagata, T. (2005). Reducing Climatology Bias in an Ocean-Atmosphere CGCM with Improved Coupling Physics. Journal of Climate, 18, 2344-2360.

Maier-Reimer, E., Mikolajewicz, U., Hasselmann, K. (1993). Mean Circulation of the Hamburg LSG OGCM and Its Sensitivity to the Thermohaline Surface Forcing. Journal of Physical Oceanography, 23, 731-757.

Marsland, S. J., Haak, H., Jungclaus, J. H., Latif, M., Röske, F. (2003). The Max-Planck-Institute global ocean/sea ice model with orthogonal curvilinear coordinates. Ocean Modelling, 5, 91-127.

Masson-Delmotte, V., Kageyama, M., Braconnot, P., Charbit, S., Krinner, G., Ritz, C., Guilyardi, E., Jouzel, J., Abe-Ouchi, A., Crucifix, M., Gladstone, R., Hewitt, C., Kitoh, A., LeGrande, A., Marti, O., Merkel, U., Motoi, T., Ohgaito, R., Otto-Bliesner, B., Peltier, W., Ross, I., Valdes, P., Vettoretti, G., Weber, S., Wolk, F., Yu, Y. (2006). Past and future polar amplification of climate change: climate model intercomparisons and ice-core constraints. Climate Dynamics, 27, 437-440.

Meeus, J. (1998). Astronomical Algorithms. Willmann-Bell, Richmond, 2nd edn.

Merico, A., Tyrrell, T., Wilson, Paul A. (2008). Eocene/Oligocene ocean de-acidification linked to Antarctic glaciation by sea-level fall. Nature, 452, 979 - 983.

Milankovitch, M. M. (1941). Canon of Insolation and the Ice Age Problem. Königlich Serbische Academie, Belgrade. English translation by the Israel Program for Scientific Translations, United States Department of Commerce and the National Science Foundation, Washington D.C.

Mikolajewicz, U., Maier-Reimer, E., Crowley, T. J., Kim, K.-Y. (1993). Effect of Drake and Panamanian Gateways on the circulation of an ocean model. Paleoceanography, 8, 409-426.

Monaghan, A. J. and Bromwich, D. H. (2008). Advances describing recent Antarctic climate variability. Bulletin of the American Meteorological Society. 89, 1295-1306.

Naish, T. R., Woolfe, K. J., Barrett, P. J., Wilson, G. S., Atkins, C., Bohaty, S. M., Bucker, C. J., Claps, M., Davey, F. J., Dunbar, G. B., Dunn, A. G., Fielding, C. R., Florindo, F., Hannah, M. J., Harwood, D. M., Henrys, S. A., Krissek, L. A., Lavelle, M., van der Meer, J., McIntosh, W. C., Niessen, F., Passchier, S., Powell, R. D., Roberts, A. P., Sagnotti, L., Scherer, R. P., Strong, C. P., Talarico, F., Verosub, K. L., Villa, G., Watkins, D. K., Webb, P.-N., Wonik, T. (2001). Orbitally induced oscillations in the East Antarctic Ice Sheet at the Oligocene/Miocene Boundary. Nature, 413, 719-723.

Nicholls, R., Tol, R., Vafeidis, A. (2008). Global estimates of the impact of a collapse of the West Antarctic ice sheet: an application of FUND. Climatic Change, 91, 171-191.

Nong, G. T., Najjar, R. G., Seidov, D., Peterson, W. H. (2000). Simulation of ocean temperature change due to the opening of Drake Passage. Geophys. Res. Lett., 27, 2689-2692.

Pagani, M., Zachos, J. C., Freeman, K. H., Tipple, B., Bohaty, S. (2005). Marked Decline in Atmospheric Carbon Dioxide Concentrations During the Paleogene. Science, 309, 600-603.

Pälike, H. and Laskar, J. (2004). Geologic constraints on the chaotic diffusion of the solar system. Geology, 32, 929-932.

Pearson, P. N., Foster, G. L., Wade, B. S. (2009). Atmospheric carbon dioxide through the Eocene-Oligocene climate transition. Nature, 461, 1110-1113.

Pearson, P. N. and Palmer, M. R. (2000). Atmospheric carbon dioxide concentrations over the past 60 million years. Nature, 406, 695-699.

Petit, J. R., Jouzel, J., Raynaud, D., Barkov, N. I., Barnola, J.-M., Basile, I., Benders, M., Chappellaz, J., Davis, M., Delayque, G., Delmotte, M., Kotlyakov, V. M., Legrand, M., Lipenkov, V. Y., Lorius, C., Pépin, L., Ritz, C., Saltzman, E. (1999). Climate and atmospheric history of the past 420,000 years from the Vostok ice core, Antarctica. Nature, 399, 429-436.

Picard, G., M. Fily, Gallee, H. (2007). Surface melting derived from microwave radiometers: a climatic indicator in Antarctica. Ann. Glaciol., 46, 29-34.

Pollard, D. and DeConto, R. M. (2005). Hysteresis in Cenozoic Antarctic ice-sheet variations. Global and Planetary Change, 45, 9-21.

Prange, M., G. Lohmann, Paul, A. (2003). Influence of Vertical Mixing on the Thermohaline Hysteresis: Analyses of an OGCM. Journal of Physical Oceanography, 33, 1707-1721.

Press, W. H., Flannery, B. P., Teukolsky, S. A., Vetterling, W. T. (1988). Numerical Recipes in C. The Art of Scientific Computing . Cambridge University Press.

Raymo, M. E. (1991). Geochemical evidence supporting T.C. Chamberlin's theory of glaciation. Geology, 19, 344-347.

Ritz, C., Fabre, A., Letréguilly, A. (1997). Sensitivity of a Greenland ice sheet model to ice flow and ablation parameters: Consequences for the evolution through the last climatic cycle. Climate Dynamics, 13, 11-24.

Rockel, B., Raschke, E., Weyres, B. (1991). A parameterization of broad band radiative transfer properties of water, ice, and mixel clouds . Beitr. Phys. Atmos., 64, 1-12.

Roeckner, E., Bäuml, G., Bonaventura, L., Brokopf, R., Esch, M., Giorgetta, M., Hagemann, S., Kirchner, I., Kornblueh, L., Manzini, E., Rhodin, A., Schlese, U., Schulzweida, U., Tompkins, A., (2003). The atmospheric general circulation model ECHAM 5. Part I: model description. Hamburg, Max Planck Institute for Meteorology.

Royer, D. L., Berner, R. A., Montañez, I. P., Tabor, N. J., Beerling, D. J. (2004). CO_2 as a primary driver of Phanerozoic climate. GSA Today, 14, 4-10.

Royer, D. L., Wing, S. L., Beerling, D. J., Jolley, D. W., Koch, P. L., Hickey, L. J., Berner, R. A. (2001). Paleobotanical evidence for near present-day levels of atmospheric CO2 during part of the tertiary. Science, 292, 2310-2313.

Schäfer-Neth, C. and Paul, A. (2001). Circulation of the Glacial Atlantic: a Synthesis of Global and Regional Models. The Northern North Atlantic: A Changing Environment, Springer, 441-459.

Scher, H. D. and Martin, E. E. (2006). Timing and Climatic Consequences of the Opening of Drake Passage. Science, 312, 428-430.

Schulz, J.-P., Dümenil, L., Polcher, J. (2001) On the land surface-atmosphere coupling and its impact in a single-column atmosphere model. J. Appl. Meteorol., 40, 642-663.

Schwerdtfeger, W. (1984). Weather and climate of the Antarctic, Developments in atmospheric science 15, Elsevier (Amsterdam), 261 pp.

Semtner, A. J. (1976). A model for the thermodynamic growth of sea ice in numerical investigations of climate. J. Phys. Oceanogr., 6, 379-389.

Siegert, M. J. (2009). Numerical Modelling of the Antarctic Ice Sheet. In: Antarctic Climate Evolution. F. Florindo and M. Siegert (eds.), Elsevier.

Siegert, M. J. and Florindo, F. (2008). Antarctic Climate Evolution. In: Antarctic Climate Evolution. F. Florindo and M. Siegert (eds.), Elsevier.

Siegert, M. J., Carter, S., Tabacco, I., Popov, S., Blankenship, D. D. (2005). A revised inventory of Antarctic subglacial lakes. Antarct. Sci., 17, 453-460.

Simmonds, I., Keay, K., Lim, E.-P. (2003). Synoptic Activity in the Seas around Antarctica. Monthly Weather Review, 131, 272-288.

Simmons, A. J. and Burridge, D. M. (1981). An energy and angular-momentum conserving vertical finite difference scheme and hybrid vertical coordinates. Mon. Wea. Rev., 109, 758-766.

Summerhayes, C., Ainley, D., Barrett, P., Bindschadler, R., Clarke, A., Convey, P., Fahrbach, E., Gutt, J., Hodgson, D., Meredith, M., Murray, A., Pörtner, H.-O., Di Prisco, G., Schiel, S., Speer, K., Turner, J., Verde, C., Willems, A. (2009). The Antarctic Environment in the Global System. In: Antarctic Climate Change and the Environment. Cambridge, UK, Scientific Committee on Antarctic Research, Scott Polar Research Institute.

Talarico, F. M. and Kleinschmidt, G. (2008). The Antarctic Continent in Gondwanaland: A Tectonic Review and Potential Research Targets for Future Investigations. In: Antarctic Climate Evolution. F. Florindo and M. Siegert (eds.), Elsevier.

Tiedtke, M. (1989). A comprehensive mass flux scheme for cumulus parameterization in large-scale models. Mon. Wea. Rev., 117, 1779-1800.

Toggweiler, J. R., and Bjornsson, H. (2000). Drake Passage and paleoclimate. J. Quaternary Sci., 15, 319-328.

Toggweiler, J. R. and Samuels, B. (1995). Effect of Drake Passage on the global thermohaline circulation. Deep Sea Research Part I: Oceanographic Research Papers, 42, 477-500.

Tripati, A., Backman, J., Elderfield, H., Ferretti, P. (2005). Eocene bipolar glaciation associated with global carbon cycle changes. Nature, 436, 341 - 346.

Turner, J., Bindschadler, R., Convey, P., Di Prisco, G., Fahrbach, E., Gutt, J., Hodgson, D., Mayewski, P. A., Summerhayes, C. (2009). Antarctic Climate Change and the Environment. Cambridge, UK, Scientific Committee on Antarctic Research, Scott Polar Research Institute.

Valcke, S., Caubel, A., Declat, D., Terray, L. (2003). OASIS Ocean Atmosphere Sea Ice Soil users's guide. CERFACS Tech. Rep. Toulouse, 85.

Van de Berg, W. J., Van den Broeke, M. R., Reijmer, C. H., Van Meijgaard, E. (2005). Characteristics of the Antarctic surface mass balance, 19582002, using a regional atmospheric climate model. Annals of Glaciology, 41, 97-104.

Van der Wateren, F.M. and Cloetingh, S.A.P.L. (1999). Feedbacks of lithosphere dynamics and environmental change of the Cenozoic West Antarctic Rift System. Global Planet. Change 23, pp. 1-24.

Vaughan, D. G., Bamber, J. L., Giovinetto, M., Russell, J., Cooper, A. P. R. (1999). Reassessment of net surface mass balance in Antarctica. J. Climate, 12, 933-946.

Wetzel, P., Haak, H. The Max-Planck-Institute Global Ocean/Sea-Ice Model MPI-OM. Technical Report, Max-Planck-Institute for Meteorology, Hamburg, Germany. Available online at: http://www.mpimet.mpg.de/

Wilson, D. S. and Luyendyk, B. P. (2009). West Antarctic paleotopography estimated at the Eocene-Oligocene climate transition. Geophys. Res. Lett., 36, L16302.

Wright, A. and Miller, K. G., (1993). Southern ocean influences on late Eocene to Miocene deep-water circulation, The Antarctic paleoenvironment: A perspective on global change Antarctic research series, 1-25.

Zachos, J., Dickens, G. R., Zeebe, R. E. (2008). An early Cenozoic perspective on greenhouse warming and carbon-cycle dynamics. Nature, 451, 279-283.

Zachos, J. C. and Kump, L. R. (2005). Carbon cycle feedbacks and the initiation of Antarctic glaciation in the earliest Oligocene. Global and Planetary Change, 47, 51-66.

Zachos, J. C., Pagani, M., Sloan, L. C.,Thomas, E., Billups, K. (2001). Trends, rhythms, and aberrations in global climate 65 Ma to present. Science, 292, 686-693.

Acknowledgements

Thanks to my supervisor Prof. Dr. Gerrit Lohmann, for giving me the opportunity to work on this Ph.D. project and for initiating me to the study of the paleoclimate.

Thanks to Dr. Klaus Grosfeld for his inestimable helpfulness in these three years and for reviewing my thesis.

Thanks to all the colleagues of the "Paleoclimate dynamics" working group at the Alfred Wegener Institute, especially Dr. Martin Butzin, Dr. Martin Werner, Dr. Thomas Laepple, Dr. Petra Langebroek, Dr. Malte Thoma, Dr. Monica Ionita and Axel Wagner for their unique help in many ways and on various time scales during my Ph.D. project.

Thanks to the colleagues of the AWI Computing Center, especially Dr. Kerstin Fieg and Dr. Chresten Wübber, for their technical assistance.

Thanks to Prof. Dr. Philippe Huybrechts and the colleagues of the "Ice and climate" working group at the University of Brussels, for the fruitful suggestions and the nice time during my stay.

Thanks to Prof. Dr. Dierk Hebbeln, Dr. Uta Brathauer, Dr. Ulrike Holzwarth and all the GLOMAR students, post-docs and directorate, for their support and the countless opportunities for education, scientific discussion and friendship.

Thanks to Dr. Eberhard Fahrbach and all the participants of the Polarstern expedition ANT/XXIV-3 for sharing that incomparable life and scientific experience with me.

Thanks to all the marvellous persons I have met since I arrived in Germany, too many people to be listed in a page. Thanks for the welcome, the support, the help, the company, the friendship. Special thanks go to Diana Magens, for enthusiastically motivating my research and for her willingness to read my thesis. Thanks also to the "Italian community" in Bremen, for keeping my passion vivid.

Immeasurable thanks go to Torben Stichel, for his endless patience, for reviewing my thesis, and for everything else.

I would have done nothing without the manifold support of by beloved family. My most important thanks go to my parents, Vittorio and Laura Cristini, for always believing in me more than I do. And to my sister Elena, for her struggle in keeping me connected to the reality.